SPINTRONICS BASED QUANTUM COMPUTING ARCHITECTURES

Ph.D. THESIS

by

KULKARNI ANANT ARAVIND

DEPARTMENT OF ELECTRONICS & COMMUNICATION ENGINEERING
INDIAN INSTITUTE OF TECHNOLOGY ROORKEE
ROORKEE - 247667, INDIA
AUGUST, 2019

SPINTRONICS BASED QUANTUM COMPUTING ARCHITECTURES

A THESIS

Submitted in partial fulfilment of the requirements for the award of the degree

of

DOCTOR OF PHILOSOPHY

in

ELECTRONICS AND COMMUNICATION ENGINEERING

by

KULKARNI ANANT ARAVIND

DEPARTMENT OF ELECTRONICS & COMMUNICATION ENGINEERING
INDIAN INSTITUTE OF TECHNOLOGY ROORKEE
ROORKEE - 247667, INDIA
AUGUST, 2019

INDIAN INSTITUTE OF TECHNOLOGY ROORKEE
ROORKEE

STUDENT'S DECLARATION

I hereby certify that the work presented in the thesis entitled **"SPINTRONICS BASED QUANTUM COMPUTING ARCHITECTURES"** is my own work carried out during a period from July 2015 to August 2019 under the supervision of Dr. Brajesh Kumar Kaushik.

The matter presented in the thesis has not been submitted for the award of any other degree of this or any other Institute.

Dated: **(KULKARNI ANANT ARAVIND)**

SUPERVISOR'S DECLARATION

This is to certify that the above mentioned work is carried out under my Supervision.

Dated: (**BRAJESH KUMAR KAUSHIK)**
Supervisor

ABSTRACT

A quantum computer performs computations on the principles of quantum mechanics that enables faster speed and higher security than classical computers, and also has the ability to process large amount of information due to its inherent ability of parallel processing. The important building blocks of the quantum computer are qubit, quantum register, quantum logic, quantum network, quantum reversibility, quantum teleportation, quantum data compression, quantum cryptography, universal quantum computing, and quantum algorithm. Quantum computers rely on basic quantum principles of superposition and entanglement. The time evolution of an arbitrary quantum state is computationally more powerful than evolution of a digital logic state. Theoretical quantum computing based on the rotation of the qubits has proved that there is a possibility of quantum devices to address the complex computing problems. However, presently, there is no computer in existence that can completely work on the principles of quantum mechanics. Therefore, the enormous advantages of quantum computing in comparison to its classical counterpart have forced researchers to explore the possibilities of physical realization with the help of emerging technologies. The basic requirements of Divincenzo criteria have to be fulfilled for the successful implementation of the quantum computing. This criteria suggest that the system realizing the quantum computing should have well characterized qubit; proper initial state of all qubits; enough isolation to the qubit(s); precise qubit state manipulation and facilitation of qubits interaction should be in time less than the qubit decoherence time; and the physical system should facilitate the measurement of each qubit to obtain the output of the quantum computation.

Spintronics is one of the most efficient ways to physically realize quantum computing due to strong analogy of electron spin to the qubit. Spin-torque based on-chip qubit architecture paves the way for the research in spintronics based physical realization of quantum computer. However, the qubit decoherence is a critical issue in spin qubit architecture from the complex computing point of view. This issue can be dealt by two ways in this thesis; firstly, by utilizing the materials with spin qubits having very high spin coherence, and secondly, by reducing and optimizing the number of elementary quantum operations with the help of elementary quantum gate

library. This thesis presents both ways in detail with demonstrations of reduction in number of elementary operations by elementary quantum gate library. A computing platform is realized using reduced elementary gates such as CNOT, SWAP, Toffoli, and Fredkin wherein the reduction in number of elementary operations is 36.36%, 36.36%, 35.44%, 35.64%, respectively. The optimization of the reduced number of operations for the quantum circuits representing the Boolean logics AND, OR, XOR, Hall Adder (HA), and Full Adder (FA), is also achieved with a reduction after optimization of 37.97%, 41.58%, 45.45%, 40%, and 40.55%, respectively. A quantum Fourier transform that is an integral part of the Shor's algorithm for the number factorization is also reduced and optimized. The reduction of 35.71% in number of elementary operations for the quantum Fourier transform is also demonstrated. Various other complex computing operations can be realized using the spin torque based qubit architecture. This thesis lays strong foundation for researchers aspiring to work in the area of quantum computing using spintronics platform and also discusses the associated challenges.

ACKNOWLEDGEMENT

First and foremost, I wish to express my sincere regards and gratitude to my supervisor and mentor, Dr. Brajesh Kumar Kaushik for his constant encouragement and precious direction during my Ph.D. work. I thank him from the bottom of my heart for all his support, positive inspiration, and motivation that made this research possible. Besides gaining from his broad knowledge, I have learned a lot from his exceptional professionalism. I have enjoyed the inspiring discussions that we had during the Ph.D. I especially thank him for promptly reading and careful assessment of my thesis. Throughout my life, I will get benefit from the experience and knowledge that I have gained while working with him.

I am grateful to Prof. Sudeb Dasgupta, Head, Electronics & Communication Engineering (ECE) department, Prof. M. V. Kartikeyan, Chairman, Student Research Committee (SRC), Prof. N. P. Pathak, Chairman, Departmental Research Committee (DRC), Dr. A. Patnaik, Ex-Chairman, DRC, Dr. A. Bulusu, Internal Expert, and Prof. K. L. Yadav, External Expert, Department of Physics, for being members of my SRC, and for sparing their precious time even with their busy schedule, for carefully examining the work and providing their valuable suggestions. I am also thankful to all the faculty members of Microelectronics and VLSI (MEV) Group including Dr. S. Manhas, Dr. A. Datta, Dr. B. P. Das, Dr. B. Kumar, Dr. V. S. Poonia, and Dr. S. Roy, for helping me at various stages of my work.

My sincere thanks to Mr. Naveen Kanwar and other non-teaching staff of ECE department for providing the basic lab facilities and support. I would like to sincerely thank my colleagues Sanjay, Vikas, Sonal, Namita, Seema, Bhushan, and Gaurav for their kind support and having many technical discussions. Also, I would like to pay my regards to fellow class mates Prabahat, Amit, Swati, Gyanendra, Neeraj, Inder, Priyamvada, Poorvi, Sandeep, Narendra, Lalit, Chotmal, Sunil, Prashant, Sumant, Hemant, Riteish, Shobhit, Shashank, and Dinesh for helping me in different stages of my work. I have been fortunate to interact with my Ph.D. seniors and would like to pay my genuine thanks to Dr. M. K. Mujumder, Dr. V. R. Kumar, Dr. P. K. Pal, Dr. S. Verma, Dr. R. Gupta, Dr. S. Sharma, Dr. A. Sharma, Dr. Govinda, Dr. A. Acharya, and Dr. N. Bagga. I have learned a lot from them during the initial stages of my work.

I would like to praise and thank my spiritual leader Chinmayanand Swami for giving me strength and patience to accomplish this work. I would like to acknowledge my grandfather Late Mr. Limbraj Kulkarni for his sacrifices made for my education. I would like to thank my parents Mr. Aravind Kulkarni and Mrs. Shobha Kulkarni for their selfless love and affection for my well-being. I could not have been successful in my life without their eternal support and encouragement. I am grateful to my wife Neelima Kulkarni who sacrificed her career to look after the children and made me free to pursue Ph.D. It would be incomplete if I forget my son Ojaswa and daughter Ananya for giving me positive energy through their everyday activities. My niece Shamika, nephews Varad and Atharva always encouraged through their conversation whenever I went home during my Ph.D. work.

Date: (Kulkarni Anant Aravind)

TABLE OF CONTENTS

LIST OF FIGURES

LIST OF TABLES

LIST OF ABBREVIATIONS

CMOS	complementary metal oxide semiconductor
QC	quantum computing
CNOT	controlled NOT
CU	controlled unitary
DFT	discrete Fourier transform
DOS	density of states
M	Magnetization
LLG	Landau–Lifshitz–Gilbert
QFT	quantum Fourier transform
QRs	quantum repeaters
CNT	carbon nanotube
STT	spin transfer torque
MATLAB	matrix laboratory
QD	quantum dot
FSM	fully specified matrix
PMD	physical machine description
SHE	spin Hall effect
TB	tunnel barrier
AEP	average error probability
CCNOT	controlled CNOT
CSWAP	controlled SWAP
AND^R	reversible AND
OR^R	reversible OR
XOR^R	reversible XOR
$NAND^R$	reversible NAND
NOR^R	reversible NOR
$XNOR^R$	reversible XNOR
HA^R	reversible half adder
FA^R	reversible full adder

LIST OF SYMBOLS

R/W	read/write
$\mathbb{C}^2$	complex vector space
ψ	quantum state
U	unitary operator
$\hbar$	Planck's constant
I	identity matrix
$U^\dagger$	adjoint of complex conjugate of U
$\sigma_x, \sigma_y, \sigma_z$	Pauli matrices
a	complex variable
b	complex variable
X	NOT gate
R_ϕ	phase shift gate
H	Hadamard gate
φ	quantum state
P	quantum gate
Q	quantum gate
E	energy consumption per bit
T	temperature
K	Boltzmann's constant
Z	quantum gate performs π rotation around z-axis
S	quantum gate performs π/2 rotation around z-axis
T	quantum gate performs π/4 rotation around z-axis
U_A	unitary gate A
U_B	unitary gate B
U_C	unitary gate C
O_n	n qubit operation
E_f	Fermi energy
γ	gyro-magnetic ratio
α	damping constant
$Heff$	effective field
M	magnetic moment
α_J	moment generated due to the flux of electrons

S	unit vector along the spin polarized magnetic moment
$V(\theta, \phi)$	general rotation of a single qubit
E_g	Energy band gap
$J(t)$	time-dependent exchange constant
S_1	spin operator of qubit 1
S_2	spin operator of qubit 2
$B(z)$	magnetic field
$E(x)$	electric field
$2d$	inter-dot distance
S_3, S_2, S_1, S_0	qubits embedded in spin-coherent semiconductor channel
V(x, y)	barrier potential
R_i, G_i	barrier gates
B_0, B_1, B_2	channel barriers
$Q_1, Q_2, \ldots, Q_n$	Qubits
J	exchange interaction
T_1	relaxation time
T_2	coherence time
Ic_1	charge current
Is_1	spin current
A_{NM}	cross-sectional area of the nanomagnet
A_{HM}	area of heavy metal
θ_{SH}	spin Hall angle
λ_{SF}	spin-flip length
t_{HM}	thickness of heavy metal
Q	electron charge
Sw_1, Sw_2	Switches
Ii_1	charge current
d_{12}	distance between qubits Q_1 and Q_2
ρ_d	density matrix representing the desired final state
P	density matrix
F	fidelity
Op	number of elementary operations
Θ	angle of rotation
$Sz_1, Sz_2, Sz_3, \ldots, Sz_n$	qubit states
R_x	qubit rotation about x-axis
R_y	qubit rotation about y-axis

R_z	qubit rotation about *z*-axis
v	electron velocity
Γ_{inj}	injection side barrier height
T,S	single qubit rotations
$\|n\rangle$	input states of qubits
$\|k\rangle$	output states of qubits
X	CNOT gate
δ, β, γ	phase angles
ρ_o	obtained states spin density matrix
ρ_{in}	input states spin density matrix
E_B, E_B^*	switching energy barrier between P and AP configuration
E_F	Fermi energy level
e	magnitude of charge on an electron
m^*	effective mass of electron
p	momentum operator of electron
$\tilde{S}_i$	standard basis matrix
$\rho_{Q_1}, \rho_{Q_2}, \rho_{Q_3}, ..., \rho_{Q_n}$	spin density matrices of qubits
$\hbar$	reduced Plank's constant
t_s	singlet transmission coefficient
t_t	triplet transmission coefficient
α	interaction factor

Chapter 1

Introduction

1.1 Introduction

The present day computing systems perfectly obeys the laws of classical physics. Quantum computing would provide the computing power required to solve problems that are currently intractable for classical computers—at least in a timeframe that's practical. At atomic levels, the quantum dynamics which is analogous to the classical dynamics, fails to follow the laws of classical physics. The laws of quantum mechanics are followed by the system in terms of motion, energy, and momentum. The obstacles in classical computing at the atomic level pave the way to quantum dynamics based quantum computing (QC) [1].

Qubit is a basic building block of the quantum computation. Qubit represents a two level quantum system which is manipulated and measured in a controlled way. A quantum computer is composed of N qubits, and its wave function resides in a 2^N-dimensional complex Hilbert space. A particular quantum state of a specific isolated system is mathematically represented by its wave function. The quantum computation is performed through the input qubit state preparation, desired unitary transformation acting on the prepared state, and output state measurement. The time evolution of quantum wave function is unitary and governed by Schrodinger's equation provided that its interaction with the environment is negligible. Schrodinger's equation represents the description of matter in terms of wavelike properties of particles in a field. The probability density of a particle represents the solution of the Schrodinger's equation. The measured output states are probabilistic and basic postulates of quantum mechanics set the probabilities of different possible outputs. A quantum algorithm is required to be repeated until the probability of the measured output becomes 1 so as to reach the desired output. Therefore, the quantum algorithms are analogous to probabilistic classical algorithms. The superposition and entanglement properties of quantum dynamics make quantum computers more powerful than their classical counterparts and solve the certain computational problems like integer factorization more efficiently than a classical computer.

The successful implementation of quantum computer needs some basic requirements to be fulfilled. Scalability of the device performing quantum computation is an important aspect to construct quantum computers of practical use. A challenging issue in most of physical setups is that it should be possible to enlarge the device so as to contain many qubits, and meet all the requirements. These are known as the Divincenzo criteria [2] and can be summarized in the following:

The Divincenzo criteria are required to be fulfilled for the successful implementation of quantum computer. The quantum computers need to be scalable for its practical use. The criteria are as follows:

1. **Storage of quantum information (qubit) –** The information is encoded in a scalable system till the computation is performed.
2. **Initial state preparation**-The state of all qubits should be set to zero before computation begins.
3. **Isolation**- The isolation of the system from external environment is needed to reduce the decoherence effects. Decoherence is defined as the loss of information from a quantum system into the environment.
4. **Quantum gate implementation-** For the realization of quantum gate, the individual qubit state isolation, manipulation, and controlled interactions are required. Moreover, the gate operation time should be less than the decoherence time.
5. **Read out**- Scalable physical system should have measured the final state of qubits at the end of the computation to obtain the output.

Conventional electronics employ electron's charge to store, process, and communicate with the help of analog and digital information. However, conventional electronics has not utilized the spin of electron for the information processing. The spin of an electron is observed as tiny magnetic moment attached to the electron (Figure 1.1). Elementary particles, composite particles, and atomic nuclei also carry spin in the form of angular momentum. The quantum mechanical spin of an electron is a pseudo-vector quantity. A pseudo-vector is a quantity that transforms like a vector under a proper rotation, but in three dimensions. It gains an additional sign flip under an improper rotation such as reflection. By placing a single electron in a magnetic field, we can make its spin polarization bi-stable since only polarizations parallel and anti-parallel to the field are stable (or meta-stable). These two

polarizations could represent logic bits 0 and 1 [3, 4, 5]. In solid state devices, the study of electronic charge, electron spin along with its magnetic moment forms spintronics. The basic concept of spintronics is the manipulation of spin-polarized currents in contrast to mainstream electronics in which the spin of the electron is not considered. Also spintronics deals with the interaction of static spins [6]. The spin degree of freedom provides new effects, new capabilities, and new functionalities to the electron [4, 7, 8].

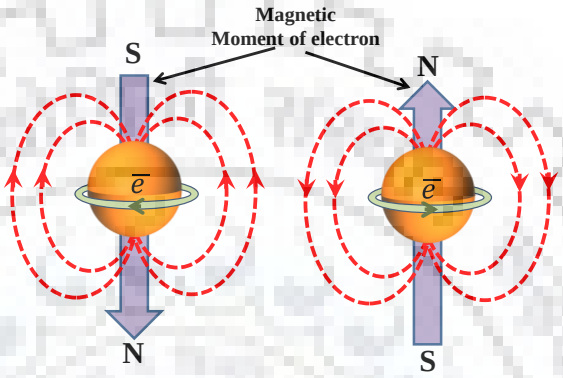

Figure 1.1 Electron spin and associated magnetic moment.

There is gradual shift from semiconductor devices based industry to spin devices based industry due to the non-volatility of spin-electronic devices. The non-volatility helps to retain the data, high speed, and compatible with fabrication processes. These will certainly help to meet sensing, storage, and computing needs of the information technology [9].

1.2 Background and Motivation

Feynman proposed a quantum mechanics based computing framework in 1982 [10]. He observed that a quantum dynamics based computing system does computation tasks faster than classical mechanics based systems. Many physicists laid the QC foundation by proposing mathematical models like Turing machine [11] and quantum logic gates [12]. QC machine is a hypothetical example of Turing machine. Turing machine works on the Church-Turing principle [13].

1.2.1 Turing Machine

A Turing machine is a hypothetical machine first proposed by the mathematician Alan Turing in 1936 [14] (Figure 1.2). Any computing algorithm can

be simulated by a Turing machine, irrespective of the complexity of the algorithm. There are four basic elements of a Turing machine.

1. Program
2. Finite state control
3. Magnetic tape
4. Read-write tape head

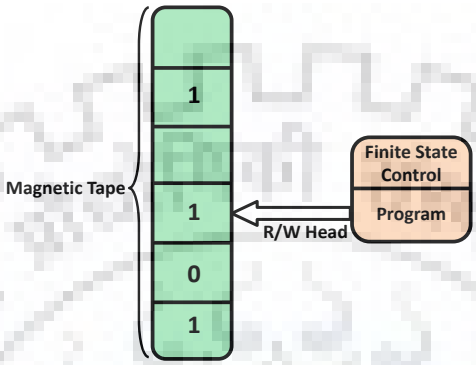

Figure 1.2 Turing machine.

The tape is infinite-long which acts like a memory in a typical computer, or any other form of data storage. The blocks on the tape are usually blank at the start and can be written with symbols. The Turing machine processes symbols '0', '1', and 'blank'. Head of the Turing machine is positioned over one of the squares on the tape. It reads the symbol, edits the symbol by writing or erasing a symbol, and shifts the tape left or right by one square so that the machine can read and edit the symbol on a neighboring square according to the given program.

1.2.2 Principles of Quantum Mechanics

Quantum Mechanics [15] is a framework for the maturity of physical theories. Quantum mechanics is a foundation for the actual physical theories such as quantum electrodynamics. It states four mathematical postulates that a physical theory must pacify. The four postulates of quantum mechanics imply the state of a closed system, evolution of closed system, the interaction of the system with external systems, and state of a composite system in terms of its constituent parts. These postulates provide a general background to explain the behavior of a physical system.

- **First postulate**

Any physical system is a complex inner product space (or Hilbert space) known as the state space of the system. The system is completely described by its state vector, which is a unit vector in its state space. A system whose state space can

be described by the two dimensional complex vector space $\mathbb{C}^2$, can serve as an implementation of a qubit, wherein states of system represent the state of the qubit. Some systems may require an infinite dimensional state space.

- **Second postulate**

The time evolution of a closed quantum system is described by the Schrodinger equation

$$i\hbar \frac{d|\psi\rangle}{dt} = H|\psi\rangle \tag{1.1}$$

where, $\hbar$ is Planck's constant, and H is fixed Hermitian operator known as the Hamiltonian of the system. The transition of quantum system state from a state $|\psi\rangle$ at time t_1 to a new state $|\psi\rangle'$ at time t_2 is through the unitary transformation

$$|\psi\rangle' = U|\psi\rangle \tag{1.2}$$

where, U is a unitary operator $U(t_1, t_2) = \exp\left[\frac{-iH(t_2 - t_1)}{\hbar}\right]$ which preserves the norm. Unitary operator U satisfies $U^\dagger U = UU^\dagger = I$, where $U^\dagger$ is the adjoint of complex conjugate of U, and I is the identity operator. A two-qubit gate is a unitary operator on $\mathbb{C}^4$. Identity operator and Pauli gates are unitary operators (1.3).

$$I = \begin{bmatrix} 1 & 0 \\ 0 & 1 \end{bmatrix}, \sigma_x = \begin{bmatrix} 0 & 1 \\ 1 & 0 \end{bmatrix}, \sigma_y = \begin{bmatrix} 0 & -i \\ i & 0 \end{bmatrix}, \sigma_z = \begin{bmatrix} 1 & 0 \\ 0 & -1 \end{bmatrix} \tag{1.3}$$

- **Third postulate**

For a quantum system having set of M possible outputs, the state measurement is described by a collection of measurement operators. The measurement operators are linear and act on the state space of the system. Let, a quantum system is in state $|\psi\rangle$ before the measurement, the probability *p(m)* of a outcome *m*(P_m *:m*$\in$*M*) is $p(m) = |\psi\rangle P_m^\dagger P_m |\psi\rangle$. The state of the system after measurement is $\frac{P_m|\psi\rangle}{\sqrt{|\psi\rangle P_m^\dagger P_m |\psi\rangle}}$.

The measurement operators satisfy the completeness equation, *i.e.* sum of the probabilities of all outcomes is 1.

- **Fourth postulate**

The state space of a composite physical system is the tensor product of the state space of the individual components of physical systems. If one component is in state $|\psi_1\rangle$, and a second component is in state $|\psi_2\rangle$, then the state of the combined system is $|\psi_1\rangle \otimes |\psi_2\rangle$. A state of a combined system is separable if it can be expressed as the tensor product of states of the components, otherwise the state is entangled.

1.3 Basic Concepts of Quantum Computing

1.3.1 Qubits

Qubit is analogous to bit in Boolean computing. It represents the fundamental unit of QC and quantum information. In a two dimensional vector space, a qubit is represented by a vector. Photon polarization state, two energy levels of electron around the atom, spin of an electron, etc., are examples of the qubit. In quantum mechanics, Bloch sphere (Figure 1.3) is a geometrical representation of the pure state space of a two-level quantum mechanical system (qubit).

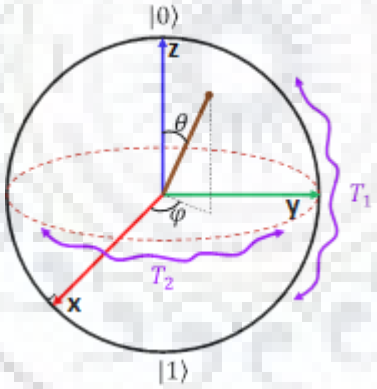

Figure 1.3 Bloch sphere representing qubit state.

The pure states represented by the points on the surface of the Bloch sphere, however, mixed states are represented by the interior points of the sphere. Moreover, *n*-qubit quantum system can be represented on Bloch sphere. The spin eigenstates [1 0]^T ($|0\rangle$), and [0 1]^T ($|1\rangle$) of an electron form the basis unit vectors in the two dimensional spin ½ linear vector space. Qubits exist in a superposition or a linear combination of states. If a measurement is done on a qubit with a spin state $a|0\rangle + b|1\rangle$ (superposition state), the qubit is found in only one of the states of $|0\rangle$ and $|1\rangle$, with probabilities a^2 and b^2, respectively, where, *a* and *b* are complex variables. In case of classical computing, superposition or linear combination of states does not exist. A

QC device remains in all possible states simultaneously. Therefore, measurement of a particular state is probabilistic. The qubit state upon measurement leads to quantum collapse.

1.3.2 One-Qubit Gates

The 2x2 unitary matrices are one-qubit gates, which transform the single qubits. All Pauli gates, identity gate, NOT gate, phase shift gate, combination of NOT and phase shift gate, and Hadamard gate are single qubit gates. The single qubit gates are summarized in Table 1.1.

Table 1.1: One-qubit gates

Sr. No.	Gate	Matrix representation
01	Pauli gates	$\sigma_x = \begin{bmatrix} 0 & 1 \\ 1 & 0 \end{bmatrix}$, $\sigma_y = \begin{bmatrix} 0 & -i \\ i & 0 \end{bmatrix}$, $\sigma_z = \begin{bmatrix} 1 & 0 \\ 0 & -1 \end{bmatrix}$
02	Identity gate	$I = \begin{bmatrix} 1 & 0 \\ 0 & 1 \end{bmatrix}$
03	NOT gate	$X = \begin{bmatrix} 0 & 1 \\ 1 & 0 \end{bmatrix}$
04	Phase shift gate	$R_\phi = \begin{bmatrix} 1 & 0 \\ 0 & e^{i\varphi} \end{bmatrix}$
05	Hadamard gate	$H = \frac{1}{\sqrt{2}} \begin{bmatrix} 1 & 1 \\ 1 & -1 \end{bmatrix}$

1.3.3 Two-Qubit Gates

A composite quantum system consists of quantum systems A and B with basis sets *n*-dimensional $\{|\psi\rangle\}$, and *m*-dimensional $\{|\varphi\rangle\}$, respectively. The tensor product of $\{|\psi\rangle\}$, and $\{|\varphi\rangle\}$ representing the composite quantum system is $\{|\psi\varphi\rangle = |\psi\rangle \otimes |\varphi\rangle\}$. The resulting basis state has *m***n* dimensions. The state space of quantum computation grows exponentially with the increase in physical size of composite systems. The two-qubit gates perform the controlled operations in the form '*If A is true then do B*'. The two-qubit gates are CNOT (Controlled NOT), and CU (Controlled Unitary).

1.3.3.1 CNOT Gate

The CNOT gate flips the qubit $|b\rangle$ if qubit $|a\rangle$ is $|1\rangle$, otherwise keeps $|b\rangle$ unchanged as shown in Table 1.2.

Table 1.2: CNOT gate

Quantum Circuit	**Matrix Representation**
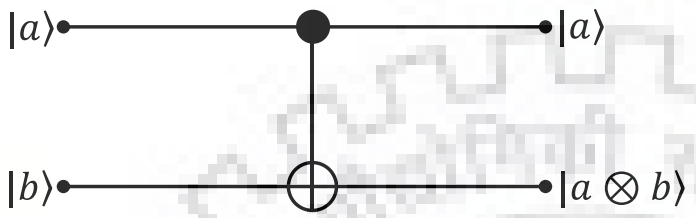	$\begin{bmatrix} 1 & 0 & 0 & 0 \\ 0 & 1 & 0 & 0 \\ 0 & 0 & 0 & 1 \\ 0 & 0 & 1 & 0 \end{bmatrix}$

1.3.3.2 CU Gate

The operator U performs the unitary operation on qubit $|b\rangle$ if qubit $|a\rangle$ is $|1\rangle$ and does not change the state of qubit $|b\rangle$ if qubit $|a\rangle$ is $|0\rangle$. The CU gate and its matrix representation are shown in Table 1.3.

Table 1.3: CU gate

Quantum Circuit	**Matrix Representation**
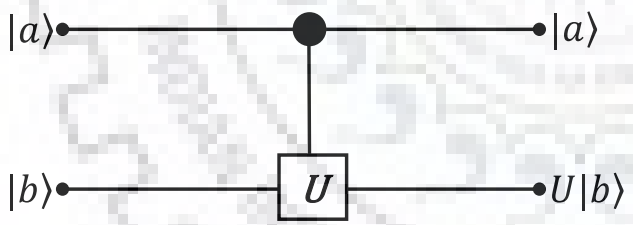	$X = \begin{bmatrix} a & b \\ -e^{i\varphi}b^* & e^{i\varphi}a^* \end{bmatrix}$, $a^2 + b^2 = 1$

1.3.4 Three-Qubit Gates

The Toffoli gate is a 3-qubit gate (Table 1.4). Toffoli gate is universal gate for reversible computation. Reversible gates provide the input information at the output (NOT gate in case of Boolean computing). Any 2^n x 2^n permutation matrix can be implemented using Toffoli gates. A permutation matrix is a square unitary matrix where all entries are 0 or 1. Permutation matrix specifies a reversible Boolean function.

Table 1.4: Toffoli gate

Quantum Circuit	**Matrix Representation**
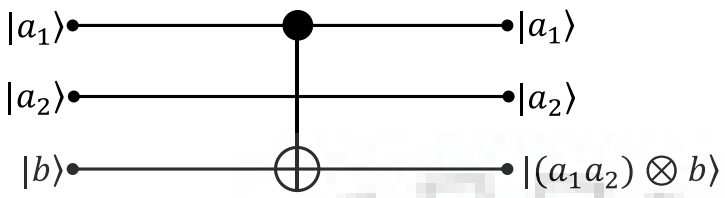	$\begin{bmatrix} 1 & 0 & 0 & 0 & 0 & 0 & 0 & 0 \\ 0 & 1 & 0 & 0 & 0 & 0 & 0 & 0 \\ 0 & 0 & 1 & 0 & 0 & 0 & 0 & 0 \\ 0 & 0 & 0 & 1 & 0 & 0 & 0 & 0 \\ 0 & 0 & 0 & 0 & 1 & 0 & 0 & 0 \\ 0 & 0 & 0 & 0 & 0 & 1 & 0 & 0 \\ 0 & 0 & 0 & 0 & 0 & 0 & 0 & 1 \\ 0 & 0 & 0 & 0 & 0 & 0 & 1 & 0 \end{bmatrix}$

The Toffoli gate can be implemented using 2-qubit quantum gates as shown in Figure 1.4.

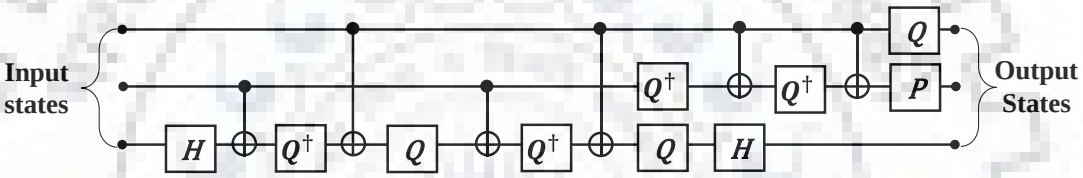

Figure 1.4 Toffoli gate implementation with 2-qubit quantum gates.

where, $P = \begin{bmatrix} 1 & 0 \\ 0 & i \end{bmatrix}$ and $Q = \begin{bmatrix} 1 & 0 \\ 0 & e^{i\frac{\pi}{4}} \end{bmatrix}$.

In a universal set of gates, any unitary operation on *n* qubits can be implemented by a sequence of 2-qubit operations. A unitary operation can be approximated to any required degree of accuracy using only CNOTs, *H*, *P*, and *Q* gates.

1.3.5 Reversibility/Irreversibility of Classical and Quantum Gates

The classical gates such as AND, OR, NAND, NOR, etc. are irreversible except the NOT gate. The output state of NOT gate provides the input state information and there is no loss of information during the operation. But in case of other classical gates, the input(s) state(s) information cannot be recovered from the output state. In an AND gate operation, the information is lost during the transformation of two inputs into a single output and it is same for other classical gates. According to the Landuaer's principle [16], the amount of energy consumption per bit loss of information to the external environment is

$$E = KT \ln 2 \tag{1.4}$$

where, K is Boltzmann's constant and T is the temperature of the external environment.

In a complex classical circuit, the amount of information lost due the large number of gate operations which results in high energy consumption. It is an important issue when the circuits are implemented with the switching device dimensions reaching the atomic level. The unitary operators are used for quantum computation to transform the qubits in a reversible way. The single qubit quantum gates, two-qubit quantum gates, and Toffoli gate are reversible gates. During the measurement, quantum state collapses into the classical state. Hence, upon measurement the quantum state cannot be recovered. Therefore, the measurement process/operation is irreversible.

1.3.6 Quantum Circuits and Algorithms

A quantum circuit is a sequence of unitary operations and measurements on n-qubit states. The input state of each qubit is prepared in some known state before the computation begins. The input states of quantum circuit shown in Figure 1.5, undergo unitary transformations U_A, U_B, U_C, and U_D. The dimensions of each unitary matrix in the quantum circuit is 2^nx2^n, where n is the number of qubits in the quantum circuits. Also, the gates Z, and H operate on single qubits only.

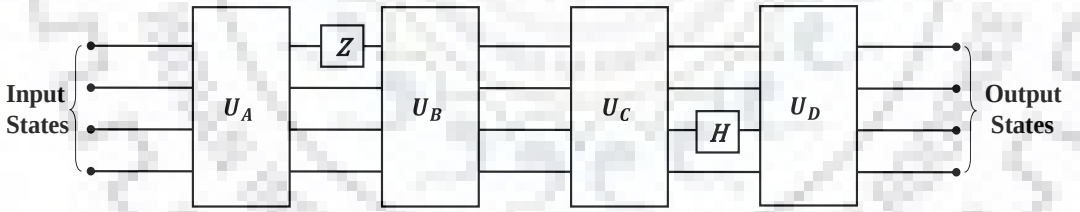

Figure 1.5 Quantum circuit.

Quantum circuit model is generally utilized to run the quantum algorithms. The number of steps constitutes a quantum algorithm. Each step of quantum algorithm is executed sequentially on quantum computer. A quantum algorithm specifies for each n, a sequence $O_n = O_1 \ldots\ldots\ldots O_k$ of n qubit operations. The map $n \rightarrow O_n$ must be computable *i.e.* the individual circuits must be generated from a shared pattern.

Quantum algorithms use some essential features such as quantum superposition or entanglement. The Shor's algorithm and Grover's algorithm are used for number factoring and searching unstructured database, respectively.

1.3.6.1 Shor's Algorithm

Quantum computers perform some tasks efficiently than classical computers. Finding factors of a number by classical computation takes a longer time due to the exponential number of operations required to perform the factorization. Quantum computation performs the same task in n^2 operations if the number of qubits used for the operation is *n*. Shor proposed a polynomial quantum algorithm for factoring a number *M* in 1994 [17].

- **Algorithm**

1. $f(n) = a^n \pmod{M}$, choose the values of *a* and *n*.
2. Find the period *'r'* of sequence $f(n)$ by using quantum discrete Fourier transform (DFT).
3. Find the '*greatest common divisor*' of $(a^{\frac{r}{2}} - 1), (a^{\frac{r}{2}} + 1)$ and *M* by using Euclid's algorithm.
4. A nontrivial common divisor (*h*), is factor of *M*.
5. If $\frac{M}{h}$ is non-prime integer, go to step1.
6. Else go to step 7.
7. End

1.3.6.2 Grover's Search Algorithm

A search algorithm is used to obtain the shortest path from one place to another. The classical search algorithms perform $O(N)$ operations to obtain the shortest path from *N* paths. Grover proposed the search algorithm to obtain the shortest path with $O(\sqrt{N})$ operations [18].

- **Algorithm**

1. Apply the Hadamard transformation on $|0\rangle$ to prepare the initial state $|\psi_0\rangle$.
2. Apply the oracle operation $|\psi_1\rangle \leftarrow (-1)^{f(\psi_0)}|\psi_0\rangle$.

3. Apply the '*inversion about mean*' operation $\left|\hat{G}\right\rangle \leftarrow 2\left|\psi_0\right\rangle\left\langle\psi_0\right| - I$ to make the high probability amplitude of solution state.
4. Repeat the steps 2 and 3.
5. Measure the final state.

1.4 Spintronics Fundamentals

The imbalance of the spin populations at the Fermi level creates spin transport in the materials such as ferromagnetic metals. The shift in energy states produces unequal filling of energy bands (Figure 1.6). Due to this inequality, there is transport of net spin polarization. However, the magnitude and polarity of spin polarization is based on the specific measurement. In a ferromagnetic metal-semiconductor material, the ferromagnetic metal acts as a source for spin polarized electrons injected into the semiconductor through the tunnel barrier [19].

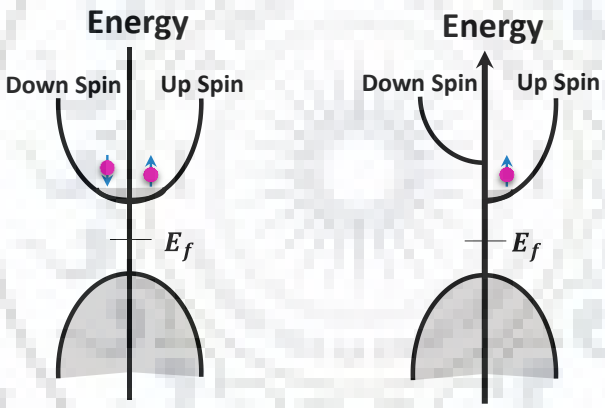

Figure 1.6 Band structure (Energy vs DOS) of nonmagnetic material (left) and ferromagnetic material (right)

1.4.1 Spin Accumulation and Injection

Spin accumulation is defined as creation of non-equilibrium electron spins in metals and semiconductors. The spin accumulation is achieved through spin injection, optical spin orientation, and spin resonance. The spin accumulation through spin injection is possible through injection of spin polarized electrons from one material into another with the help of electric current. The source material could be a ferromagnetic metal (Fe). When spins are injected from ferromagnet into a metal such as Al, the spins injected are of non-equilibrium form *i.e.* Spin accumulation. The type of spin accumulation is possible through electrical spin injection between two

nonmagnetic materials (Al and Cu). In case of optics based spin injection, the material is exposed to circularly polarized light. Electron spins in the material gains the angular momentum from the light photons. This procedure is called optical orientation. One more technique used for the spin accumulation is spin resonance. For this, magnetic field is applied to split the spin up and spin down electron states. The process is called Zeeman splitting. The spin resonance is mostly used in metals and semiconductors.

Electrical spin injection is of most interest in spintronic devices. The injected spin polarization travelling under the influence of electric field is the spin drift transport (Figure 1.7). The non-equilibrium spin can travel diffusively due to concentration gradient called as spin diffusion [19]. There is power dissipation in spintronic devices [20] due to spin-polarized current [21].

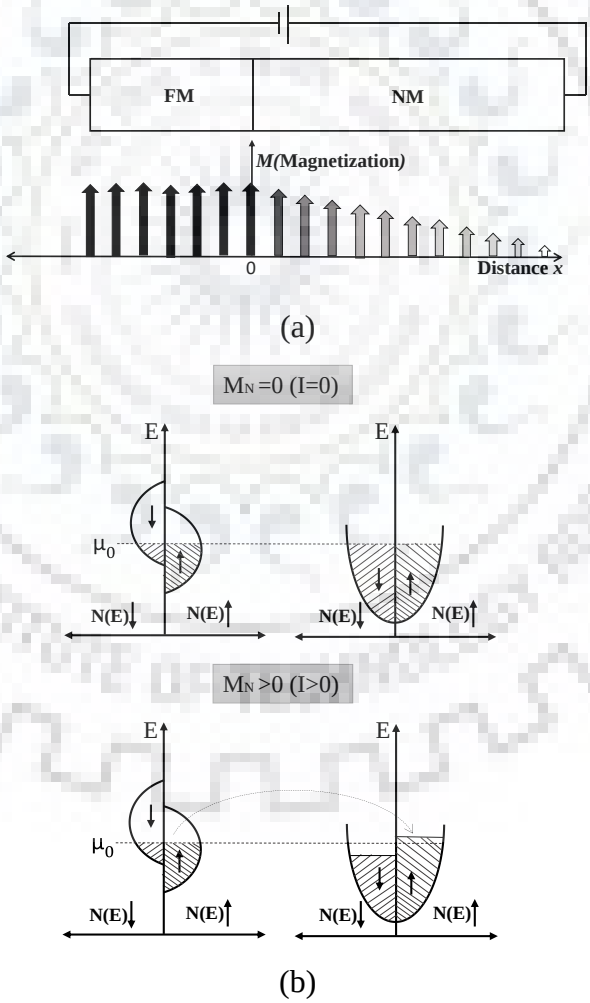

Figure 1.7 (a) Electrical spin injection (b) Energy band diagrams.

1.4.2 Spin Detection

Spin current can be detected by the phenomenon called as moment exchange between the flux of electrons and magnetization orientation of the ferromagnetic layer also called as spin transfer torque or STT effect [8], [22], [23]. The dynamic behavior (Figure 1.8) of M (Magnetization) in a ferromagnetic film can be described by the Landau–Lifshitz–Gilbert (LLG) equation

$$\frac{1}{\gamma}\frac{dM}{dt} = (\vec{M} \times H_{eff}) - \alpha \frac{\vec{M}}{M} \times (\vec{M} \times H_{eff}) \tag{1.5}$$

where γ is the gyro-magnetic ratio, $\gamma = {}^{2\mu_s}/_{\hbar}$, α is the damping constant and H_{eff} is the effective field.

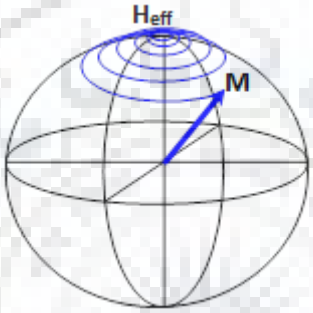

Figure 1.8 Precession of magnetic moment *M* around a magnetic field H_{eff}.

Under the influence of flux of electrons, a net moment will be generated which will produce an additional spin torque to modify the equation as above

$$\frac{1}{\gamma}\frac{dM}{dt} = (\vec{M} \times H_{eff}) - \alpha \frac{\vec{M}}{M} \times (\vec{M} \times H_{eff}) - \alpha_J \frac{\vec{M}}{M} \times (\vec{M} \times s) \tag{1.6}$$

Where α_J is the moment generated due to the flux of electrons and *s* is the unit vector along the spin polarized magnetic moment [22]. If the third term in the above equation is large above a critical value, then the magnetization of the target layer or magnetization of the magnet will switch.

1.4.3 Spin Relaxation

Spin relaxation refers to the process by which a non-equilibrium population of electron spins is brought to its equilibrium value in a material. If an electron suddenly changes its spin orientation, then it is referred to as spin flip. However, if spin population changes gradually with time, then it is referred to as spin relaxation [8].

Spin relaxation is of supreme importance in spintronics, since everyone is concerned with using the spin polarization of either a single charge carrier or the net spin polarization of an ensemble of charge carriers to encode and decode information. Relaxation of nuclear spins requires a microscopic mechanism for a nucleus to change orientation with respect to the applied magnetic field and/or interchange energy with the surroundings [24].

1.4.4 Spin Interaction

When an electron trapped in a cavity is placed in the magnetic field, the spin polarization of the electron is switched between the two states 0 and 1 by making the magnetic field parallel and antiparallel to electron polarization. Electrons trapped in cavities formed in tiny semiconductor structure are called quantum dots. Parallel and antiparallel polarizations of each quantum dot representing the bits 1 and 0 are stable states. Spin of each quantum dot interacts only with the spin of its nearest quantum dot. The interaction is quantum mechanical and called as exchange interaction. Spins of certain chosen quantum dots (inputs) are polarized using local magnetic fields (Figure 1.9).

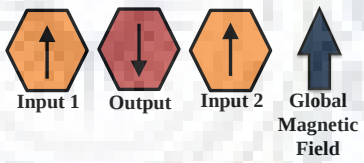

Figure 1.9 Spin interaction.

The input states take the interacting system from ground state to an excited state. The system is then allowed to get relaxed to the ground state by releasing the energy. The spin orientation of a certain quantum dot (output) represent the result of a specific computation due to the exchange interaction of inputs. The exchange interaction represents the only hardware based system [4].

1.5 Evolution of Spintronics Based Computing

The evolution of the spintronic based QC is elaborated in the subsequent subsections.

1.5.1 Evolution of Spintronics Based QC

The classical computing follows the laws of physics till the size of transistors reaches the size of atom. Quantum computing would provide the computing power required solving problems that are currently intractable for classical computers—at least in a timeframe that's practical. Therefore, it is necessary to accomplish the computing at atomic size that follows non-classical physics called quantum mechanics. A quantum computer does the computations based on the quantum mechanics. Moreover, quantum computers guarantee faster speed and higher security than classical computers and have the ability to store large amount of information. Quantum computers rely on quantum principles i.e. superposition and entanglement. The time evolution of a random quantum state is more capable computationally than evolution of a digital logic state. However, presently, there is no computer in existence that can completely operate on the quantum mechanics.

Quantum computers contradict from the classical computers in a way in which information is stored [26]. In former, information is stored in the form of qubits. The polynomial time problems for which no solution exists on any classical machine, can be solved by quantum computer [27]. The realization of Boolean logic gates can be analogous to the computation by a specific pair of two-qubit quantum gates through their interactions [28].

There are various ways to explore the physical realization of the quantum computation. Spintronics is one of the most adequate ways to physically realize QC due to the electron spin comparable to the qubit. Spintronics is a branch of physics which deals with the manipulation, storage, and transfer of information with the aid of electron's spin in extension to or in place of the electron charge [29]. Moreover, intensive research is going on to create new ways of spintronics based QC by utilizing electron spin as qubit [30]. The exploration of nuclear quantum computer, quantum dot architectures, and spin-torque based on-chip qubit architecture etc. pave way for the research in spintronics based physical realization of quantum computer.

1.6 Problem Definition

The focus of the thesis is towards second order transmission coefficient matrix based modeling of spin-torque based *n*-qubit architecture and optimal decomposition of the quantum circuits with the help of the reduction and optimization techniques.

The thesis work is divided into five phases:

i. Second order transmission coefficient matrix modeling of the spin-torque based *n*-qubit architecture.

ii. Reduction in number of operations for the elementary gates such as CNOT, SWAP, Toffoli, and Fredkin gates and their implementation.

iii. Optimization of the quantum circuits for the reversible Boolean logic and their implementation.

iv. Implementation and analysis of the reversible D-Latch.

v. Implementation and analysis of the spin-torque based quantum Fourier transform (QFT).

1.7 Outline of the Work

The thesis work is based on the modeling of the spin-torque-based qubit architecture, wherein, a modified matrix is proposed to analyze the effect of ratio of reflection barrier height to exchange interaction, on electron–qubit interaction, deviation of axis of rotation for single-qubit rotation, and average error probability for two qubit rotation in a spin-torque-based *n*-qubit reconfigurable architecture. Moreover, reduction and optimization techniques are developed to reduce the number of operations required to perform the QC in terms of fidelity and number of electrons required to realize any quantum operation/gate.

Seven chapters are included in the thesis. Each chapter contains motivation behind the problem under study. Moreover, implementation, results, and analysis are also thoroughly presented in a coherent manner. A brief discussion of each chapter is presented as below:

Chapter 1 provides the introduction to QC and spintronics. Moreover, it explains the evolution of the spintronics based QC and neuromorphic computing. In addition, the chapter presents summary of the thesis.

In **Chapter 2**, the extensive literature related to optical and spintronics based quantum devices such as quantum electrodynamic cavity based qubits, quantum dot based qubits etc., is discussed. Moreover, spintronics based neuromorphic computing is also explained in brief.

In **Chapter 3,** a modified (second order) transmission coefficient matrix is proposed to analyze the effect of ratio of reflection barrier height to exchange interaction on electron–qubit interaction, deviation of axis of rotation for single-qubit rotation, and average error probability for two qubit rotation in a spin-torque-based *n*-qubit reconfigurable architecture.

In **Chapter 4**, the conventional and reduced quantum gates are compared for existing and modified matrices. The quantum gates performance is analyzed in terms of number of electrons required per gate for the electron–qubit interaction, gate fidelity, number of elementary quantum operations per gate, and gate execution time.

Optimal quantum circuit decompositions of Boolean logic are presented in **Chapter 5** with the help of developed elementary quantum library $\{ R_y^\theta, R_z^\theta, \sqrt{SWAP} \}$ for the spin-torque-based QC architecture. The reversible Boolean logic performance is analyzed and compared for the conventional, reduced, and optimal decompositions on the first- and second-order transmission coefficient matrix based spin-torque QC architecture.

An implementation and analysis of the reversible D-Latch is presented in **Chapter 6**. An optimized quantum circuit for the reversible D-Latch is presented to obtain the fidelity and number of electronics required to implement the latch over the five clock cycles.

Chapter 7 is devoted towards the optimal decomposition and implementation of the Quantum Fourier Transform (QFT). The spin-torque based architecture has been modeled with the help of optimized decomposition of quantum circuits for the QFT. Moreover, an optimal-depth Clifford+T gates set based quantum circuit is utilized to implement the QFT. The performance analysis in terms of fidelity, magnitude, and phase difference of respective density matrices for different forms of three-qubit QFT, is presented.

The conclusions drawn based on the obtained results, and future scope are presented in **Chapter 8**.

A list of references and list of publications based on work carried out, is presented at the end of the thesis.

Chapter 2

Quantum Computing Architectures: A Literature Review

2.1 Introduction to Quantum Computing

The QC works on Schrodinger equation that provides the quantum description of matter in terms of waves. Its solution is related to the probability density of an element in time and space. The measured output states are probabilistic and basic postulates of quantum mechanics set the probabilities of the possible outputs. The superposition and entanglement properties of quantum dynamics make quantum computers more powerful than their classical counterparts and solve certain computational problems like integer factorization much more efficiently than a classical computer.

The possibilities of computation with the help of quantum physics are elaborated in [31]. The two-state quantum system is represented by a unit vector in Hilbert space C^2, where C are complex numbers. The two states $|0\rangle$ and $|1\rangle$ are represented by unit vectors (1, 0) and (0, 1), respectively. These two states form orthogonal basis to the Hilbert space. There is a need of many such two-state qubits (particles) to build a quantum computer. The Hilbert space for *n* qubits is the tensor product of *n* spaces $C^2*C^2*C^2$. The 2*n* vectors form the computational basis. A physical entity representing the two state quantum system ($|0\rangle/|1\rangle$) is called qubit [32]. $|0\rangle$ is called "ground state" and $|1\rangle$ is called "excited state." A Hilbert space of 2^n forms a quantum system, wherein 2^n mutually orthogonal quantum states represent 2^n different things. The 2*n* mutually orthogonal states of n qubits are written as $\{|i\rangle\}$, where *i* is *n* bit binary number.

2.1.1 Quantum Register

Quantum register state is a vector in a multi-dimensional Hilbert space, in a system that comprises of a number of qubits. Within a quantum register, calculations are performed by manipulating qubits. Quantum and classical computers have a conceptual difference. Classical computers have an array of n flip-flops called as classical register while in case of quantum computing, collection of n qubits is termed as quantum register. In quantum registers, information is stored in binary form [33].

2.1.2 Quantum Logic

The individual qubit rotation and its interaction with other qubits in a quantum system are needed for the evolution of its state from one to other. This is done with the help of simple quantum logic operations called quantum gates. The fundamental single-qubit quantum gates are *I*, *X*, *Z*, *Y* and *H*. However, there are only two single-bit gates in classical computing i.e. Identity and NOT gates. For a two-qubit controlled gate, evolution/rotation of quantum state of second qubit is possible if quantum state of first qubit is $|1\rangle$. Two-qubit quantum gates are CNOT, controlled SWAP (CSWAP), controlled CNOT (CCNOT), etc. Moreover, classical gates such as AND, OR, NAND, NOR, XOR etc. can be realized with the help of single- and two-qubit quantum gates. Fundamental arithmetic operations such as addition and multiplication performed by many quantum gates architectures are given in [34].

The quantum computer and factorization are reviewed in [35]. Moreover, the quantum computing concepts are elaborated in [1] and [36]. The universal quantum gate helps to generate the quantum operation of any other quantum gate. The most easy representation of the universal quantum gate is by a pair of a gate $V(\theta, \phi)$ and CNOT or controlled XOR. $V(\theta, \phi)$ represents a general rotation of a single qubit.

$$\mathbf{V}(\theta,\phi) = \begin{pmatrix} \cos\left(\frac{\theta}{2}\right) & -ie^{-i\phi}\sin\left(\frac{\theta}{2}\right) \\ -ie^{-i\phi}\sin\left(\frac{\theta}{2}\right) & \cos\left(\frac{\theta}{2}\right) \end{pmatrix} \tag{2.1}$$

The universal quantum gates are given in [37-40]. A quantum gate is a powerful and a significant concept as two-qubit gates are appreciable for quantum computation.

2.1.3 Quantum Network

Quantum networks form a significant element of quantum computing. Basically, they allow the communication of quantum information between quantum processors. Quantum network consists of quantum logic gates wherein each gate executes unitary operations on one or more than one quantum system called qubits. Unitary operations are reversible. Because of this, Quantum networks affecting underlying arithmetic operations cannot be directly drawn from their classical Boolean counterparts. For the basic arithmetic operations, quantum networks can be built up in various ways. Quantum gates employing two or more number of qubits can act as a building block of networks [33].

2.1.4 Quantum Reversibility

Quantum gates are reversible. Reversible gates have the same number of inputs and outputs. They are useful as they are the promising ways to enhance the energy efficiency of computers beyond the classical Von-Neumann Landauer limit of KT ln 2 energy dissipated per irreversible bit operation, where, K is the Boltzmann constant and T is the temperature [34].

2.1.5 No-cloning Theorem

The unique property of quantum computation is no-cloning. It is not possible to clone a quantum state if it is not known i.e. it is not possible to create the replica of unknown quantum state unless it is already known. For example, one cannot clone an entangled quantum state [41]. No-cloning theorem is an essential element in quantum cryptography as it blocks observers from creating the copies of transmitted quantum cryptography key. However, no cloning theorem is a final limitation for error correction.

2.1.6 Dense Coding

Basically, in dense coding, quantum entanglement is utilized to increase the rate at which information is sent via noiseless quantum channel. Qubits are utilized to store and transmit the information. Sending a single qubit between two parties will ensure secure communication and reduced communication complexity in computations. Moreover, dense coding establishes the relationship between classical information, qubits, and information in the quantum entanglement [33].

2.1.7 Quantum Teleportation

A known state can be used to communicate a single qubit just by sending the classical information. However, if the state is not known, any measurement may change the state and the state cannot be cloned. Therefore, the only way to communicate the information is by sending the physical qubit such as electron or by swapping the state into another quantum system and send it. The quantum information can be transferred from one location to another by the means of quantum teleportation. The information is sent with the aid of classical communication and already shared quantum entanglement. However, quantum teleportation has only achieved between molecules [42].

2.1.8 Quantum Data Compression

The information extraction from a classical system and quantum system is different. In the case of classical system, the information extracted and information required to describe the system is precisely same. However, in case of quantum system, infinite information would be required to describe a single qubit, and upon measurement, only one bit of information can be obtained from that qubit. This shows that the data is compressed in case of quantum system. Therefore, quantum mechanics based systems are the one where ensemble of identically prepared quantum systems provide much more information [43].

2.1.9 Quantum Cryptography

The cryptographic tasks are possible with the help of properties of quantum systems. The main aspect of the quantum cryptography is quantum key distribution. A random secret key is established for cryptography through the method of quantum key distribution. The impressive feature of quantum cryptography is that it permits the possibility of device independent cryptography in a way that the protocols can be executed on untrusted devices [44].

2.1.10 Quantum Algorithm

A quantum algorithm is an array of unitary steps/operations to manipulate initially prepared quantum state to achieve desired quantum state upon measurement at the final state. Quantum algorithms solve some problems quicker than classical algorithms. The algorithms for factoring and unorganized data searching are Shor's algorithm and Grover's algorithm [45]. Shor's algorithm runs exponentially faster and Grover's algorithm runs quadratically faster than their classical equivalents.

2.2 Physical Realization of Quantum Computation

The most important aspect of the quantum computing is its physical realization. Some basic requirements should be fulfilled for the successful realization of the quantum computing. These requirements are known as Divincenzo criteria [46]. For the construction of a practical quantum system, scalability is an important issue. In most of the physical setups, the incorporation of as many qubits as possible along with meeting Divincenzo criteria is a major challenge. Therefore, in this section, myriad ways to physically realize a quantum computing system are presented.

One of the ways for the realization of quantum logic is to consider the individual photon as flying qubit. [47]. The single-photon level between two-distinct levels in an optical resonator is utilized through the demonstration of conditional dynamics. The other way is through the neutral atoms trapped in one- and two-dimensional arrays of dipole traps with a laser beam (see Figure 2.1) focused with microfabricated arrays of microlens [48]. A lateral separation of 125 μm is provided to selectively address the trap sites.

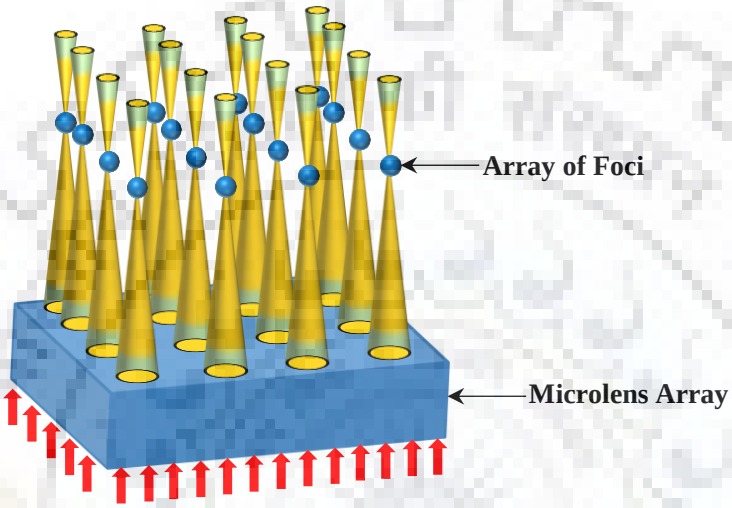

Figure 2.1 One- and two-dimensional arrays of dipole traps with a laser beam.

The implementation of many quantum gate operations would be possible by creating two interleave sets of trap arrays with reconfigurable separation. A general technique is proposed to generate and manipulate the strong interactions between spin states of nearby atoms in an optical lattice [49]. The optical potentials are varied to modulate the spin exchange interaction. This technique helps for the applications such as scalable quantum computation and complex topological order that supports external particle excitations.

The interaction between atoms and the quantized electromagnetic modes inside a cavity is studied under the cavity quantum electrodynamics [50]. In Figure 2.2, a laser is utilized to energize the cavity. The changes in the cavity are observed through cavity transmission due to coupling to atoms. Moreover, the spontaneous emission of atoms is also observed. The spontaneous emission lifetime of atoms is in nanoseconds which makes it difficult to measure the state of the atom when passed through the cavity. A superconducting waveguide and superconducting qubit are utilized as cavity and atom, respectively. Moreover, a number of superconducting quantum circuits can

play the role of atom. A simple architecture composed of two lossy cavities which are coupled permits switching between Markovian and non-Markovian regimes for the dynamics of a qubit inserted in one of the cavities [51]. If the cavity without qubit is perfect, qubit coherence is preserved. Moreover, if there is a small photon leakage in the cavity without qubit, qubit coherence can be precisely maintained.

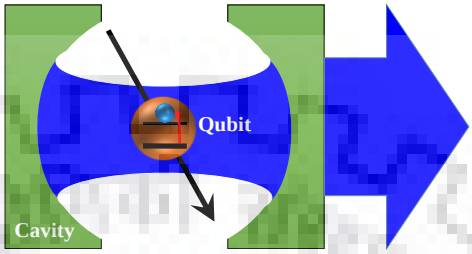

Figure 2.2 Cavity quantum electrodynamics system.

A pair of flying and stationary qubits is utilized for the robust and scalable quantum computation [52]. This proposal helps to get rid of difficulty in storing the photons in linear optics setup. As there is no direct qubit-qubit interaction, it reduces decoherence and helps to realize a distant quantum gate with fewer control errors. Therefore, the architecture designed with the help of this proposal is distributed in nature and can find applications in integrated quantum computation and quantum communication. In connection with distributed quantum computing, the stable ground states of source atoms are used for encoding the qubits. Two photons are created simultaneously to realize two-qubit gate [53]. These photons are passed through a linear optics network to perform the measurement on them to avoid the explicit interaction between the qubits. The obstacles in the realization of quantum gates is imperfections in coupling strengths. From the distributed quantum computing point of view, quantum networks play a vital role. One such quantum network is proposed [54] based on a single atom trapped in the optical cavity. The atom and cavity together form a node to manipulate the quantum information. The interaction between two nodes is made possible by coherent exchange of a photon. Due to the node approach, quantum network provides a way towards scalable architecture. To provide a robust SWAP and entangling quantum gates, optical fibres are utilized between two distant cavity atoms in cavities and these gates are very promising for high level of coherent control [55]. One more obstacle in realization of the robust multi-qubit quantum computer is effect of temperature. A superconducting charge qubits are located in a microwave cavity [56]. It is observed that the quantum operations are

unaffected by thermal effects and random operation errors. This contribution helps in realization of high fidelity quantum computing.

The alkaline earth atoms can also be utilized for the quantum information processing. Two independent lattices, one used for encoding the qubit on nuclear spin and other for moving qubits for quantum gate operations [57]. The examples are realization of spin models in optical lattices and reservoir gas interaction with atoms in optical lattice. There is a need of strong long distance interaction for the fruitful realization of quantum gates. Rydberg atoms have unique properties of dipole-dipole interactions and radiative lifetimes [58]. These two properties depend on principle quantum number (>>1) of Rydberg atom. It has been proved in the past that the Rydberg atoms have the ability to facilitate long distance qubit interaction. This helps to realize quantum information processing.

The vibrational modes of molecules with shaped lasers can also be used for quantum operations [59]. The 2^n vibrational computing states are encoded as qubits on the ground electronic surface of the molecule. The amplitudes are cycled between these states along with a gateway state (shaped laser pulse) for the quantum operations from basic gates to prime factorization. A realistic Hamiltonian and dipole surface are used for the molecular quantum computation. A multilayer microwave integrated quantum circuit is proposed [60]. It sets the way towards the realization of progressively complex superconducting devices to achieve the target of a scalable quantum computer. It approves for high density connectivity to external measurement and control circuitry.

To design a scalable quantum computer which is based on long wavelength radiation quantum gates, blueprint for a trapped ion based scalable quantum computer module is presented in [61]. A fully scalable design is presented that uses ion transport between different modules that are connected together to form a large scale device. The model is also appropriate for alternative trapped ion quantum computer architectures like schemes using photonic interconnects. The proficient quantum communication over long distances remains eminent challenge because of operation errors and fibre attenuation [62]. Quantum repeaters (QRs) can overcome this problem and hence, can increase the communication rate. QRs can be categorized in three generations. The improved quantum repeater architecture is also identified for particular set of experimental parameters.

It is very complicated to trap and cool the atoms and ions in vacuum for the quantum computing [63]. Therefore, there is a need of replacement entities motivated to use quantum dots and single dopants. It is comparatively very easy to cool the quantum dots to form array of qubits. For example, an electron or hole is bound in a localized potential with discrete energy levels in a semiconductor nanostructure. In the next section, spin quantum dots are reviewed for the realization of quantum computing.

2.2.1 Spin Quantum Dots

Quantum dots are the electrons trapped in a cavity. They are categorized in two types i.e. electrostatic and self-assembled. The electrostatic quantum dots are formed when the confinement is formed by the controlled voltage on the metallic gate. The self-assembled quantum dots are formed through a random semiconductor growth that creates confinement potential [64, 65]. The depth of potential required for the confinement is the basis for the difference between electrostatic and self-assembled quantum dots. Moreover, electrostatic quantum dots and self-assembled quantum dots operate at very low temperature and high temperature, respectively. Electrostatic quantum dot is controlled electrically whereas self-assembled quantum dot is controlled optically.

Danial Loss and DiVincenzo proposed array of electrostatic quantum dots for quantum computation [28]. Each quantum dot comprises a single electron. Spin state of the electron is utilized as qubit state. The quantum logic is realized by modulating the voltage on the electrostatic gates present between confined electrons to move the electrons near to each other or away from each other. This results in voltage controlled exchange interaction between the quantum dots [66]. When an electron is confined, the states are quantized. The current voltage relationship for the quantum dot can be described with the help of interaction model [67]. The emission wavelength or emission colour of a quantum dot depends on the dot size. A bulk semiconductor and quantum dot energy gap are shown in Figure 2.3(a) and Figure 2.3(b), respectively [68]. The energies are determined by the radius of the quantum dots.

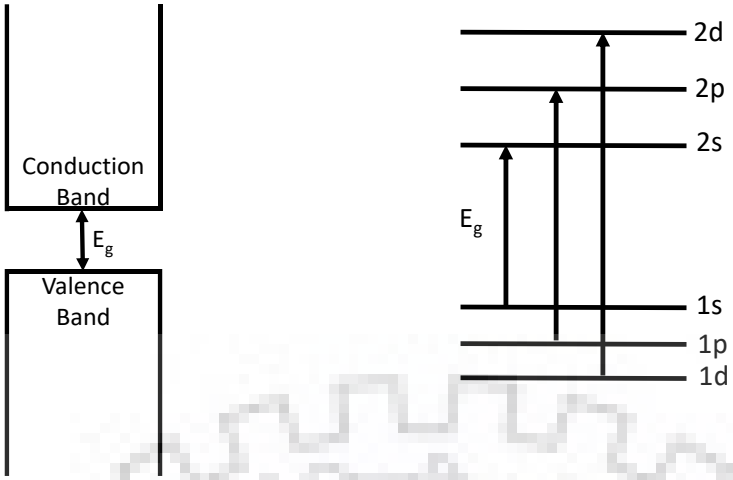

Figure 2.3 (a) Energy band gap in a bulk semiconductor, and (b) Quantized energy levels for quantum dot.

Spin-orbit interaction helps to couple an alternating electric field to the electron spin of a quantum dot (Figure 2.4). Several mechanisms are presented [69] for the efficient control of the spin in the quantum dots. A transverse magnetic field is produced due to Dresselhaus and Rashba spin-orbit interaction in the presence of a Zeeman splitting [70]. Decoherence [71] is hindrance in fruitful realization of the quantum gates. The spin dynamics of electrons and various decoherence effects are presented in [72].

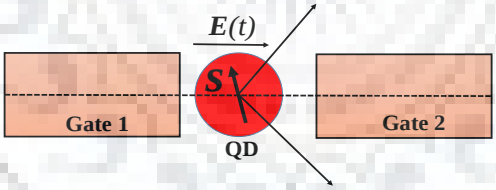

Figure 2.4 Electric field control of spin via the spin-orbit interaction.

Carbon materials have excellent property of weaker nuclear-spin interactions as ^{13}C with nuclear spin ½ are available with 1% only [73]. Therefore, carbon structures provide encouraging materials to build quantum dots with considerably long decoherence time. An electron confined to carbon nanotube or graphene quantum dot structure is presented in [74]. In graphene, it is observed that only hyperfine interactions couple with the electron. However, in case of carbon nanotube (CNT), the decoherence is due to curvature as it induces hybridization of the electron orbitals. These nuclear-spin interactions affect the related spin dynamics. Spin relaxation in heavy-hole quantum dots in low external magnetic fields is studied [75]. The two-

phonon processes and spin-orbit interaction are responsible for saturation for the spin relaxation rate in heavy-hole quantum dots.

A linear triple-quantum-dot array is used in [76] to demonstrate a coherent time evolution of two interacting distant spins via a quantum mediator. Single-shot spin readout is used to calculate the coherent time evolution of the spin states on the outer dots. Dependence of the exchange frequency as a function of the detuning between middle and outer dots is also observed. This gives the way for scaling up spin qubit circuits using quantum dots. It is presented that the spin information conveyed by one or two electrons can be transmitted between two quantum dots which are separated by 4 μm with a classical fidelity of 65% [77].

2.2.2 Quantum Computing with Quantum Dots

DiVincenzo criteria [2] directs the physical system to realize the quantum gate operations, therefore, spin states of coupled single electron quantum dots are utilized for the realization of a universal set of one- and two-quantum bit gates. A qubit is realized as spin of excess electron on a single electron quantum dot (Figure 2.5) [28]. Electrical gating is facilitated between the qubits. If the barrier potential between two-qubits is high, the qubits are isolated and are not allowed to interact. The exchange interaction between two qubits grows as the barrier potential is lowered. The spin states of qubits 1 and 2 are used for the realization of universal set of one and two quantum gates.

The Heisenberg exchange is modelled as

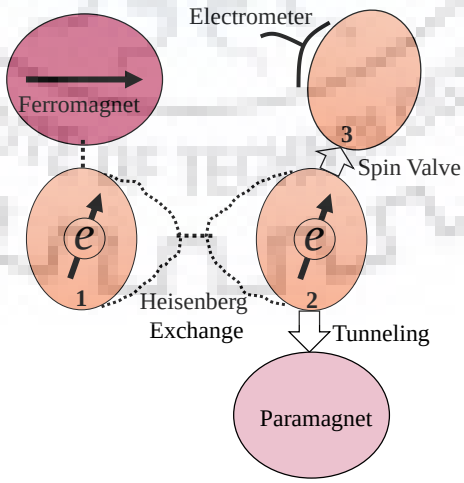

Figure 2.5 Heisenberg exchange interaction between two quantum dots.

$$H_s(t) = J(t)\, S_1 \cdot S_2 \qquad (2.2)$$

where, $J(t)$ is time-dependent exchange constant. S_1 and S_2 are ½ spin operators of first and second qubits, respectively. The dependence of J on magnetic field $B(z)$ or electric field $E(x)$ or by modulating the inter-dot distance $2d$ (Figure 2.6) is elaborated in [64]. V(x, y) is the barrier potential. This helps to design quantum gates by adapting $J(t)$.

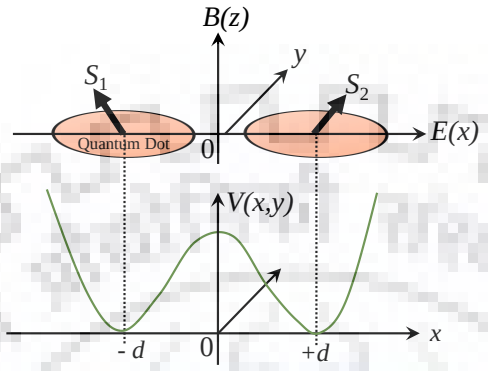

Figure 2.6 Laterally coupled quantum dots.

A singlet-triplet qubit is implanted in the presence of homogenous magnetic field to propose a set of universal gates [78]. It is all gate manipulation by varying the potential offset or misalignment between the two dots by applying electrical voltage. It does not depend on the tunnel coupling between the dots (Figure 2.7). With the help of this topology, single qubit rotation and two-qubit entanglement are realized to constitute universal quantum gates. Toffoli-Fredkin gate is a universal reversible logic gate. The inherent property of a reversible gate is non-dissipation of energy [79]. A linear array of exchange coupled three quantum dots is utilized to implement a Toffoli-Fredkin gate [80].

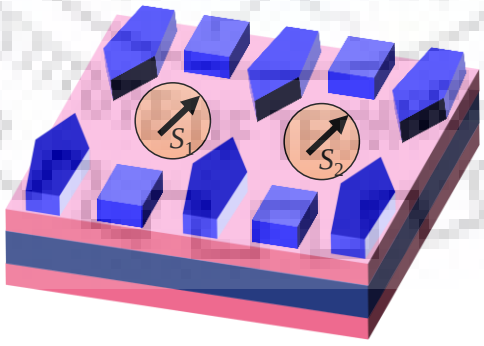

Figure 2.7 Double quantum dot.

AC magnetic field needs to be generated to selectively drive spin resonance in the coupled spin system. The frequency of qubit rotation (Rabi frequency) is proportional to electron-g factor. The value of g-factor is different for different

materials [81]. For a graphene quantum dot, the value of g-factor is 2. Due to this, the graphene quantum dot can be rotated five times faster for the same external magnetic field [82] than others. This rotation in graphene quantum dot at faster rate helps to realize fault-tolerant quantum computing. A quantum dot on bilayer graphene is shown in Figure 2.8.

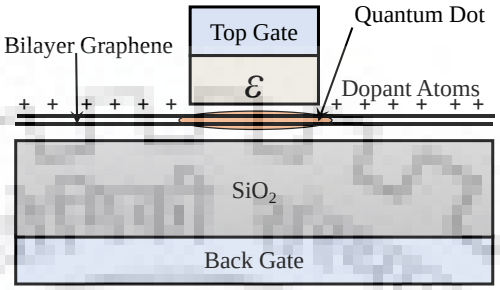

Figure 2.8 Bilayer graphene based quantum dot.

Spin qubits of graphene nanoribbons have small bandgaps. Moreover, additional flexibility is provided for two-qubit quantum operation. Single electron spin qubit is realized in [83]. It has electrical control speed (upto 30 MHz) and enhanced phase coherence time (20 μs) mediated by extrinsic spin electric coupling. This qubit shows excellent performance with single-qubit gate fidelities exceeding 99.9% on an average. It offers a path to large scale spin qubit systems with fault tolerant controllability.

The long-distance interaction of three-quantum gates is shown in Figure 2.9. In this, two distant qubits can be strongly coupled without disturbing the intermediate qubit states. The electrical control of graphene quantum dots is possible due to formation of tuneable bandgap by electric fields [84].

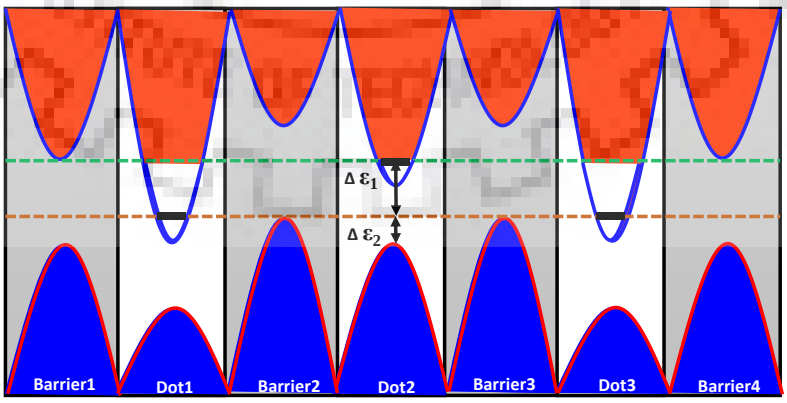

Figure 2.9 Electric-field-tunable electronic properties of graphene quantum dots .

Hole spins in Ge/Si nanowire quantum dots for universal and electrically controlled quantum gates are proposed in [85]. Electric dipole induced spin resonance is utilized for the single qubit rotation. Cavity electric field of a superconducting transmission line resonator facilitates the two-qubit entanglement. The precise control over qubits (Figure 2.10a and Figure 2.10b) is made possible due to the weak Dresselhaus spin-orbit interaction and strong Rashbha spin-orbit interaction via external electrical field applied in perpendicular direction. Due to the strong Rashbha spin-orbit interaction, g-factor is precisely controlled to perform single- and two-qubit gates independently.

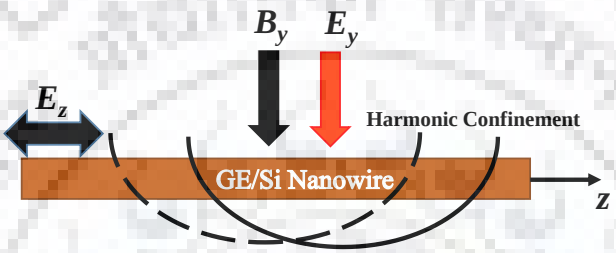

(a)

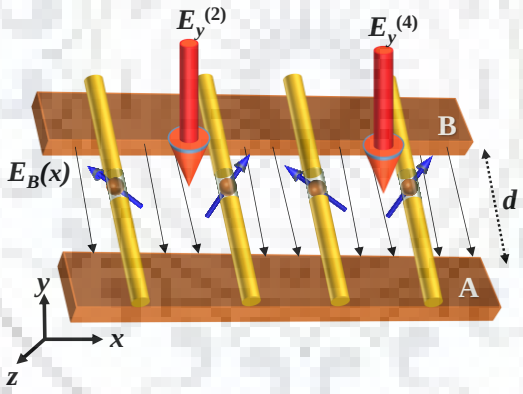

(b)

Figure 2.10 (a) Perpendicular electric field and, (b) Two-qubit quantum gate realization between qubit 2 and 4.

2.2.3 Spin Torque Based Quantum Computing Architecture

Spin is a primary entity envisioned for the physical realization of qubits. The quantum computing is based on individual qubit rotations and two qubits interactions in composite systems. To accomplish the task, the external magnetic field is used to manipulate the qubits. In complex computing systems, it is very difficult to precisely control and manipulate the individual qubits through external magnetic field. In the recent past, STT (Spin Transfer Torque) is used to switch the polarization of

nanomagnets to achieve the classical computing [7][23]. Spin torque like effects can be used to implement quantum processes involving single qubit initialization and rotation as well as two qubit entanglement. Qubit readout can be implemented using the same architecture.

The architecture shown in Figure 2.11 consists of four qubits S_3, S_2, S_1, and S_0 embedded in a spin-coherent semiconductor channel. The static qubits could be ^{29}Si nuclear spin, ^{31}P donor level, electronic donor spin, or nanoscale magnet embedded in the semiconductor [86]. A nanomagnet is a sub micrometric system that presents spontaneous magnetic order (magnetization) at zero applied magnetic field. The small size of nanomagnets prevents the formation of magnetic domains. The magnetization dynamics of sufficiently small nanomagnets at low temperatures, typically single-molecule magnets, presents quantum phenomena, such as macroscopic spin tunnelling. At larger temperatures, the magnetization undergoes random thermal fluctuations present a limit for the use of nanomagnets for permanent information storage. The spin reservoir injects the iterant spins into the channel to control the qubit operations. The spin reservoirs are held at some specific spin potentials. The spin potentials are generated by magnetic contacts [87- 91], giant spin Hall Effect [92-106], or spin pumping [107] at low and room temperature. The barrier gates R_i and G_i of each qubit are controlled to carry out a specific operation. Also, the semiconductor channel has barriers B_0 to B_2 to provide the isolation and control of the flow of electrons through the channel. Integration of qubits with semiconductors provides device fabrication prospect [108].

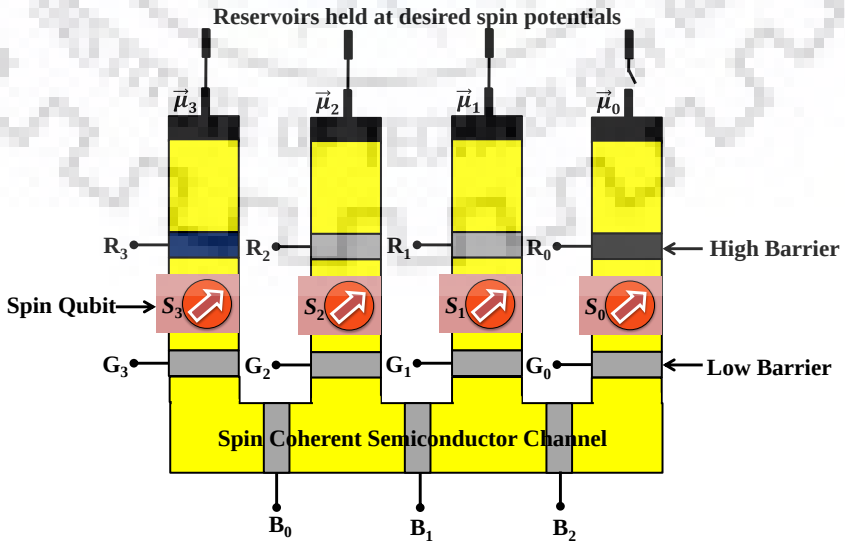

Figure 2.11 Spin-torque based qubit-architecture.

2.2.4 Fabrication Aspects of Qubit

The most challenging issue of the architecture is the fabrication of the qubit. There are several technologies proposed by researchers for the qubit fabrication. Specifically, the measurement of the qubit adds challenge to the realization of the architecture as quantum computer from the qubit initialization to the qubit measurement. Detection of the single spins in silicon is not yet realized [109], there could be a possibility of fast single charge detection due to RF single electron transistor (SET) technology [110]. There are several proposals given by researchers in these directions such as single atom Si nanoelectronics using controlled single-ion implantation [111], single atom devices by ion implantation [112], atomically precise placement of single dopants in Si [113], single ion implantation method for single-dopant devices [114], controlled shallow single-ion implantation in silicon [115], integration of single ion implantation method in focused ion beam system [116], etc. These proposals could help to perform the qubit manipulations and measurements.

2.3 Technical Gaps

Based on literature review, it is observed that the spintronics based architectures have the potential to realize the QC. Further exploration is necessary to realize the important aspects of QC such as a set of reversible quantum gates, classical gates, quantum Fourier transform (QFT) on the generalized simulation platform. High fidelity quantum operations are targeted for the realization of the spin-torque-based fault tolerant quantum computing.

The research gaps evaluated based on the literature survey are as follows:

- **Lack of Generalized simulation platform:** A generalized simulation platform is not provided by the previous models [82] to realize the spin torque based initialization, manipulation, and measurement of the spin qubit in an *n*-qubit system architecture. Also, a set of high fidelity quantum gates are required to be realized on the generalized simulation platform.
- **Optimal decomposition of the quantum circuits:** The spin-torque-based architecture needs the sequence of single-qubit rotation and two-qubit entanglements for the realization. The reduction in number of operations required for the realization of the complex computation is needed to preserve the qubit

coherence. Therefore there is a need of optimized quantum circuits decomposition.

- **Reversible Boolean logic exploration:** The previous models [82] have realized only single-, two-qubit manipulations. In addition, a two-qubit CNOT gate is realized as a capstan example. The model is required to be further explored to realize the Boolean logic in terms of reversible AND, NAND, OR, NOR, etc. gates to achieve the no information loss at low power dissipation.
- **Quantum Fourier transform:** In quantum computing, the quantum Fourier transform (QFT) [117-125] is a linear transformation on qubits. In addition, QFT is an important operation for the quantum algorithms. The physical realization of QFT is achieved by multilevel atoms, linear optics operators, cavity quantum electrodynamics, and photonic lattices. But, these methods have difficulties in realizing scalable architecture. The spin-torque-based architecture is scalable, and it will help to get rid of the difficulties posed by previous methods for the realization of the QFT.

The entire thesis covers the solution to aforementioned problems. The results are obtained through extensive and rigorous simulations on MATLAB.

Chapter 3

Transmission Coefficient Matrix Modeling of the Spin-Torque Based *n*-Qubit Architecture

3.1 Introduction

In the modern era, classical computing is facing several challenges such as inability to solve the complex problems efficiently [17], scaling limitation, high power dissipation [126], etc. There is a pressing need to deal with the aforementioned problems associated with classical computing. Quantum computing (QC) [1] can become an exciting option due to its unique characteristic of imitating the particle behavior at subatomic levels. In addition, QC performs the quantum operations in less time compared to classical computing due to parallel information processing. This helps to solve the complex problems such as integer number factoring, and unorganized data searching efficiently.

QC is required to be physically realizable and needs rigorous efforts for real implementation. Any physical system implementing the QC has to fulfill the DiVincenzo criteria [2]. Spintronics [127] can be the most efficient way to physically realize QC due to the electron spin analogous to the qubit [128]. Spintronics based computing architectures such as nuclear quantum computer [129], and quantum dot (QD) architecture [28, 130, 131] have shown encouraging prospects for the physical realization of the QC. However, these architectures have some implementation issues. In the case of QDs, precisely controlling and manipulating individual electron is very difficult. Other critical issues with QDs are long-distance interaction inability, spin decoherence, spin measurement complexities, and computing architecture scaling limitation. To get rid of problems encountered due to long distance interaction inability in the aforementioned architectures, several models were proposed such as interaction [132] between static and flying qubits in a carbon nanotube [133], static and mobile spins interaction in graphene [134], static and flying qubit entanglement in degenerate mesoscopic systems [135], flying conduction band electron-static qubit interaction model [136], and electrical control of a solid-state flying qubit [137]. Moreover, a spin-torque [138, 139] based architecture for QC to realize single-qubit rotation and two-qubit exchange interaction through the first order transmission

coefficients matrix model is presented in [108]. However, investigation of effects such as ratio of reflection barrier height to exchange interaction (Γ_{Rfl} / J) on quantum operations are not considered. As an improvement over previous models, a modified transmission coefficient matrix is proposed in this chapter to include the effect of Γ_{Rfl} / J on single-qubit rotation and two-qubit entanglement.

The analytical and matrix methods proposed in [108] to realize the single-qubit rotation and two-qubit entanglement do not provide a general simulation framework to trace the performance of more than two-qubit quantum circuits [140]. Therefore, in this work, a fully specified matrix (FSM) based general methodology is utilized for the spin-torque based *n*-qubit reconfigurable architecture. Moreover, for the fault-tolerant QC, an optimized quantum library is essential for every physical machine description (PMD) [141]; and no optimized quantum gate library is introduced for the spin-torque based QC. This work includes modeling of modified matrix-based single-qubit rotation and two-qubit entanglement for *n*-qubit architecture.

This chapter consists of three sections including the current introductory section. Section 3.2 explains spin-torque based QC architecture. Section 3.3 discusses the modified matrix-based single-qubit rotation and two-qubit entanglement models for *n*-qubit architecture performed with the help of generalized FSM method.

3.2 SHE Based Spin-Torque QC Architecture

The spin-torque based *n*-qubit architecture performs the single-qubit rotation and two-qubit entanglement. The single- and two-qubit architectures form the basic building blocks of the *n*-qubit architecture.

3.2.1 Single-Qubit QC Architecture

The spin-torque based single-qubit architecture is shown in Figure 3.1(a). The static spin qubit Q_1 is embedded in a spin-coherent channel. Architecture facilitates controlled barrier gates R_1 and G_1. The G_1 is set to high barrier height and the pair of R_1-G_1 barriers isolates or allows qubit for the rotation. The distance between barrier G_1 and qubit Q_1 is *d*. The channel carries quantum information. The heavy metal-nanomagnet assembly injects electrons into the channel with the desired spin-polarization. Switches Sw_1 and Sw_2 remain *ON* and *OFF*, respectively for spin

generation [142, 143], and *OFF* and *ON*, respectively for non-local spin injection [144].

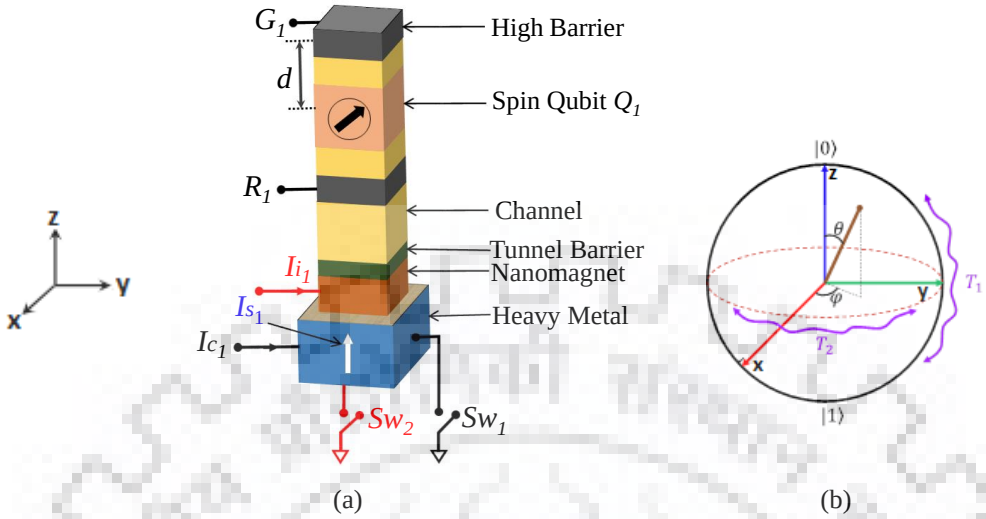

(a) (b)

Figure 3.1 Single-qubit (a) Architecture (b) Qubit state evolution on Bloch sphere.

Bloch sphere representation of spin qubit state evolution is depicted in Figure 3.1(b). The deviation in the qubit state from its desired state depends on relaxation time T_1 and coherence time T_2 (shown in Figure 3.1b). The variation in angles θ and φ depends on T_1 and T_2, respectively. The variation in φ represents the qubit dephasing; therefore, T_2 of spin-qubits is the fundamental requirement for the physical realization of QC architectures.

The heavy metal allows charge current Ic_1 to pass along x-axis. The Ic_1 produces spin current Is_1 along z-axis. The Is_1 exerts a torque on nanomagnet next to heavy metal to set nanomagnet spin polarization to the desired spin state. The magnitude and direction of torque depend on the magnitude and direction of Ic_1. It also depends on the spin-Hall angle of the material used. Is_1 can be expressed as [138]

$$Is_1 = \frac{\hbar}{2q}\frac{A_{NM}}{A_{HM}}\theta_{SH}\left(1-\cosh\left(\frac{\lambda_{SF}}{t_{HM}}\right)\right)Ic_1 \tag{3.1}$$

where, A_{NM} is cross-sectional area of the nanomagnet, A_{HM} is the area of heavy metal, θ_{SH} is the spin Hall angle, λ_{SF} is the spin-flip length, and t_{HM} is the thickness of heavy metal. In addition, Is_1 can be greater than Ic_1 due to the continuous scattering of electrons on the surface. The spin state of nanomagnet makes the nanomagnet to act as a spin reservoir.

To perform non-local spin injection from the spin reservoir into the channel, switch positions Sw_1 and Sw_2 are reversed. The heavy metal allows charge

current Ii_1 to pass along z-axis. The current Ii_1 injects spin-polarized electrons from nanomagnet through TB into the semiconductor channel. The injected spin-polarized electrons traverse through the channel to constitute spin current. Spin current in the channel depends on two factors *i.e.* channel material and temperature. The spin current exerts the torque on static qubit to modulate its quantum state. The increase in barrier height of R_1 increases the interaction by producing standing waves between barriers R_1 and G_1. Subsequent to the interaction, the barrier G_1 reflects electrons back to the reservoir. The qubit state measurement is performed after the process of qubit-electron interaction.

From the material perspective, qubits can be represented by Si nuclear spin, P donor level, or nanoscale magnet embedded in the semiconductor [86]. For electrons bound to donors in silicon, at low temperature, T_1 becomes very long i.e. minutes to hours. The increase in temperature reduces T_1 due to the valley-orbit excited state of the donor. T_2 is comparatively shorter than T_1 for donor electrons. In literature, experiments have been carried out to measure T_2. A T_2 of 0.52 ms is obtained for a P donor doped in isotopically enriched ^{28}Si [145]; T_2 is measured approximately 60 ms for a P donor in ^{28}Si at 7 K [146]; in [147], an antimony ^{121}Sb is implanted in isotopically pure ^{28}Si. A T_2 of Sb electron at 50 nm below the Si/SiO_2 surface is measured as 0.3 ms, however, it is increased to 0.75 ms at same depth below the surface when the surface is passivated with hydrogen. Therefore, effect of silicon surface on T_2 due to surface defects and ion implantation plays a significant role in spin-qubit dephasing; the decoherence time of free electrons is measured as 3 μs [148] at 4.2 K which is sufficient to perform more than 100 basic quantum operations. The gate execution time of spin-torque based quantum gates is comparatively less than the aforementioned decoherence times. Moreover, a single qubit rotation can be carried out in 10 ns through the flying spin electrons and qubit interaction. The spin lifetimes of over 500 ns at 60 K have been reported in undoped Si [149] that is more than sufficient to perform complex quantum gates. The major source of decoherence in architecture is when electrons moving in semiconductor channel. Moreover, decoherence depends on the material of which semiconductor channel is made up of and temperature. Therefore, for the quantum computing, isotopically enriched ^{28}Si doped with P is more significant than other forms of Si due to its long enough coherence time to physically realize QC gates.

Channel can be made up of semiconductor materials such as Si, graphene, etc. The spin diffusion lengths of silicon and graphene are 200 nm [150, 151] and 5 μm [152], respectively at room temperature. Therefore, graphene has better spin transport characteristics at room temperature than Si. The nanomagnet used for spin injection can be prepared of Fe, CoFe, CoFeB, or full-Heusler alloys. Spin injection efficiency of Fe, CoFe, or CoFeB reported is ~60-70% [150]. Whereas, the spin polarization of Heusler alloys is ~100% [153, 154]. Hence, researchers are working on the Heusler alloys based spin injection for the futuristic spintronics devices. Among heavy metals available, Pt, β-Ta, β-W, or CuBi alloys [138] can be preferred for spin generation due to their ability to generate large spin current.

To reduce power dissipation due to the charge current required to inject spin-polarized electrons into a semiconductor channel, a novel two-switch based assembly is incorporated in the architecture for spin generation and injection. The spin Hall Effect (SHE) is used to generate spins and non-local spin injection facilitates electron spins insertion in the channel. Moreover, a tunnel barrier (TB) is sandwiched between nanomagnet and semiconductor channel to reduce conductivity mismatch between nanomagnet and semiconductor channel materials.

3.2.2 Two-Qubit QC Architecture

A two-qubit architecture is shown in Figure 3.2. It consists of two single-qubit structures separated by a semiconductor channel. Barrier B_1 is entrenched into the channel to control the electrostatics of electrons and facilitates qubit isolation. Two-qubit operation is performed on Q_1 and Q_2. G_1 and G_2 are set to low barrier heights to allow two-qubit interaction. The distance between Q_1 and Q_2 is d_{12}.

During a two-qubit operation, barriers used for interaction are R_1 and R_2. Electrons are injected from the side of Q_2 into the channel. Electrons traverse through the channel from Q_2 to Q_1 and interact first with Q_2 and then with Q_1. The sequential interaction of flying electrons with Q_1 and Q_2 performs two-qubit rotation. The two-qubit interaction depends on distance d_{12}.

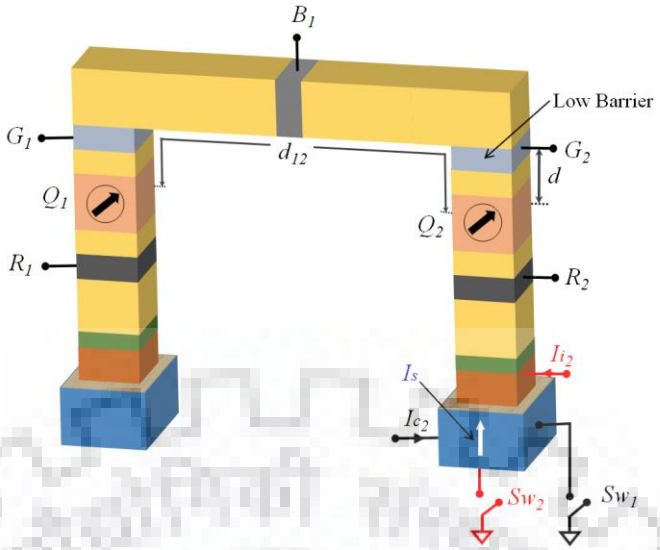

Figure 3.2 Two-qubit architecture.

3.2.3 Three-Qubit QC Architecture

A spin-torque based three-qubit reconfigurable architecture is shown in Figure 3.3. The architecture consists of three static spin qubits Q_1, Q_2, and Q_3; and barrier gates R_1-R_3, G_1-G_3, and B_1-B_2. The pair of R-G barriers isolates or allows a qubit to take part in a specified QC operation.

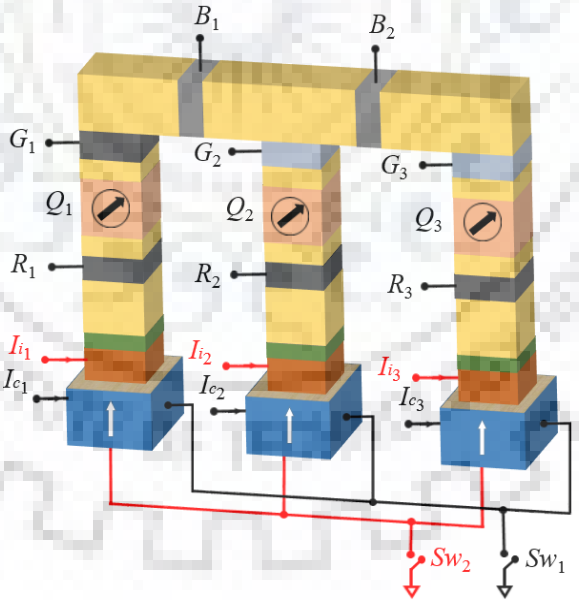

Figure 3.3 Three-qubit architecture.

The architecture performs elementary single-qubit rotation on any of the qubits; and two-qubit operation on any pair of the qubits to realize reversible quantum gates. Architecture can be extended to n qubits by adding required number of single arms.

3.3 Modified Matrix Based Single-Qubit Rotation and Two-Qubit Entanglement in *n*-Qubit QC Architecture

Spin density matrix as expressed in (3.2) represents spin polarization of injected electrons.

$$\rho_e = \frac{1}{2}[I + \sigma_x \hat{x} + \sigma_y \hat{y} + \sigma_z \hat{z}] \tag{3.2}$$

where, I, σ_x, σ_y, and σ_z are unitary Pauli spin matrices.

Hamiltonian for the interaction of injected electrons with the qubit [104] is represented as

$$H = \frac{p^2}{2m^*} + J\rho_e \cdot \tilde{S}_i \delta(x) + \Gamma_{Rfl}\delta(x - x_0) \tag{3.3}$$

where, m^* and p are effective mass and momentum operator of an electron, respectively, J is hyperfine or exchange interaction, x-x_0 represents interaction distance, and $\tilde{S}_i$ is standard basis matrix representing the i^{th} qubit. The order of $\tilde{S}_i$ matrix depends on the number of qubits that forms overall state space of the architecture. This work generalizes the order of S_i to $2^{n+1}\times 2^{n+1}$ for the n-qubit architecture.

The overall spin density matrix of n-qubit system is represented as

$$\rho_s = \rho_{Q_1} \otimes \rho_{Q_2} \otimes \rho_{Q_3} \ldots\ldots\ldots \otimes \rho_{Q_n} \tag{3.4}$$

where, ρ_{Q_1}, ρ_{Q_2}, ρ_{Q_3},….., and ρ_{Q_n} are spin density matrices of Q_1, Q_2, Q_3,…..,and Q_n, respectively. The order of ρ_s matrix is $2^n \times 2^n$. For a qubit, the transmission coefficient at the reflection barrier [136] is

$$t = \frac{4}{4 + i2\pi\Gamma_{Rfl}\rho_\varepsilon + \pi V_s \rho_\varepsilon (i2 + (e^{i2kd} - 1)\pi\Gamma_{Rfl}\rho_\varepsilon)} \tag{3.5}$$

where, ρ_ε is $\frac{2m^*}{\pi k\hbar}$, k is wave vector, $\hbar$ is reduced Plank's constant, $V_s = \frac{J}{2}(s(s+1) - \frac{3}{2})$, $s=0$ and $s=1$ are for singlet and triplets, respectively. The singlet and triplet transmission coefficients are expressed from (5) as

$$t_s = \frac{1}{1 + i4\Omega x - i3\Omega - 12\Omega^2 x\ (e^{i2kd} - 1)} \tag{3.6}$$

$$t_t = \frac{1}{1 + i4\Omega x + i\Omega + 4\Omega^2 x\ (e^{i2kd} - 1)} \tag{3.7}$$

where, $x = \frac{\Gamma_{Rfl}}{J}, \Omega = J/\hbar v$, and v is velocity of the electron. The transmission coefficient matrix containing t_s and t_t, respectively is

$$t = \begin{bmatrix} t_t & 0 & 0 & 0 \\ 0 & t_t & 0 & 0 \\ 0 & 0 & t_s & 0 \\ 0 & 0 & 0 & t_t \end{bmatrix} \tag{3.8}$$

and reflection matrix is $r = t - I$, where I is identity matrix. After simplifying (3.8), the modified t is expressed as

$$t = \frac{1}{(1 + i4\Omega x)\, I + i\tilde{S}(\Omega - (i4\Omega^2 x\ (e^{i2kd} - 1)))} \tag{3.9}$$

For $\Gamma_{Rfl} / J = 0$, (3.9) reduces to

$$t = \frac{1}{I + i\tilde{S}\Omega} \tag{3.10}$$

The generalized reflection matrix R_F for qubit rotation is

$$R_F = r - e^{i2kd} t \left[I_{2^{n+1}} + e^{i2kd} I_{2^{n+1}} R_0 \right]^{-1} I_{2^{n+1}} t \tag{3.11}$$

With the help of (3.11), singlet and triplet components of R_F are expressed as

$$R_s = \frac{a_{s_1} + ib_{s_1}}{a_{s_2} + ib_{s_2}} \text{ and } R_t = \frac{a_{t_1} + ib_{t_1}}{a_{t_2} + ib_{t_2}} \tag{3.12}$$

The terms $a_{s_1}, b_{s_1}, a_{s_2}, b_{s_2}, a_{t_1}, b_{t_1}, a_{t_2}$, and b_{t_2} used in (12) are expressed as

$$a_{s_1} = -12\Omega^2 x + (3\Omega - 4\Omega x - 24\Omega^2 x)\sin(2kd) + 24\Omega^2 x \sin(4kd) - \cos(2kd) + 12\Omega^2 x \cos(4kd) \tag{3.13}$$

$$a_{s_2} = 1 - 24\Omega^2 x \cos(2kd) + 12\Omega^2 x + 4\Omega x \sin(2kd) - 3\Omega \sin(2kd) + 12\Omega^2 x \cos(4kd) \tag{3.14}$$

$$b_{s_1} = 3\Omega - 4\Omega x + (4\Omega x - 3\Omega + 24\Omega^2 x)\cos(2kd) - 24\Omega^2 x \cos(4kd) - \sin(2kd) + 12\Omega^2 x \sin(4kd) \tag{3.15}$$

$$b_{s_2} = 4\Omega x - 3\Omega - 24\Omega^2 \sin(2kd) - 4\Omega x \cos(2kd) + 3\Omega \cos(2kd) + 12\Omega^2 x \sin(4kd) \tag{3.16}$$

$$a_{t_1} = 4\Omega^2 x - (8\Omega^2 x + 1)\cos(2kd) - (4\Omega x + \Omega)\sin(2kd) - 2\Omega^2 x \cos(4kd) \tag{3.17}$$

$$a_{t_2} = 1 + 8\Omega^2 x \cos(2kd) - 4\Omega^2 x + 4\Omega x \sin(2kd) + \Omega \sin(2kd) - 4\Omega^2 x \cos(4kd) \tag{3.18}$$

$$b_{t_1} = -4\Omega x - \Omega - (8\Omega^2 x + 1)\sin(2kd) + 4\Omega x \cos(2kd) + \Omega \cos(2kd) - 2\Omega^2 x \sin(4kd) \tag{3.19}$$

$$b_{t_2} = 4\Omega x + \Omega + 8\Omega^2 x \sin(2kd) - 4\Omega x \cos(2kd) - \Omega \cos(2kd) - 4\Omega^2 x \sin(4kd) \tag{3.20}$$

Singlet and triplet angles θ_s and θ_t are expressed as

$$\theta_s = \tan^{-1}\left(\frac{b_{s_1}}{a_{s_1}}\right) - \tan^{-1}\left(\frac{b_{s_2}}{a_{s_2}}\right) \tag{3.21}$$

$$\theta_t = \tan^{-1}\left(\frac{b_{t_1}}{a_{t_1}}\right) - \tan^{-1}\left(\frac{b_{t_2}}{a_{t_2}}\right) \tag{3.22}$$

The interaction factor α is

$$\alpha = \theta_s - \theta_t \tag{3.23}$$

Variation in α due to $\Gamma_{Rf\,l} / J$ is shown in Figure 3.4.

There is increase in scattering of electrons due to increase in $\Gamma_{Rf\,l} / J$ that results in considerable increase in α. Therefore, the number of electrons required for the desired rotation is reduced. The overall fully specified spin density matrix representing spin qubit state evolution due to the interaction of injected electron spins of spin density matrix ρ_e and spin qubit of spin density matrix ρ_s is

$$\rho = [R_F][\rho_e \otimes \rho_s]\left[R_F^{\dagger}\right] \tag{3.24}$$

The generalized FSM and partial trace methods realize single-qubit rotation and spin qubit state measurement, respectively. In addition, same methods are utilized to perform two-qubit entanglement and measurement. The process of sequential interaction and reflection changes ρ iteratively. The quantum collapse occurs during qubit state measurement.

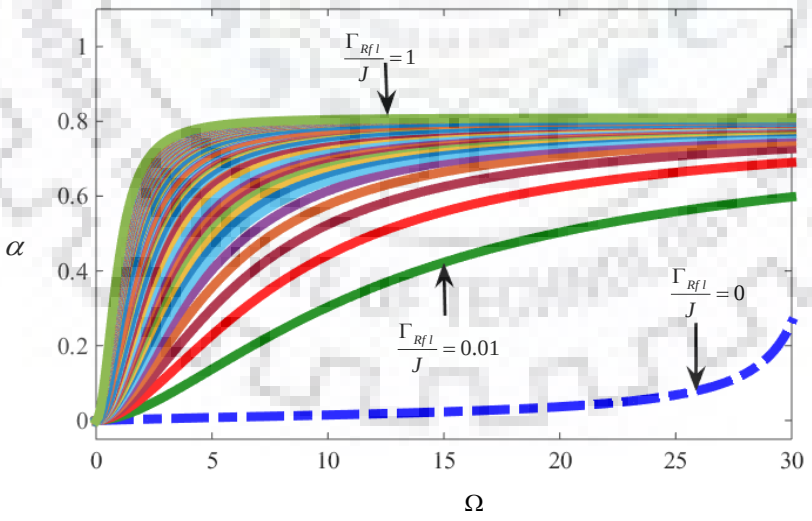

Figure 3.4 Interaction factor variation.

3.3.1 Single-Qubit Rotation

In this work, to demonstrate a single-qubit rotation, Q_1 is selected. The initial state of Q_1 is set to $|S_1\rangle = |0\rangle$ to perform the rotation about x-axis by $\pi/2$.

It is clearly seen from Figure 3.5 that there is a decrease in number of electrons due to increase in Γ_{Rfl} / J. The reduction in number of electrons is due to improvement in α (Figure 3.4). However, the component of spin state along axis of rotation deviates from initial value (not seen in Figure 3.5 due to smaller angle of rotation i.e. $\pi/2$). The deviation in axis of rotation results in decrease in fidelity for higher angle rotations. The same procedure can be carried out for any other qubit in the architecture. The effect of Γ_{Rfl} / J on product of number of electrons (N) required for single qubit rotation and α is depicted in Figure 3.6. The $N\alpha$ product is equal to the desired angle of rotation (θ) for the matrix proposed in [85]. With the help of modified matrix proposed in this work, the $N\alpha$ product is plotted for different values of Γ_{Rfl} / J. Though, there is decrease in N, the $N\alpha$ product is increasing linearly with increase in θ due to considerable improvement in α.

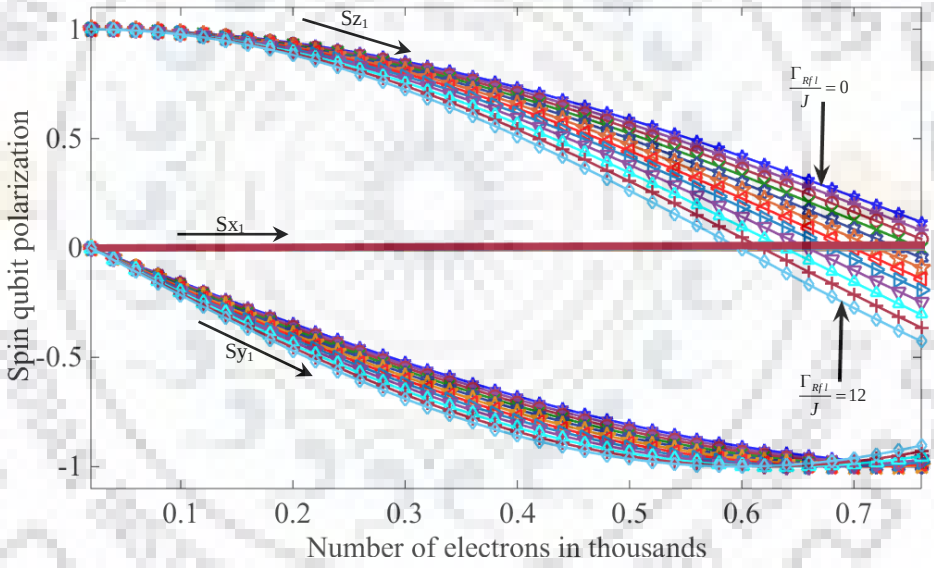

Figure 3.5 Single-qubit rotation about x-axis.

3.3.2 Two-Qubit Entanglement

Qubits Q_1 and Q_2 are selected to perform two-qubit entanglement. Transmission and reflection matrices for Q_1 are t_1 and r_1; and for Q_2 are t_2 and r_2, respectively. Moreover, barrier R_2 on the side of qubit Q_2 has reflection and transmission matrices t_b and r_b, respectively. The injection side barrier R_2 has a barrier height of Γ_{Inj}. The overall reflection matrix R_F for two-qubit interaction can be represented by qubit reflection matrices R_{F_1}, R_{F_2}, and R_{F_3} in cascade at Q_1, Q_2, and R_2,

respectively. The R_{F_1}, R_{F_2}, and R_{F_3} are functions of R_0, R_{F_1}, and R_{F_2}, respectively due to sequential interaction.

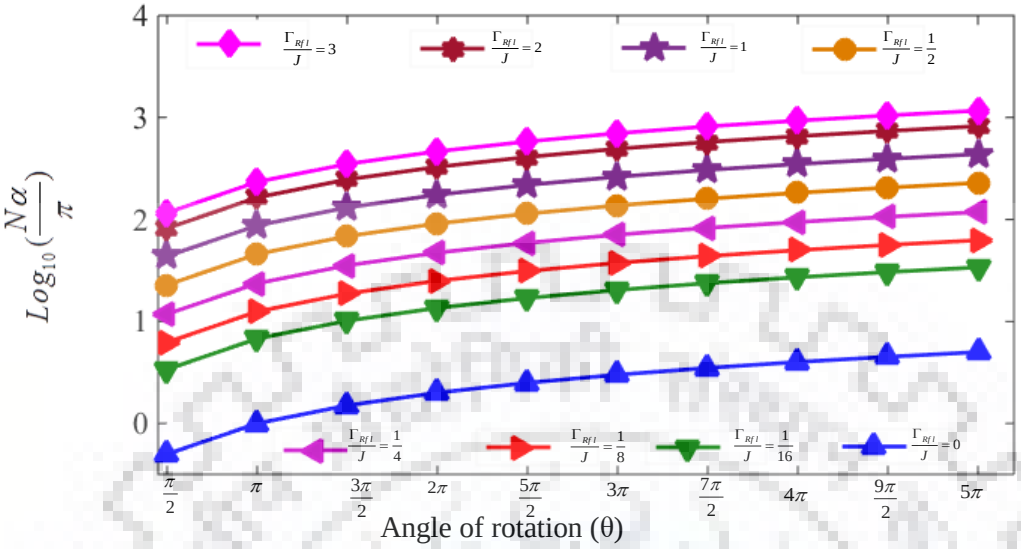

Figure 3.6 $N\alpha$ variation.

In this work, a two-qubit entanglement operation is performed on Q_1 and Q_2. The state evolution of entanglement between two-qubits is obtained (Figure 3.7). There is a considerable reduction in number of electrons and Γ_{Inj} for the entanglement. The entanglement is also called $\sqrt{\text{SWAP}}$ gate as it performs half of the SWAP gate operation.

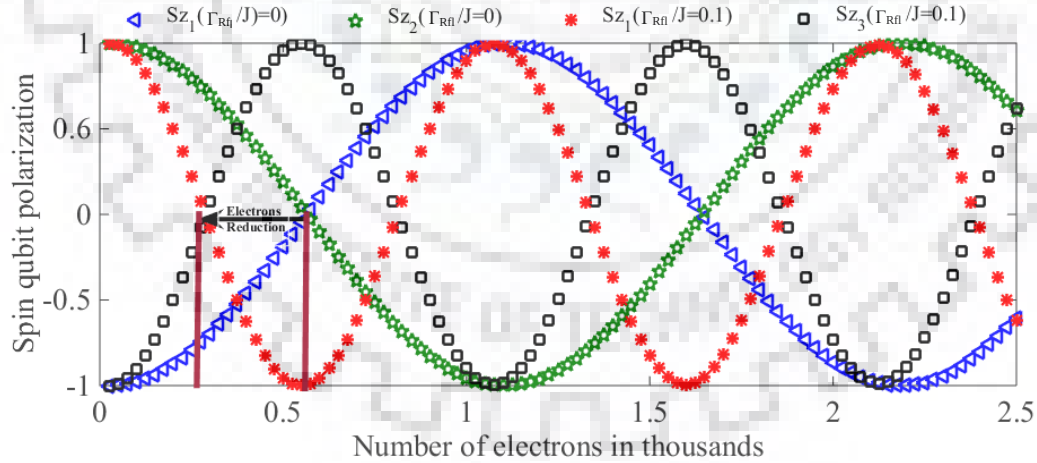

Figure 3.7 Two-qubit entanglement.

The accuracy of two-qubit entanglement depends on average error probability (AEP). The AEP based analysis for two-qubit entanglement is carried out as follows. The overall reflection matrix at injection side barrier can be represented in the form of unitary and non-unitary components as

$$R_{F\,Injb} = \begin{bmatrix} 1 & 0 & 0 & 0 & 0 & 0 & 0 & 0 \\ 0 & a & c & 0 & c' & 0 & 0 & 0 \\ 0 & c & a & 0 & c'' & 0 & 0 & 0 \\ 0 & 0 & 0 & b & 0 & c'' & c' & 0 \\ 0 & c' & c'' & 0 & b & 0 & 0 & 0 \\ 0 & 0 & 0 & c'' & 0 & a & c & 0 \\ 0 & 0 & 0 & c' & 0 & c & a & 0 \\ 0 & 0 & 0 & 0 & 0 & 0 & 0 & 1 \end{bmatrix} \quad (3.17)$$

where, a, b, and c represent unitary components while $c'$and $c''$are non-unitary components. AEP [85] are obtained by varying kd and kd_{12} (Figure 3.8). There is an increase in AEP due to the effect of $\Gamma_{Rf\,l} / J$. The effect of increase in AEP on quantum gate operation in terms of fidelity is elaborated in chapter 4.

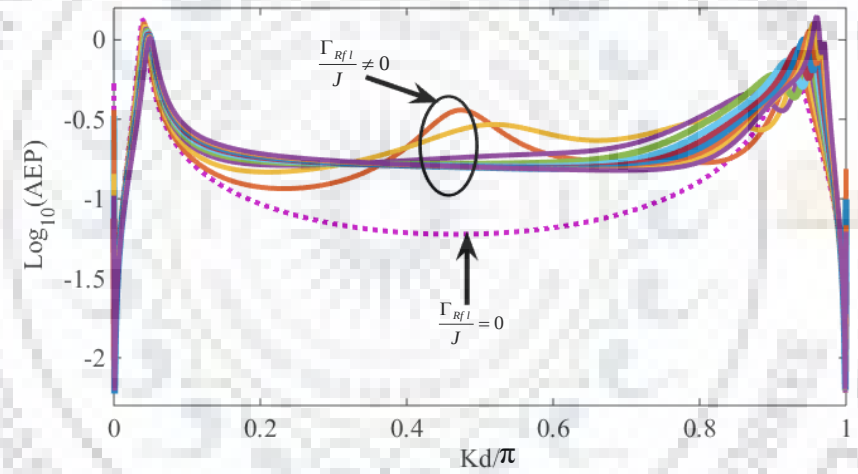

(a)

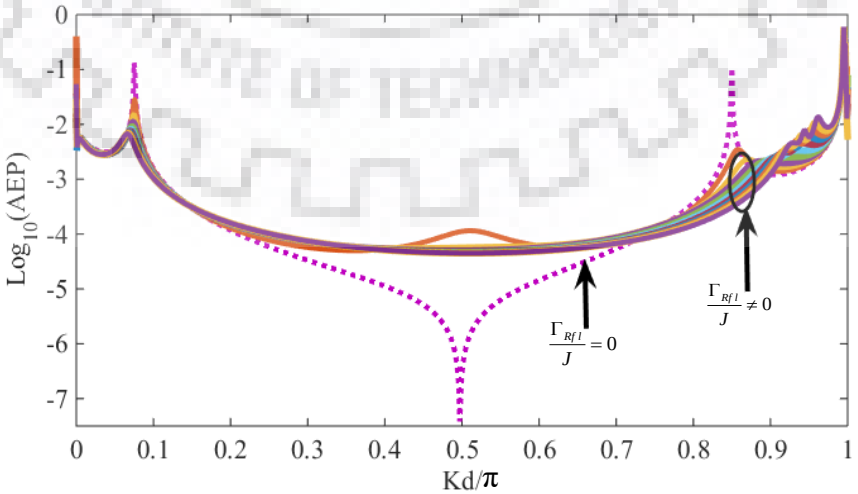

(b)

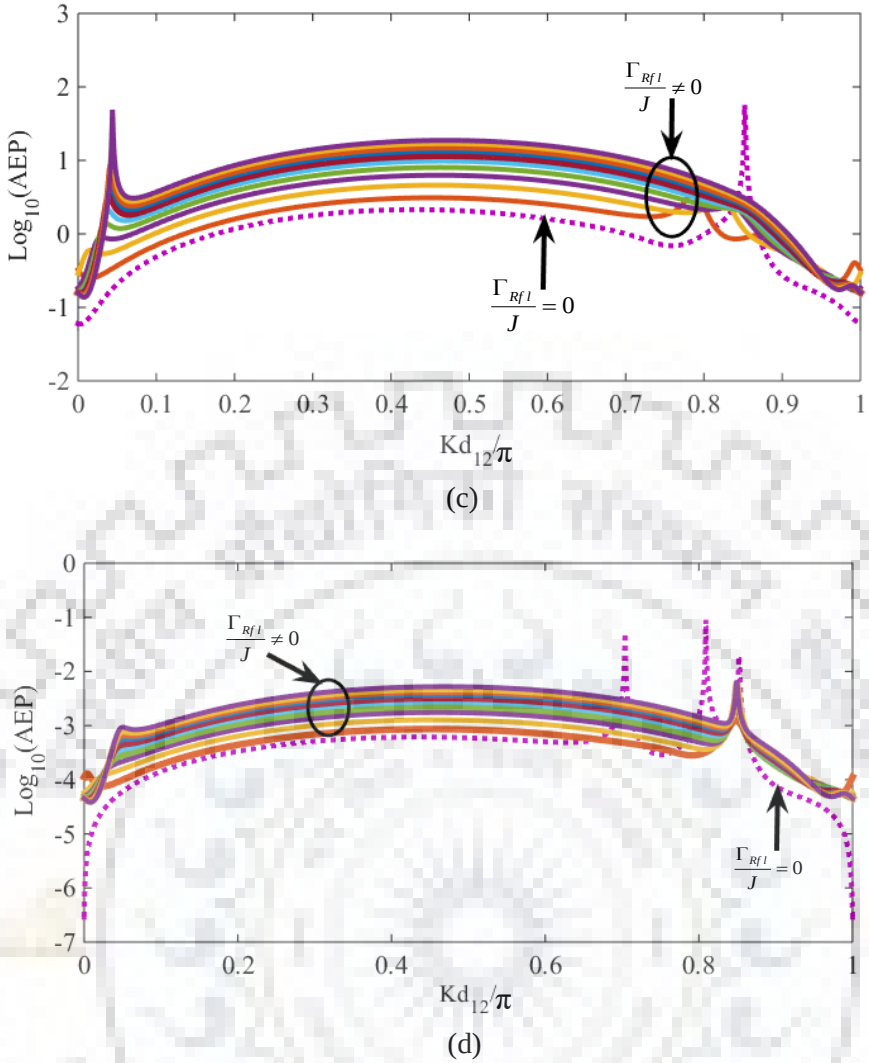

Figure 3.8 Average error probability (AEP) for (a) Kd variation at $\Gamma_{Inj} = 0$ (b) Kd variation at$\Gamma_{Inj} = 30$ (c) Kd_{12} variation at $\Gamma_{Inj} = 0$ (d) Kd_{12} variation at $\Gamma_{Inj} = 30$.

3.4 Summary

Spin-torque based QC architecture is emerging as one of the novel technologies to meet scalability challenges due to its intra-architecture spin qubit state manipulation. The existing model for spin-torque based QC does not include the ratio of reflection barrier height to exchange interaction to the transmission coefficients. Therefore, in this work, a modified matrix is proposed to analyze the effect of ratio of reflection barrier height to exchange interaction on electron-qubit interaction, deviation of the axis of rotation for single-qubit rotation, and average error probability (AEP) for two qubit rotation in a spin-torque based *n*-qubit reconfigurable architecture.

Chapter 4

Elementary Quantum Gates Reduction for the Spin-Torque Based *n*-Qubit Architecture

4.1 Introduction

Conventional and reduced decompositions of quantum circuits are utilized to evaluate the performance of complex quantum logic in terms of number of elementary gates, gate fidelity, execution time, and number of interacted electrons. The accuracy of physical realization of a quantum gate depends on fidelity, that is a measure of closeness of spin qubit state at the end of evolution to the desired state. The fidelity is expressed as

$$f = \left(Tr(\sqrt{\sqrt{\rho_d}\,\rho\sqrt{\rho_d}}) \right)^2 \tag{4.1}$$

where, ρ_d and ρ are the density matrix representing the desired final state of the operation and density matrix representing obtained state, respectively. The fidelity is required to be more than 99% for fault tolerant QC [155].

4.2 Realization of Reversible Quantum Gates

A reconfigurable simulation platform is presented in this chapter to trace the fidelity of complex quantum gates. A complex quantum gate is required to be decomposed into elementary quantum gates such as CNOT, SWAP, etc. [156]. For the spin-torque based physical realization, quantum circuits representing these elementary quantum gates are needed to be further decomposed into a sequence of elementary single- and two-qubit operations. The flowchart for *n*-qubit reconfigurable quantum gate operation is shown in Figure 4.1.

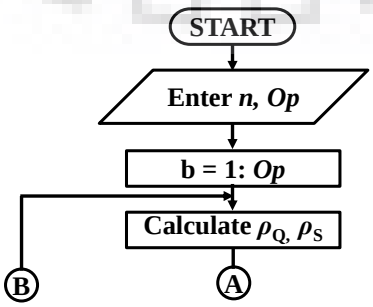

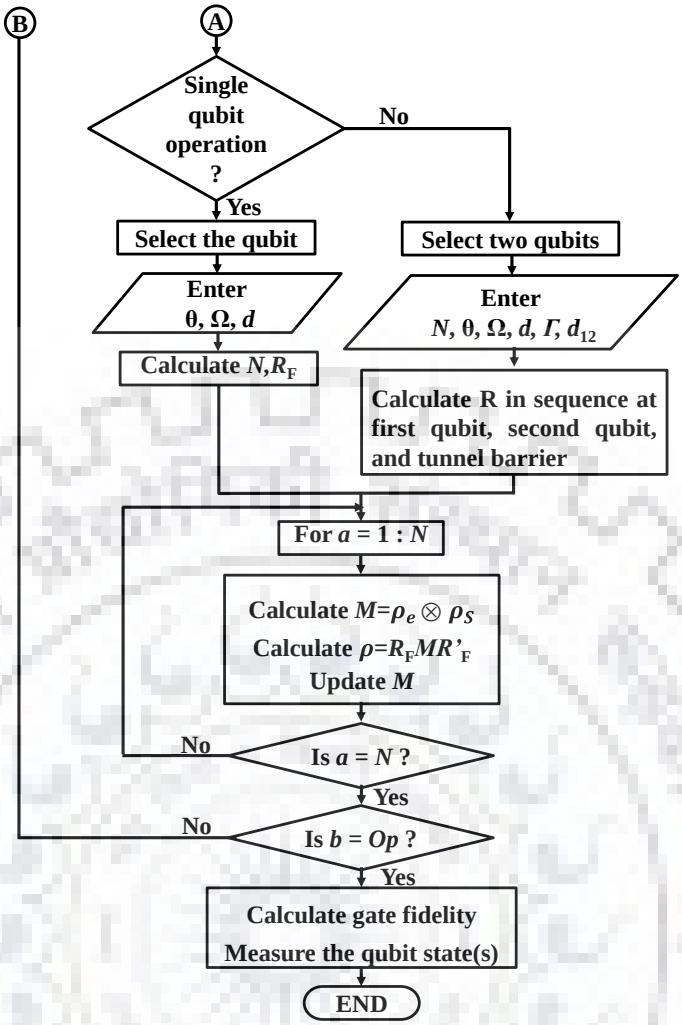

Figure 4.1 Flow chart for n-qubit reconfigurable quantum gate operations.

From the flowchart, *Op* is the number of elementary operations required to perform an *n*-qubit quantum gate, and θ is the angle of rotation, ρ_S and ρ_Q are spin density matrices representing spin states of qubit and electron, R_F is the overall spin density matrix, *d* is the qubit distance between barrier and qubit, d_{12} is the distance between two qubits, and Γ is the barrier height. Here, 1 and 2 are representing any two qubits of spin-torque based reconfigurable architecture. *N* is number of electrons required to perform single- or two-qubit operations. The physical realization and qubit state evolution of single-, two-, and three-qubit gates are presented in following subsections.

4.2.1 Realization of Single-Qubit Operations

Single-qubit gates perform specified unitary operations through controlled rotation about a specified axis. Single-qubit gates are NOT, *Z*, Hadamard, *S*, *T* etc.

NOT gate flips qubit state and Hadamard gate changes axis of qubit rotation from *x*-axis to *z*-axis and vice versa. *Z*, *S*, and *T* gates perform π, $\pi/2$, and $\pi/4$ radians rotation about *z*-axis, respectively. The NOT gate rotates the qubit by π radians about *x*-axis. In this work, Q_3 is selected to simulate Hadamard gate operation. The gate operation is performed in three steps as shown in Figure 4.2. The $|S_1\rangle$, $|S_2\rangle$, $|S_3\rangle$,…, $|S_n\rangle$ are quantum states of qubits Q_1, Q_2, Q_3,…., Q_n, respectively. Figure 4.3 and Figure 4.4 show state evolution of convention and modified Hadamard gates, respectively. The Sz_1, Sz_2, Sz_3,…., Sz_n are *z* components of states $|S_1\rangle$, $|S_2\rangle$, $|S_3\rangle$,…, $|S_n\rangle$, respectively. The initial state of $|S_3\rangle$ is $|1\rangle$.

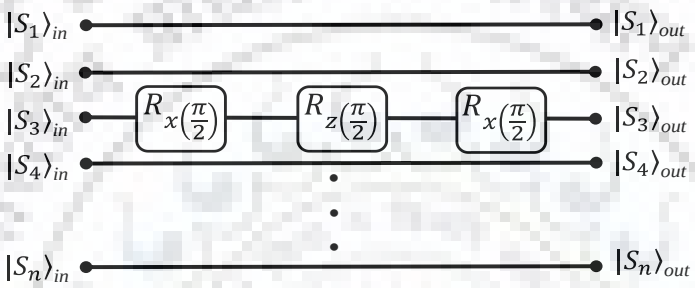

Figure 4.2 Hadamard gate.

4.2.2 Realization of Two-Qubit Operations

Two-qubit quantum gates work on the following principle: *'If A is true, then act on B*'. The two-qubit CNOT gate along with elementary single-qubit gates forms universal set of quantum gates. The SWAP gate consists of three CNOT gates in sequence to perform exchange of spin states of two qubits. Two-qubit CNOT and SWAP gates are realized by selecting Q_2 and Q_3 in *n*-qubit architecture. In the following subsections, realization of modified matrix based reduced CNOT and SWAP gates, is presented.

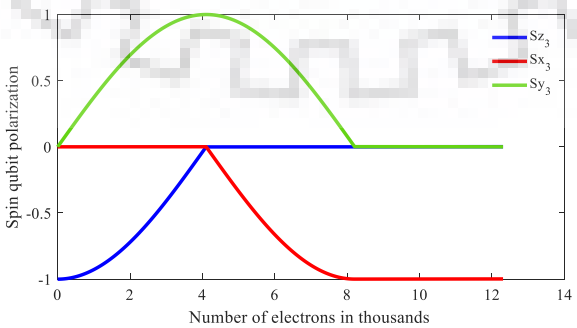

Figure 4.3 State evolution of conventional Hadamard gate.

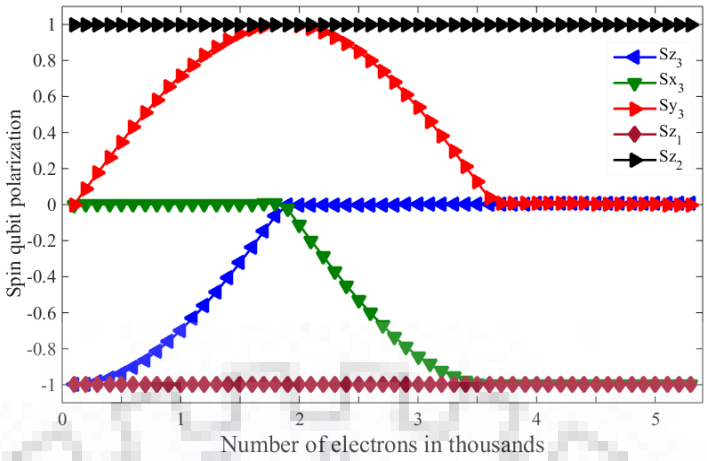

Figure 4.4 State evolution of modified Hadamard gate.

4.2.2.1 CNOT Gate

The CNOT gate is an important component of a QC architecture. The conventional decomposition of CNOT gate is shown in Figure 4.5. In addition, for higher fidelities there is a need of reduction in number of elementary operations through decomposition of CNOT gate to get rid of the obstacles of decoherence at circuit level.

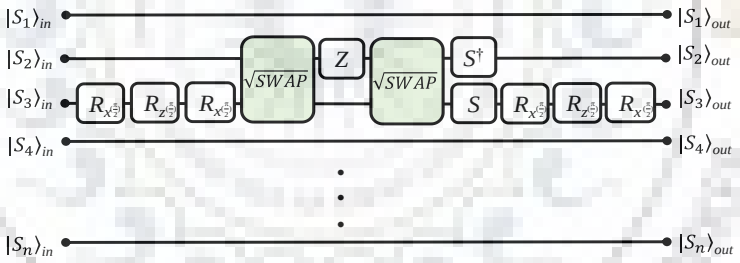

Figure 4.5 Conventional CNOT gate decomposition.

In [108], identity rules are proposed to obtain optimal quantum gate library for different physical descriptions. With the help of quantum gate library and optimal gates proposed herein, we have obtained the decomposition for the reduced CNOT gate as shown in Figure 4.6.

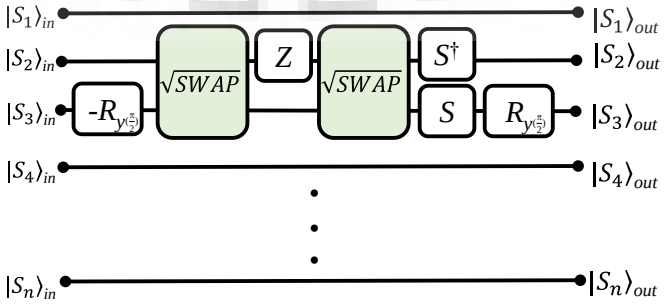

Figure 4.6 Reduced CNOT gate decomposition.

The conventional CNOT and reduced CNOT gates have 11 and 7 number of elementary operations, respectively. Figure 4.7 depicts evolution of initial state $|S_1S_2S_{3....}\rangle = |111....\rangle$ for modified matrix based reduced CNOT gate, respectively. For the reduced CNOT gate, the initial Hadamard operation is represented by the rotation of the qubit about y-axis by $\pi/2$ in counterclockwise direction. However, final Hadamard operation is represented by the rotation about y-axis by $\pi/2$ in clockwise direction. The result demonstrates that state $|S_2\rangle$ initialized to $|1\rangle$ flips state $|S_3\rangle$; and state $|S_3\rangle$ remains unchanged for state $|S_2\rangle$ initialized to $|0\rangle$.

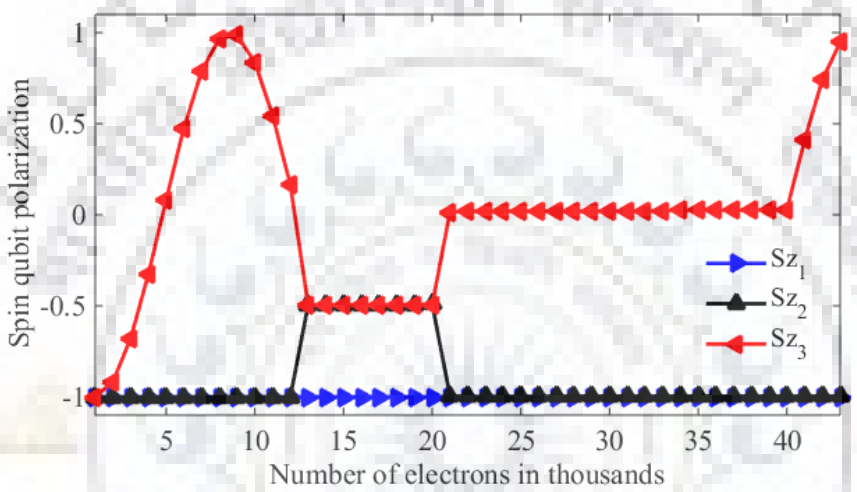

Figure 4.7 State evolution of an initial state $|S_1S_2S_3\rangle = |111\rangle$ for the modified matrix based reduced CNOT gate.

4.2.2.2 SWAP Gate

The SWAP gate consists of three CNOT gates in sequence. First, second, and third CNOT gates have qubits Q_2, Q_3, and Q_2, respectively as control qubits. The conventional decomposition of the SWAP gate is given in Figure 4.8(a). The reduced decomposition of the SWAP gate is given in Figure 4.8(b).

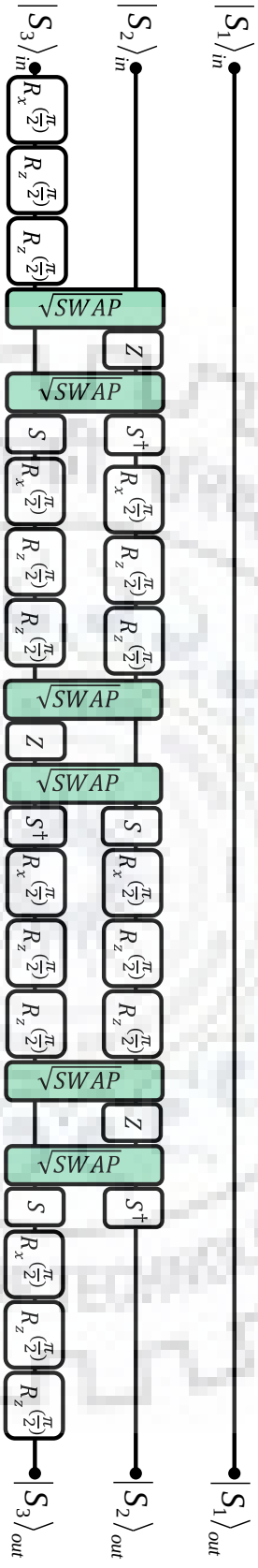
$|S_1\rangle_{in}$
$|S_2\rangle_{in}$
$|S_3\rangle_{in}$
$R_x(\frac{\pi}{2})$
$R_z(\frac{\pi}{2})$
$\sqrt{SWAP}$
Z
S
$S^\dagger$
$|S_1\rangle_{out}$
$|S_2\rangle_{out}$
$|S_3\rangle_{out}$

(a)

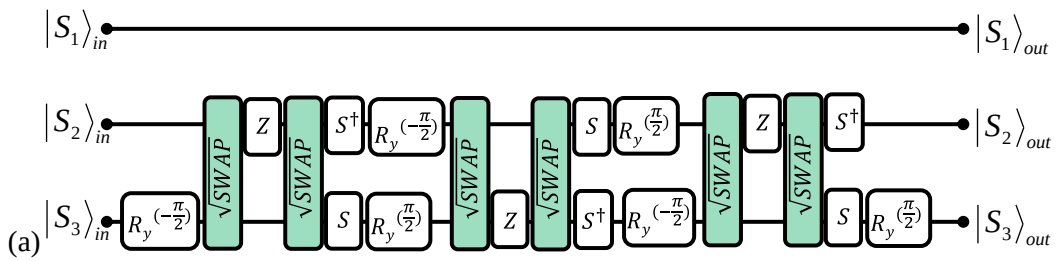

(a)

(b)

Figure 4.8 (a) Conventional decomposition of SWAP gate, (b) Reduced decomposition of SWAP gate

The SWAP gate evolution of an initial state $|10\rangle$ is shown in Figure 4.9. At the end of third stage CNOT gate state evolution, initial states of Q_2 and Q_3 are swapped and of other qubits remain in $|0\rangle$ states.

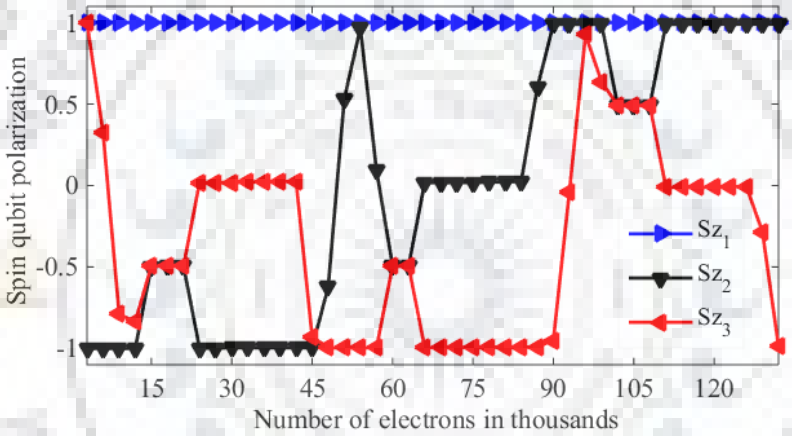

Figure 4.9 State evolution of an initial state $|S_1S_2S_3\rangle = |010\rangle$ for the modified matrix based reduced SWAP gate.

4.2.3 Realization of Three-Qubit Operations

The three-qubit gates work on the principle: *'If A and B are true, then act on C'*. Qubits are kept in isolated states except Q_1, Q_2, and Q_3 to perform three-qubit gates.

4.2.3.1 Toffoli Gate

The Toffoli gate performs CCNOT operation. In this work, Q_1 and Q_2 act as control qubits and, Q_3 acts as controlled qubit to realize three-qubit Toffoli gate. The Toffoli gate flips quantum state $|S_3\rangle$ if states $|S_1\rangle$ and $|S_2\rangle$ are in quantum $|1\rangle$ state. The conventional decomposition of the Toffoli gate is given in Figure 4.10(a). Moreover, the reduced decomposition of the Toffoli gate is presented in Figure 4.10(b).

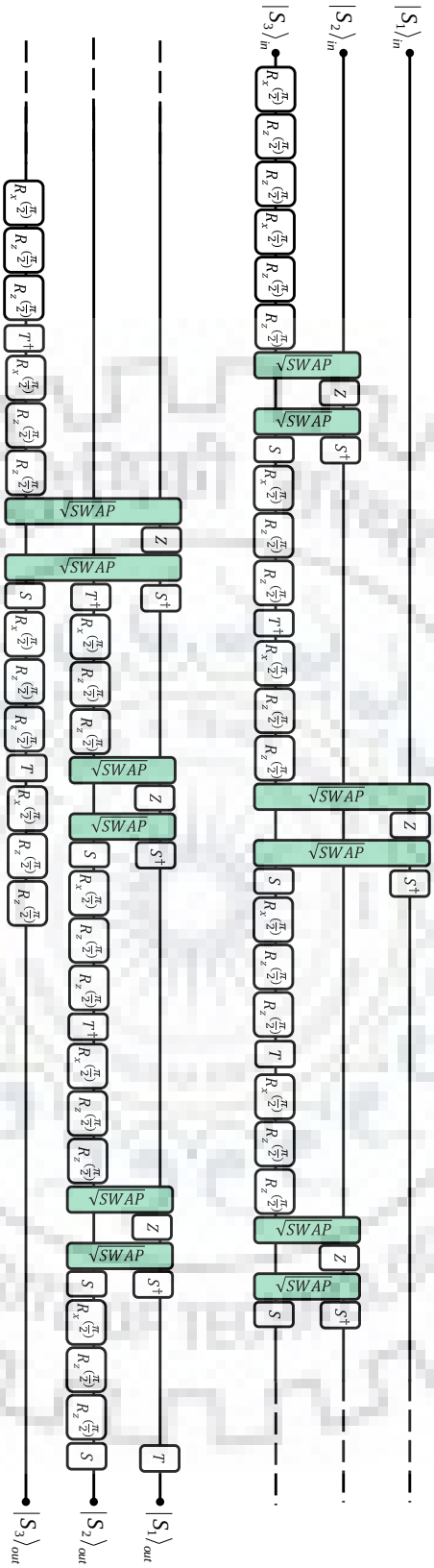
$|S_3\rangle_{in}$
$|S_2\rangle_{in}$
$|S_1\rangle_{in}$
$|S_3\rangle_{out}$
$|S_2\rangle_{out}$
$|S_1\rangle_{out}$
$R_x(\frac{\pi}{2})$
$R_z(\frac{\pi}{2})$
$\sqrt{SWAP}$
Z
S
$S^\dagger$
T
$T^\dagger$

(a)

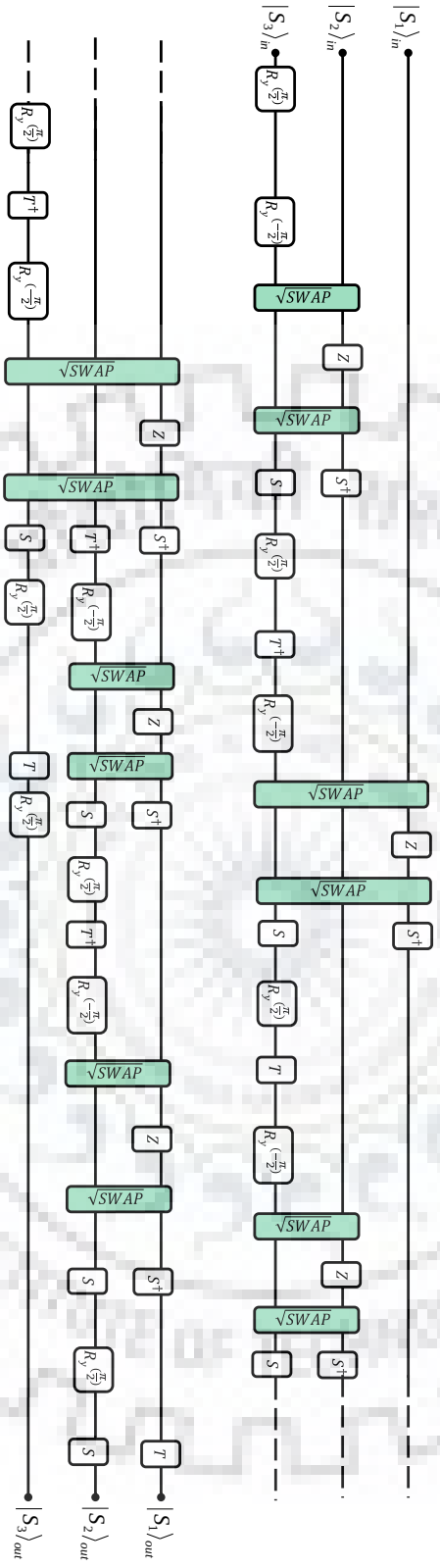

(b)

Figure 4.10 (a) Conventional decomposition of Toffoli gate (b) Reduced decomposition of Toffoli gate.

The evolution of an initial state $|111\rangle$ depicted in Figure 4.11 shows that state $|S_1S_2\rangle$ initialized to $|11\rangle$ flips state $|S_3\rangle$.

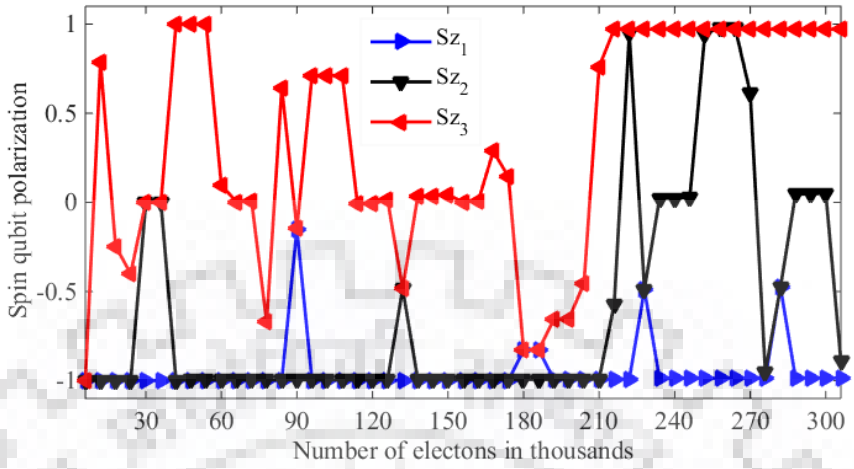

Figure 4.11 State evolution of an initial state of $|S_1S_2S_3\rangle = |111\rangle$ for the modified matrix based reduced Toffoli gate.

4.2.3.2 Fredkin Gate

Fredkin gate performs CSWAP operation. In this work, three-stage quantum circuit of Fredkin gate is simulated; first stage performs CNOT gate on qubits Q_2 and Q_3; second stage realizes Toffoli gate; and third stage performs CNOT gate on Q_1 and Q_2. For the Fredkin gate, Q_1 acts as control qubit, and Q_2 and Q_3 act as controlled qubits. Fredkin gate is also utilized in chapter 6 for the realization of reversible D-Latch. The conventional and reduced decompositions of the Fredkin gate are shown in Figures 4.12(a) and 4.12(b), respectively. The evolution of an initial state $|101\rangle$ is shown in Figure 4.13. The obtained results confirm that the state $|S_1\rangle$ initialized to $|1\rangle$ changes $|S_2S_3\rangle$ from $|01\rangle$ to $|10\rangle$.

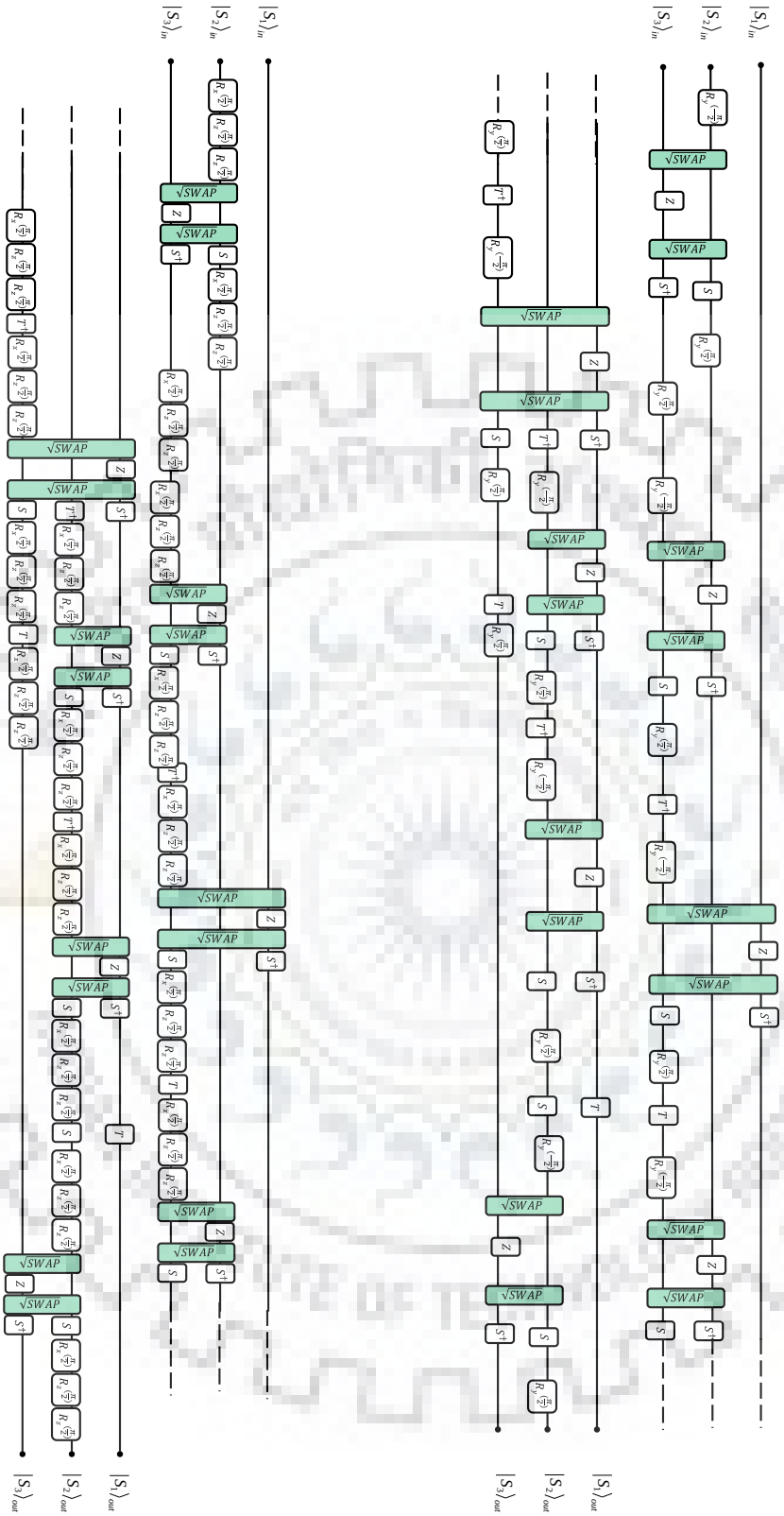

Figure 4.12 (a) Conventional decomposition of Fredkin gate (b) Reduced decomposition of Fredkin gate.

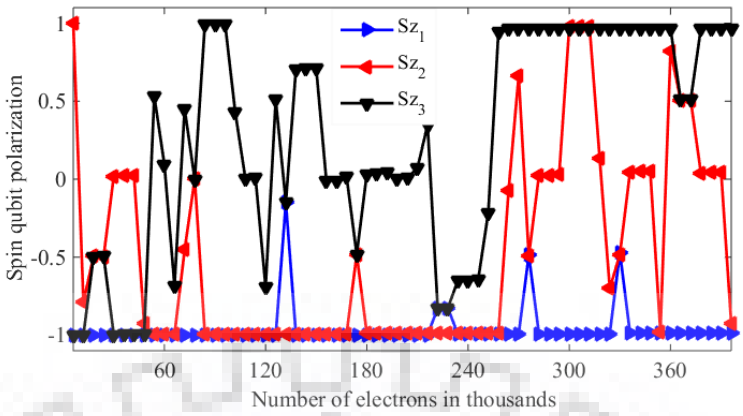

Figure 4.13 State evolution of an initial state of $|S_1S_2S_3\rangle = |101\rangle$ for the modified matrix based reduced Fredkin gate.

4.3 Performance Evaluation and Comparison

In this work, the decomposition circuits that consist of elementary operations are utilized for both forms of quantum gates i.e. conventional and reduced. Moreover, the performance is analyzed based on modified transmission coefficient matrix-based conventional and reduced forms of the quantum gates. The elementary operations comparison for each of the quantum gates realized in this work is given in Table 4.1.

Table 4.1: Gate-wise number of elementary operations (Quantum cost)

Gate	**Elementary operations**		**Reduction**
	Conventional [108]	Reduced	**(%)**
CNOT	11	7	36.36
SWAP	33	21	36.36
Toffoli	79	51	35.44
Fredkin	101	65	35.64

The comparison shows that the average reduction in number of elementary operations is ~36%. The gate execution time is very important factor from the qubit decoherence time. It is observed for reduced forms of the two-qubit and three-qubit gates that the average gate execution time is reduced by 10.58%, 13.77%, 14.30%, and 12.92% of CNOT, SWAP, Toffoli, and Fredkin gates, respectively.

The reduction in number of electrons required for realization of quantum gate is very significant from the architecture point of view. As depicted in Figure 3.1, due

to spin-generation and injection assembly, for *Op* number of quantum operations, two *Op* switching activities are required. In reduced CNOT gate, number of switching activities is considerably reduced due to 36% reduction in number of elementary operations in comparison to conventional CNOT. Moreover, it is observed for conventional and reduced gates that electrons are further decreased due to increase in $\Gamma_{Rfl} / J = 0$ (see Table 4.2). In addition, there is reduction in number of electrons required to realize a modified-matrix based conventional gate, existing matrix based reduced gate, and modified-matrix based reduced gate by 9.25%, 14.73%, and 22.64%, respectively in comparison to the first order conventional gates.

Table 4.2: $\log_{10}$ (Interacted electrons) comparison

Gate	$\Gamma_{Rfl} / J = 0$		$\Gamma_{Rfl} / J \neq 0$	
	Conventional [108]	**Reduced**	**Conventional**	**Reduced**
CNOT	4.7442	4.6747	4.7027	4.6318
SWAP	5.2213	5.1519	5.1799	5.1109
Toffoli	5.5925	5.5236	5.5492	5.4785
Fredkin	5.7009	5.6319	5.6583	5.5916

The fidelity variation is comparatively less in case of CNOT and SWAP gates. The average gate fidelity comparison of quantum gates is given in Table 4.3. The key parameters are given in Table 4.4. The CNOT and SWAP gates have gate fidelity well above the fault-tolerant fidelity. However, gate fidelity of modified-matrix based Toffoli and Fredkin gates is below the fault-tolerant fidelity that needs error correction.

There is a trade-off between fidelity and reduction in number of electrons for the second order form of quantum gates. Existing matrix-based reduced gates have higher average fidelity while modified matrix based reduced gates require minimum number of electrons. The modified matrix based reduced gates achieve both i.e. better fidelity with reduced number of electrons. Moreover, the two- and three-qubit gates are realized with the help of single-qubit rotations about y- and z-axes and two-qubit entanglement only. Therefore, quantum gate library for the spin-torque based architectures is $\{ R_y , R_z , \sqrt{\text{SWAP}} \}$.

Table 4.3: Average gate fidelity comparison

Gate	$\Gamma_{Rfl}/J = 0$		$\Gamma_{Rfl}/J \neq 0$	
	Conventional [108] **(%)**	**Reduced (%)**	**Conventional (%)**	**Reduced (%)**
CNOT	99.86	99.94	99.93	99.92
SWAP	99.59	99.68	99.51	99.61
Toffoli	99.04	99.17	98.81	98.72
Fredkin	98.74	98.96	98.13	98.72

Table 4.4: Parameters used for simulations

Symbol	Parameter	Quantity
d	Distance between qubit Q and barrier G	17.6359 nm
k	Wave number in mesoscopic systems for single qubit rotation	1.7724e8 [157]
Ω	$J/\hbar v$	$\pi/16$ [108]
Γ_{Inj}	Injection side barrier height for first order two qubit entanglement	100 [108]

4.4 Summary

Conventional and reduced quantum gates are compared for existing and modified matrices. Performance of high fidelity conventional and reduced quantum gates is evaluated with the help of quantum gate library $\{R_y, R_z, \sqrt{\text{SWAP}}\}$. The quantum gates performance is analyzed in terms of number of electrons required per gate for the electron-qubit interaction, gate fidelity, number of elementary quantum operations per gate, and gate execution time. Reconfigurability is accomplished through barrier height modulation to reduce the architecture hardware. It is observed that existing model based reduced gates have better fidelity and modified model based reduced gates require less number of electrons for the gate realization in comparison to other forms of realizations. High fidelity (~99%) of quantum gates is attained for the fault tolerant QC.

Chapter 5

Optimal Quantum Circuits Decomposition of Boolean Logic and Reversible D-Latch for Spin-Torque Based Multi-Qubit Architecture

5.1. Introduction

Researchers are intensively working on the novel technologies to meet the modern computing challenges such as power dissipation and performance [126]. The power dissipation is a key issue in applications like internet of things (IoT) [158] due to essential ultralow power operations at high speed. According to Landauer's principle [159], loss of information in irreversible process causes heat dissipation. In complementary metal oxide semiconductor (CMOS) based modern complex computing systems with high density, the heat dissipation is very high due to irreversibility. Hence, the alternate ways to realize the computing systems are essential to abate the information loss. The reduction in energy loss per bit loss of information could mitigate the problem of heat dissipation. However, this energy loss cannot go below the thermodynamic limit [160]. The other alternative would be utilization of low power and reversible computing [161-176] to circumvent the loss of information. The subsequent recourse is more significant in the epoch of transistors reaching the size of atom [177] to reduce the overall power dissipation. Therefore, with sub-nanometer technology, implementation of the CMOS based reversible Boolean logic [178] could resolve the problem of heat dissipation. However, challenges still persist as physical devices show the quantum mechanics [179] based behavior that affects the performance of metal oxide semiconductor field effect transistors (MOSFETs) in sub-nanometer scaled CMOS architectures. Moreover, for the large data processing, inherent parallelism of computing architecture is essential. Consequently, there is a need to have transpired technologies to engrave the issues such as loss of information and efficient quantum mechanics based scalable physical architectures. Therefore, the efforts are going on to develop the reversible Boolean logic circuits [180] and their modeling for physical implementation. Quantum computing (QC) [1] could be the most efficient way to realize the reversible Boolean logic due to its fundamental ineffaceable characteristic of reversibility and parallel

processing. Moreover, QC operations follow the principle of quantum mechanics which is an added advantage to realize them physically at sub-nanometer level.

Spintronics [127] emerged as a novel technology for the non-volatile memory and logic [181] that has tremendous potential for quantum computing [182], wherein electron spin can be mapped to the qubit [94]. Several spintronics based models [28, 129, 131, 136] have been proposed to realize the QC. Recently, a spin-torque based QC architecture [108] has been proposed to realize the elementary single and two-qubit operations. We have developed an elementary quantum gates library $\{R_y^{(\theta)}, R_z^{(\theta)}, \sqrt{SWAP}\}$ for the spin-torque based quantum gates, where $R_y^{(\theta)}$, $R_z^{(\theta)}$ are the rotations by an angle θ about y-axis and z-axis, respectively; and $\sqrt{SWAP}$ is the two qubit entanglement. In this chapter, the quantum gate library is utilized to design the optimal decompositions of quantum circuits representing the reversible Boolean computing blocks such as AND^R, OR^R, XOR^R, $NAND^R$, NOR^R, $XNOR^R$, half adder (HA^R), and full adder (FA^R) for the modeling of physical realization on spin-torque based QC architecture.

The exponential growth of the semiconductor industry over the years is due to the doubling of number of transistors on semiconductor chip every 18 months [183]. It results in cost reduction by 25–30% per year with increased complexity. There is an increase in power dissipation due to the scaled transistors and metal interconnects. The novel nanodevices which could implement the memory and logic on the same chip help to improve the speed. The semiconductor industry is facing several problems due to the complex computing [184]. The reasons being the transistor size reaching the size of the atom and parallel processing is required for the complex computing. Therefore, there is a need of alternatives to address these problems. Several technologies have been proposed in the past to provide the possible solutions. Quantum computing (QC) provides a suitable platform for the complex computing applications due to inherent parallel processing [1]. However, the physical realization of the quantum computing requires the technology which should imbibe quantum computing characteristics. Spintronics is one such technology which is more suitable for the quantum information processing due to electron spin analogous to the qubit [128]. However, major challenge is to preserve the spin state of the qubits for the sequential circuits due to clock cycle based operations. Therefore, in this chapter, we

have presented an optimized decomposition of the sequential circuits with the help of elementary quantum circuits. For the first time, the optimal decomposition of the sequential circuits at the elementary level is presented and realized with the help of modified transmission coefficient matrix based model for the spin-torque based qubit architecture through the iterative process. The spin-torque qubit architecture facilitates the single-qubit rotation and two-qubit entanglement through the interaction of the spin polarized electrons with the spin-qubit. The optimal decomposition of the sequential circuits reduces the number of elementary operations required for the realization of quantum circuits in comparison to the conventional decomposition.

The chapter is divided into five sections including the introduction. The section 5.2 presents the optimal decompositions of the reversible Boolean computing blocks. The performance evaluation of reversible computing blocks in terms of fidelity and number of electrons required for the realization is presented in section 5.3. The overview of reversible sequential circuits such as D- Latch, T-Latch, and Master-Slave flip-flop is presented in section 5.4. The optimized decomposition of the D-Latch and its spin qubits state evolution are elaborated in section 5.5. Finally, chapter is summarized in section 5.6.

5.2. Optimal Decomposition of Reversible Boolean Computing

The decomposition of the computing blocks depends on the physical system implementing the quantum circuit [185-186]. Therefore, physical machine description (PMD) could be different for each of the physical realizations to implement the same quantum algorithm [105]. The spin-torque based QC architecture realizes the single- and two-qubit decompositions of the quantum circuits. The elementary quantum gate library for the conventional decomposition is $\{R_x^{(\theta)}, R_z^{(\theta)}, \sqrt{SWAP}\}$.

The CNOT gate is the basic building block of the reversible Boolean computing blocks. Therefore, from the spin-torque based architecture point of view, the number of elementary operations realizing the CNOT gate is required to be reduced.

However, post-reduction, the redundant operations are required to be removed; and two sequential elementary operations about the same axis are merged as single operation through the optimization. Therefore, the quantum circuits

representing the Boolean computing blocks are further optimized as shown in Figure 5.1. Therefore, this paper considers the conventional, reduced, and optimal decompositions of the reversible computing blocks for the performance analysis.

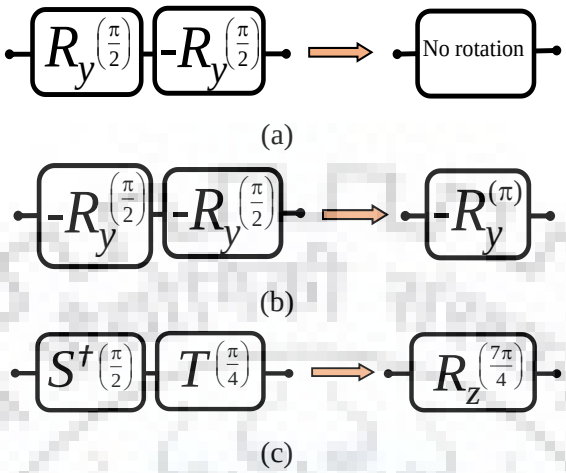

Figure 5.1 Reversible Boolean gates optimization (a) Removal of redundant single qubit rotations (b) Single rotation about y-axis by $-\pi$ (c) Single qubit rotation about z-axis by $7\pi/4$.

The gate-wise number of elementary operations for each of the optimal decompositions is shown in Table 5.1.

Table 5.1: Number of elementary operations

Computing block	Conventional decomposition	Reduced decomposition	Optimal decomposition
AND^R	79	51	49
OR^R	101	65	59
XOR^R	22	14	12
$NAND^R$	79	51	49
NOR^R	101	65	59
$XNOR^R$	22	14	12
HA^R	90	58	54
FA^R	180	116	107

In this work, we have presented only optimal decompositions of quantum circuits representing the reversible computing blocks. For the simplicity purpose, a group of elementary operations are represented by a functionally equivalent two-qubit module (shown in Figure 5.2).

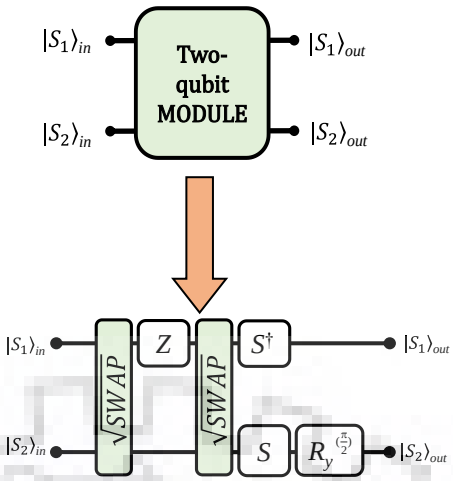

Figure 5.2 Two-qubit module.

The Z, *S*, $S^\dagger$ rotate single qubit by an angle of π, π/2, and –π/2, respectively about the z-axis. The optimal decompositions of quantum circuits representing elementary two-input XOR^R, AND^R, and OR^R gates are shown in Figure 5.3, Figure 5.4, and Figure 5.5, respectively. The *T* and $T^\dagger$ gates are single qubit rotations about z-axis by an angle of π/4 and –π/4, respectively.

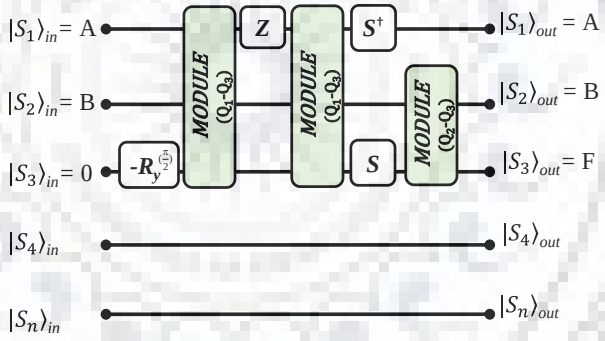

Figure 5.3 QC based optimal XOR^R gate.

For the realization of the two-input reversible Boolean gates, the Qubits Q_1, Q_2, and Q_3 are employed to perform the quantum operations and remaining qubits are kept isolated. The initial quantum states of $|S_1\rangle$, $|S_2\rangle$, and $|S_3\rangle$ are represented by inputs *A*, *B*, and 0, respectively. A quantum NOT gate is required to be added at Q_3 of each of the gates as shown in Figure 5.3, Figure 5.4, and Figure 5.5 to realize reversible XNOR^R, NAND^R, and NOR^R, respectively.

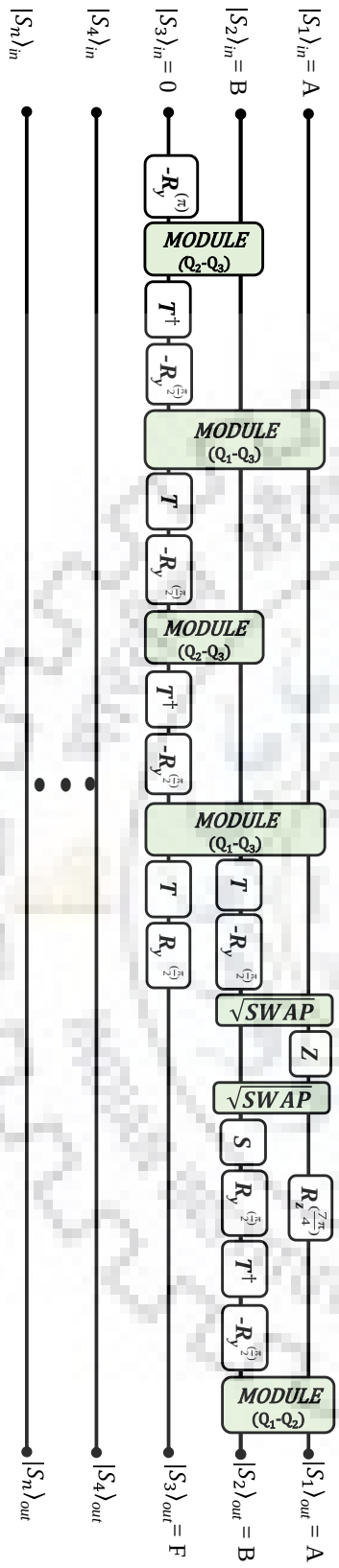

Figure 5.4 QC based optimal AND^R gate.

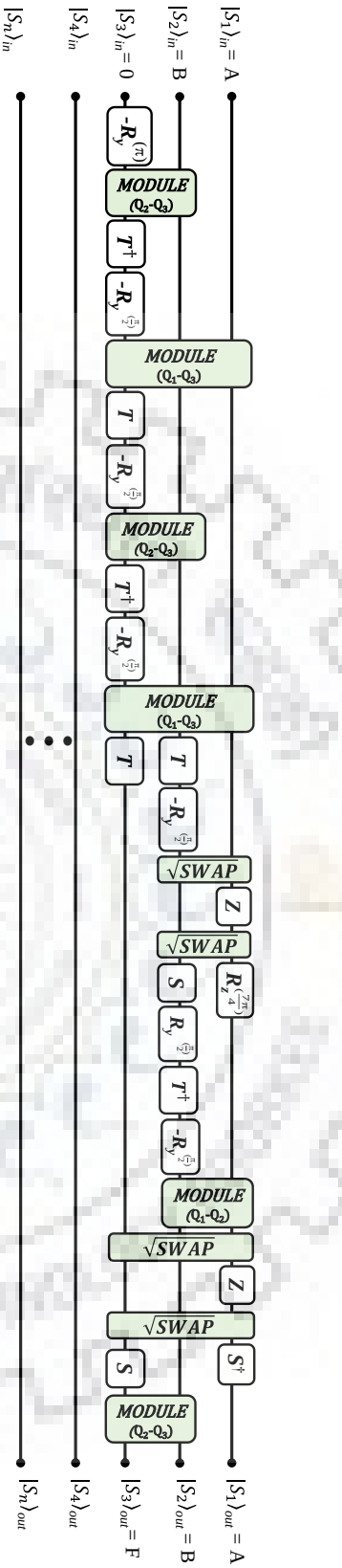

Figure 5.5 QC based optimal OR^R gate.

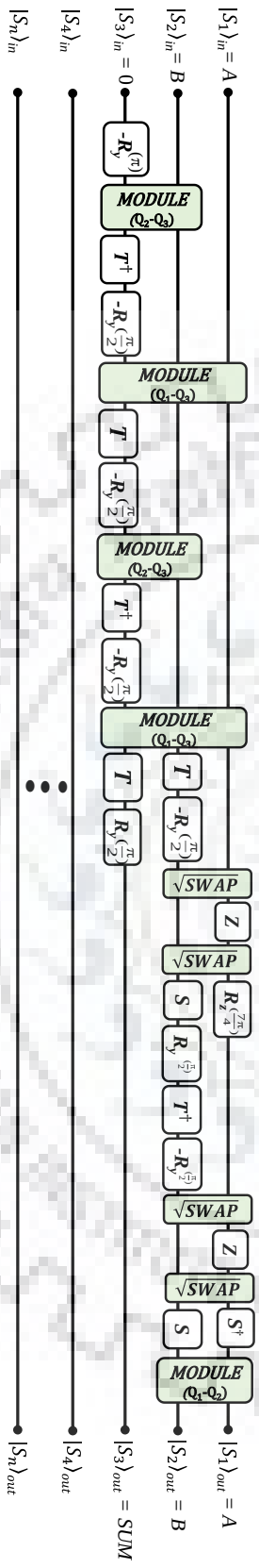

Figure 5.6 QC based optimal HA^{R}.

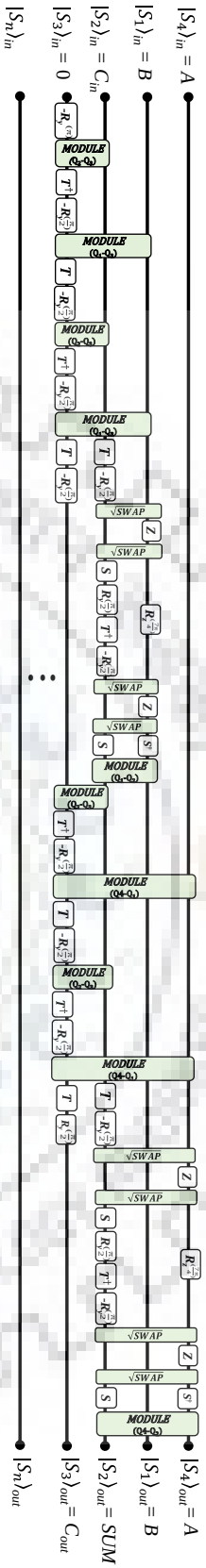

Figure 5.7 QC based optimal FA^{R}.

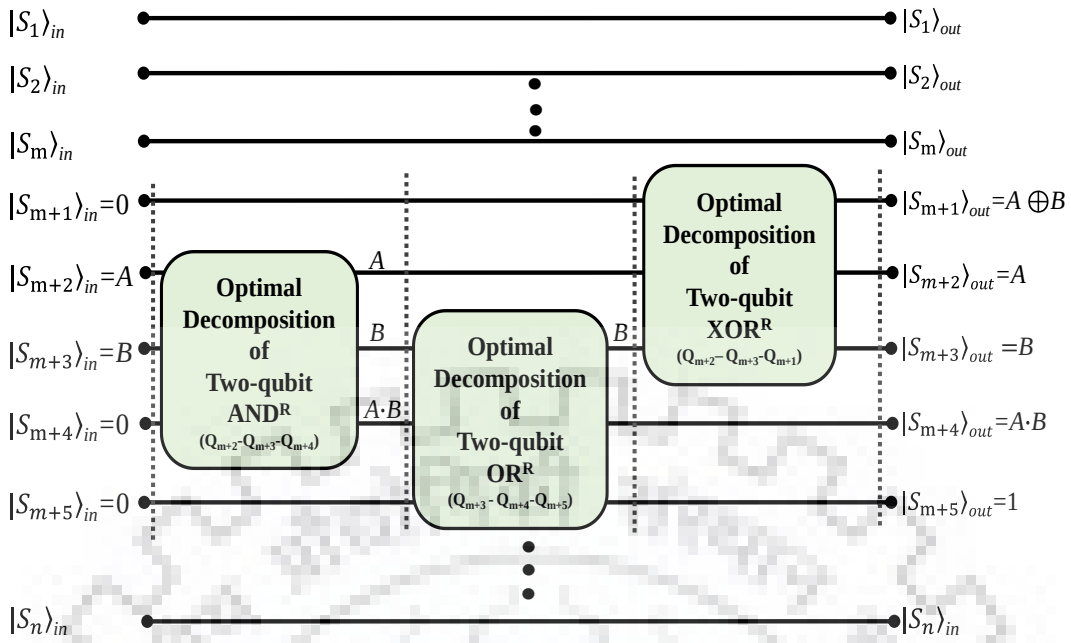

Figure 5.8 QC based optimal reversible Boolean logic.

The reversible half adder (HA^R) and full adder (FA^R) constitute the basic building blocks of reversible computing. The optimal decomposition of the HA^R is shown in Figure 5.6. Similar to the elementary Boolean gates realization, qubits Q_1, Q_2 and Q_3 are selected to realize the HA^R. For the FA^R (Figure 5.7), the operations are carried out on qubits Q_1, Q_2, Q_3, and Q_4. A sequence of reversible Boolean logic computing blocks is shown in Figure 5.8 to realize different logic blocks. It requires 202 conventional decompositions, 130 reduced decompositions, and 120 optimal decompositions for the realization. The interconnection of optimal computing blocks may need further optimization depending on the redundant elementary operations at the interface of the blocks. However, the sequence of reversible Boolean computing blocks shown in Figure 5.8 does not need further optimization.

5.3. Performance Evaluation of Reversible Boolean Computing

The performance of reversible Boolean logic computing blocks is evaluated in terms of number of switching activities of the transistors T_1 and T_2 (shown in Figure 5.9) to generate and inject the non-local spins into the semiconductor channel for the qubit rotation; and fidelity deviation of each of the computing block from the fault tolerant fidelity.

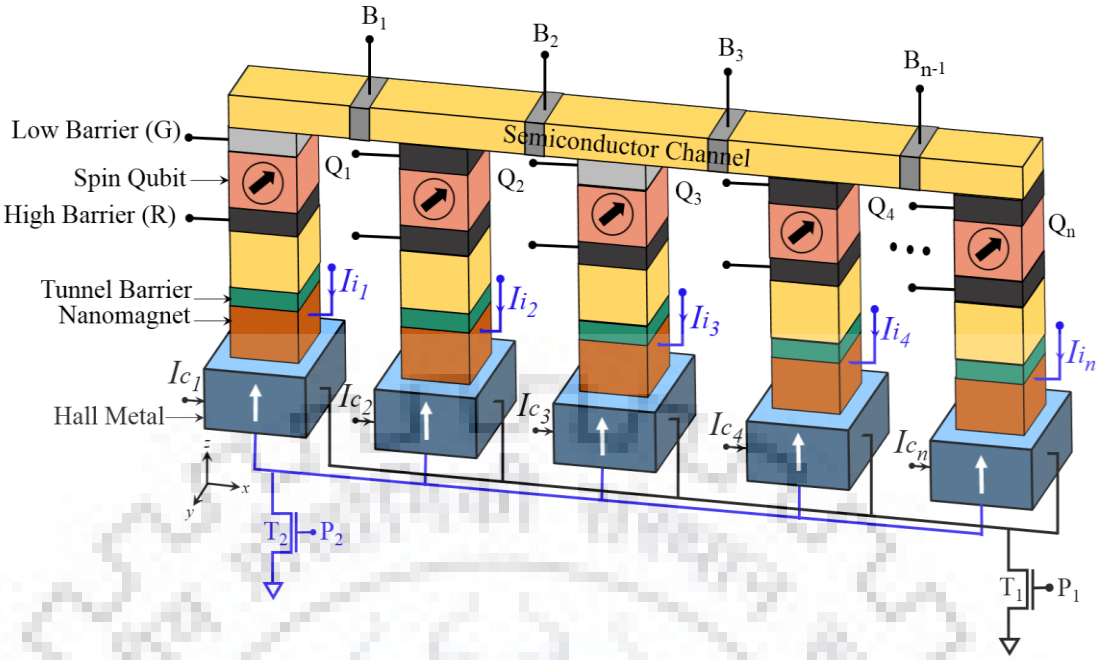

Figure 5.9 Spin qubit architecture.

In comparison to conventional decomposition, the reduction in number of switching activities of the transistors T_1 and T_2 to realize the optimal decompositions of the reversible computing blocks AND^R, OR^R, XOR^R, $NAND^R$, NOR^R, $XNOR^R$, HA^R, and FA^R is 37.97% ,41.58%, 45.45%, 37.97%, 41.58%, 45.45%, 40%, and 40.55%, respectively. We envision a decrease in power dissipation due to reduction in number of switching activities. The state evolution of the computing blocks considered for the analysis in this chapter for the second order optimal decomposition of respective computing blocks is shown in Figure 5.10 to Figure 5.17, where 1 and -1 represent the quantum logic states $|0\rangle$ and $|1\rangle$, respectively.

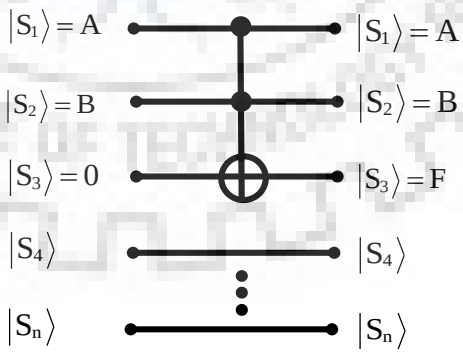

(a)

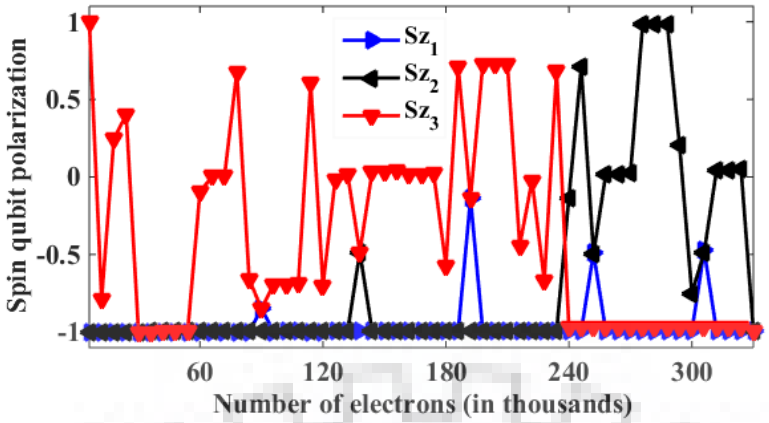

(b)

Figure 5.10 AND^{R} (a) Quantum circuit and (b) Spin qubit state evolution.

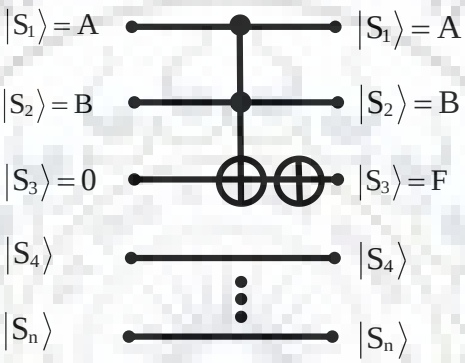

(a)

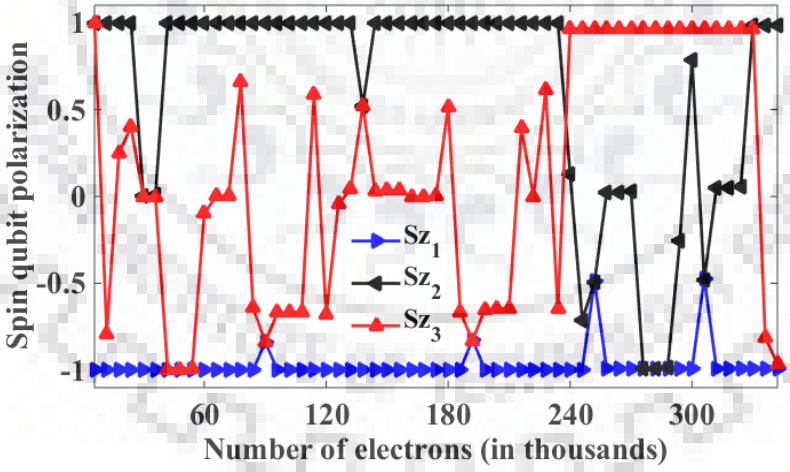

(b)

Figure 5.11 NAND^{R} (a) Quantum circuit and (b) Spin qubit state evolution.

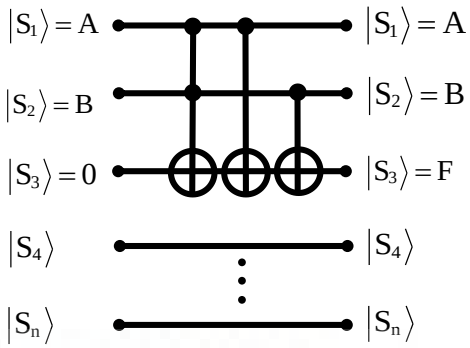

(a)

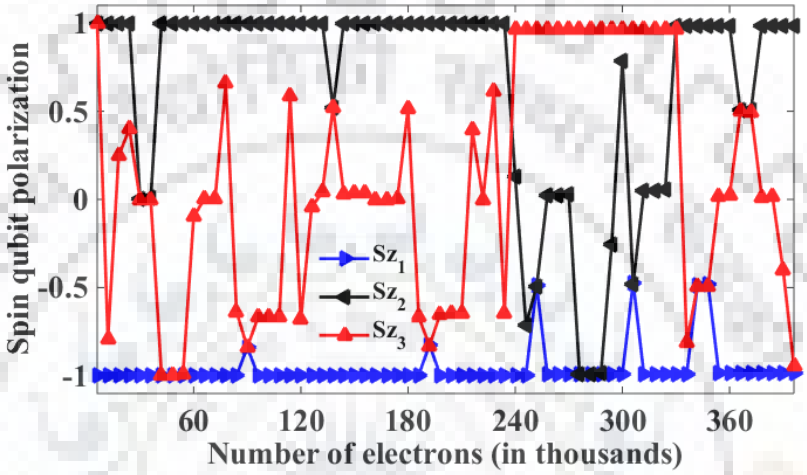

(b)

Figure 5.12 OR^R (a) Quantum circuit and (b) Spin qubit state evolution.

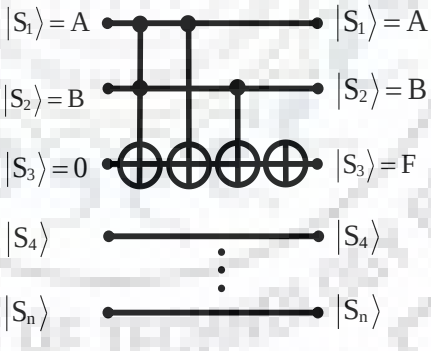

(a)

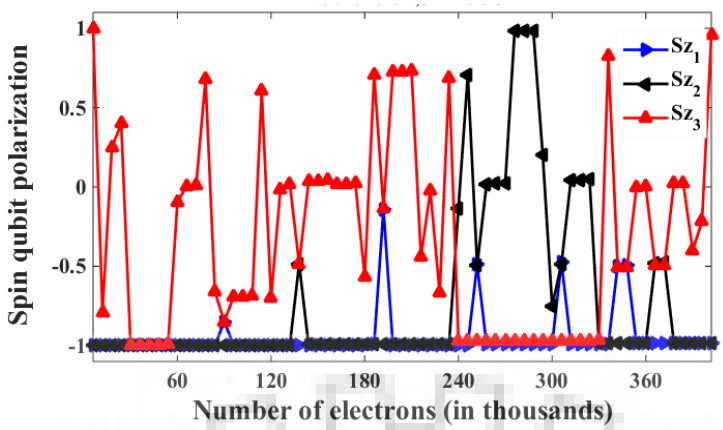

(b)

Figure 5.13 NOR^{R} (a) Quantum circuit and (b) Spin qubit state evolution.

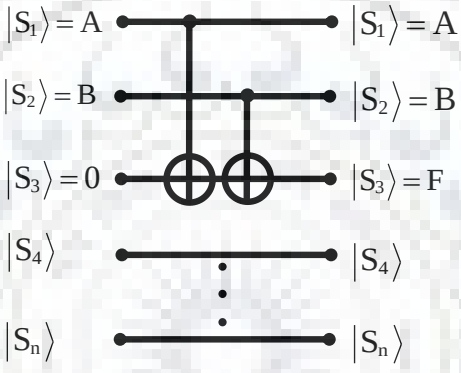

(a)

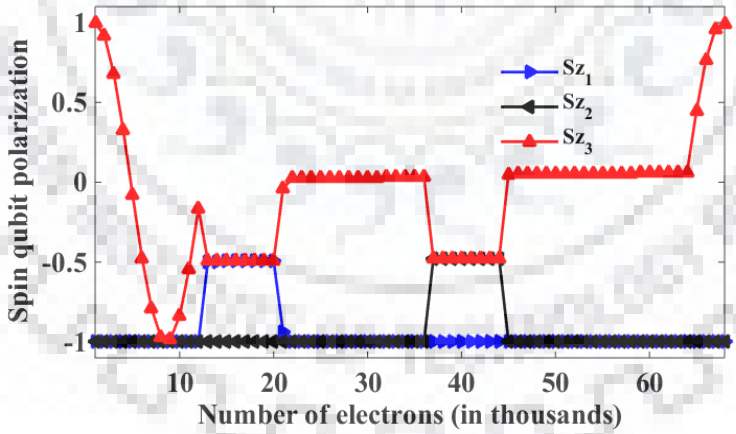

(b)

Figure 5.14 XOR^{R} (a) Quantum circuit and (b) Spin qubit state evolution.

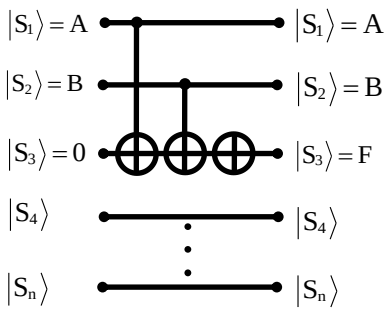

(a)

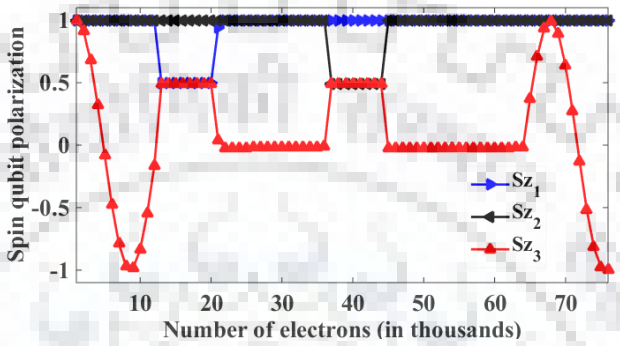

(b)

Figure 5.15 XNOR^{R} (a) Quantum circuit and (b) Spin qubit state evolution.

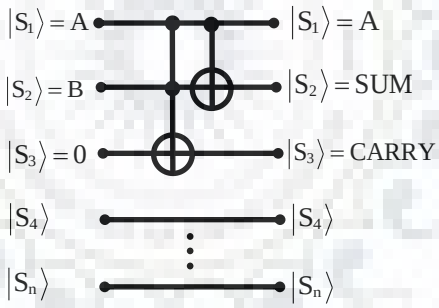

(a)

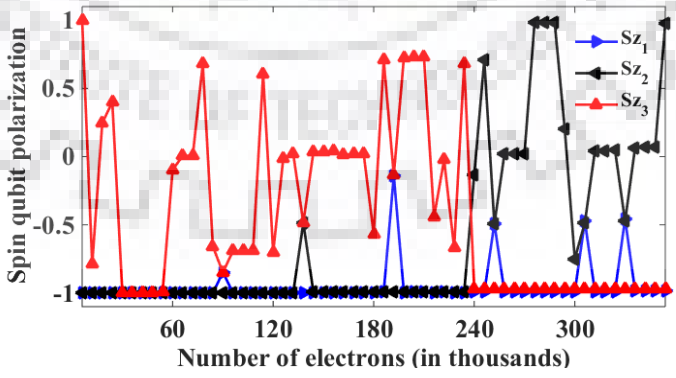

(b)

Figure 5.16 HA^{R} (a) Quantum circuit and (b) Spin qubit state evolution.

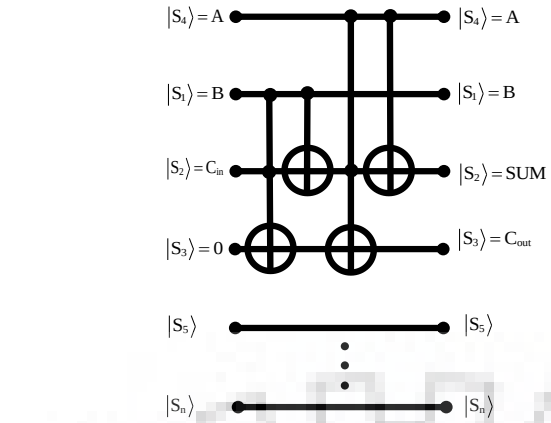

(a)

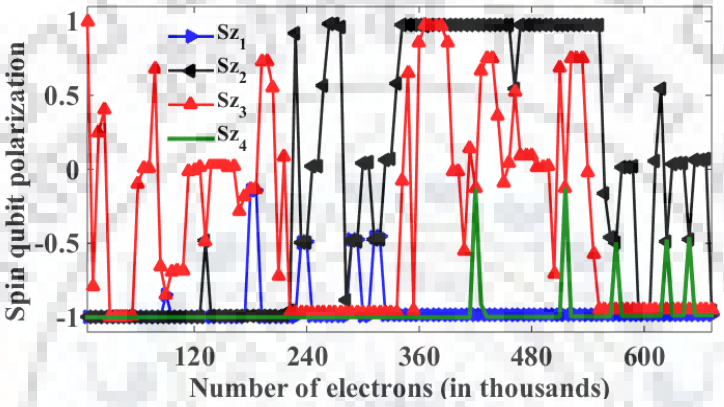

(b)

Figure 5.17 FA^{R} (a) Quantum circuit and (b) Spin qubit state evolution.

A comparison of number of electrons required to realize each of the computing blocks by first and second order conventional, reduced, and optimal decompositions is depicted in Table 5.2. It shows that the second order optimal decomposition requires a minimum number of electrons for the computing block realization due to second order singlet and triplet transmission coefficients and reduced number of elementary operations.

Table 5.2: Gate-wise number of interacted electrons

	$\log_{10}$(Number of electrons interaction)					
	First order conventional	**First order reduced**	**First order optimal**	**Second order conventional**	**Second order reduced**	**Second order optimal**
AND^R	5.59	5.56	5.54	5.52	5.56	5.52
OR^R	5.69	5.66	5.65	5.61	5.64	5.58
XOR^R	5.03	5.00	4.98	4.95	4.87	4.82
$NAND^R$	5.60	5.57	5.55	5.53	5.57	5.53
NOR^R	5.70	5.66	5.65	5.62	5.63	5.60
$XNOR^R$	5.06	5.00	5.02	4.95	4.92	4.87
HA^R	5.64	5.60	5.60	5.55	5.58	5.54
FA^R	5.92	5.88	5.90	5.84	5.86	5.82

The average fidelities obtained for reversible computing blocks are shown in Table 5.3. There is an improvement in gate fidelity for optimal decomposition of computing blocks in comparison to the reduced decomposition. The performance evaluation of HA^R and FA^R circuits is prerequisite to meet the future computing challenges. There is improvement in the fidelity of the optimal decompositions in comparison to the reduced decompositions. However, there is a considerable reduction in fidelity of FA^R in comparison to the HA^R fidelity for all forms of the decompositions due to large number of elementary operations required to realize the FA^R and needs error correction.

Table 5.3: Average gate fidelity comparison

	Fidelity (%)					
	First order conventional	**First order reduced**	**First order optimal**	**Second order conventional**	**Second order reduced**	**Second order optimal**
AND^R	99.25	99.04	99.04	99.09	98.88	98.88
OR^R	99.03	98.86	98.89	98.82	98.67	98.70
XOR^R	99.76	99.80	99.83	99.70	99.75	99.79
HA^R	99.13	98.95	98.98	98.93	98.75	98.79
FA^R	98.14	98.01	98.07	97.71	97.58	97.65

Table 5.4: Parameters used for simulations [108]

Symbol	Quantity
kx_0 for single qubit rotation	π
kx_0 for two-qubit entanglement	$\pi/2$
kx_{12} for two-qubit entanglement	π
$\Omega = J/\hbar v$	$\pi/16$
Γ_{Inj} for first order two-qubit entanglement	100

5.4. Reversible Sequential Circuits

Sequential circuit constitutes an important part of the digital logic. Unlike a combinational circuit, its output depends on the present values of the inputs as well as the past values of the outputs. In digital circuits, almost all logic devices are the mixture of combinational and sequential circuits. The major obstacles in realizing the sequential circuits are clock cycle based operation and irreversibility resulting in loss of information. According to Landauer's principle, there is heat dissipation due to loss of information [159]. For one bit loss of information, the heat dissipation is $kT \ln 2$ where k and T are the Boltzmann's constant and temperature, respectively. The absence of loss of information represents the thermodynamically reversible system. A reversible sequential circuit is one of the possible solutions to avoid the loss of information [187]. However, the design of reversible sequential circuits is a challenging task for the researchers working in the area of reversible logic design. The reason being, the one-to-one mapping of the qubit states in the presence of the clock cycles. Moreover, an extra hardware is required for one-to-one mapping. Therefore, the major focus is on the reduction of the hardware required to realize the reversible sequential logic. In the past, the reversible circuits are realized with the help of the transistors. However, the number of transistors required to realize the reversible circuits was very huge in comparison to their irreversible counterparts. Several designs have been presented for the reversible sequential circuits [188-191]. The quantum gates based reversible sequential circuits such as D-Latch, T-Latch, and Master-Slave flip-flop [190] are given in Figure 5.18, Figure 5.19, and Figure 5.20,

respectively. For the reconfigurable spin-torque based architecture, the reduction in number of elementary single-qubit rotations and two-qubit entanglements required to realize the Fredkin gate based sequential circuits is necessary. In chapter 4, the reduced decomposition of the Fredkin gate is presented. In this chapter, modeling of the spin-torque based physical realization of the D-Latch is presented through the optimal decomposition.

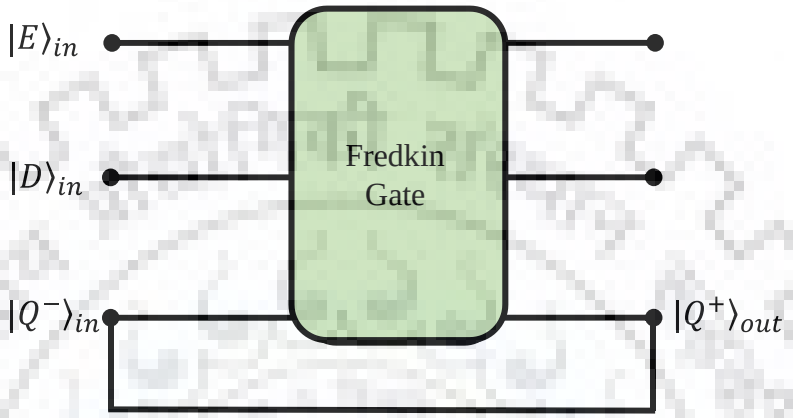

Figure 5.18 Reversible D-Latch.

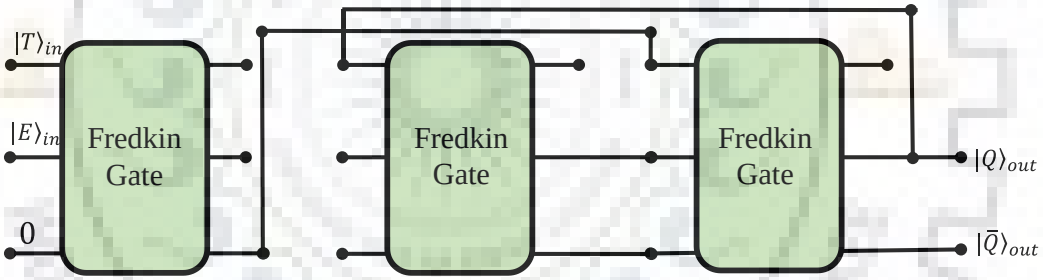

Figure 5.19 Reversible T-Latch.

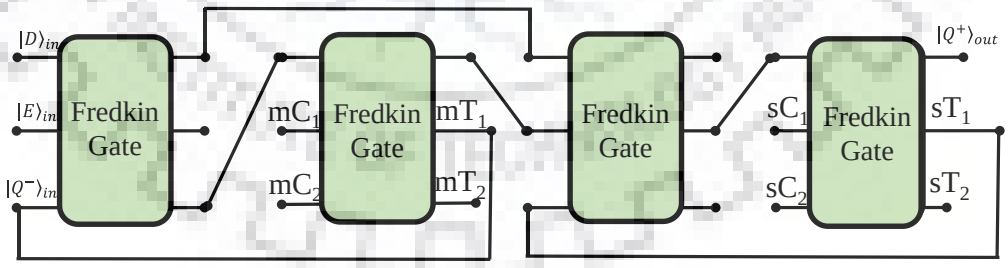

Figure 5.20 Reversible Master Slave Flip-Flop.

The Fredkin gate shown in these figures is a reversible quantum gate. Moreover, it is the basic constituent of the reversible gate. The quantum circuit

representing the Fredkin gate is shown in Figure 5.21. It is a sequence of CNOT-Toffoli-CNOT gates. The truth table for the Fredkin gate is given in Table 5.5.

5.5. Optimized Decomposition of Reversible D-Latch for Spin-Torque based *n*-Qubit Architecture

The optimization technique to reduce the number of elementary operations is presented in [9] as shown in Figure 5.22.

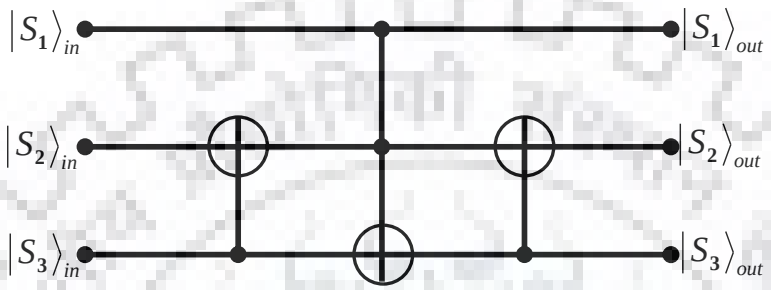

Figure 5.21 Quantum circuit for Fredkin gate.

Table 5.5: Truth table for the Fredkin gate

Input qubit states			**Output qubit states**		
$\|S_1\rangle_{in}$	$\|S_2\rangle_{in}$	$\|S_3\rangle_{in}$	$\|S_1\rangle_{out}$	$\|S_2\rangle_{out}$	$\|S_3\rangle_{out}$
$\|0\rangle$	$\|0\rangle$	$\|0\rangle$	$\|0\rangle$	$\|0\rangle$	$\|0\rangle$
$\|0\rangle$	$\|0\rangle$	$\|1\rangle$	$\|0\rangle$	$\|0\rangle$	$\|1\rangle$
$\|0\rangle$	$\|1\rangle$	$\|0\rangle$	$\|0\rangle$	$\|1\rangle$	$\|0\rangle$
$\|0\rangle$	$\|1\rangle$	$\|1\rangle$	$\|0\rangle$	$\|1\rangle$	$\|1\rangle$
$\|1\rangle$	$\|0\rangle$	$\|0\rangle$	$\|1\rangle$	$\|0\rangle$	$\|0\rangle$
$\|1\rangle$	$\|0\rangle$	$\|1\rangle$	$\|1\rangle$	$\|1\rangle$	$\|0\rangle$
$\|1\rangle$	$\|1\rangle$	$\|0\rangle$	$\|1\rangle$	$\|0\rangle$	$\|1\rangle$
$\|1\rangle$	$\|1\rangle$	$\|1\rangle$	$\|1\rangle$	$\|1\rangle$	$\|1\rangle$

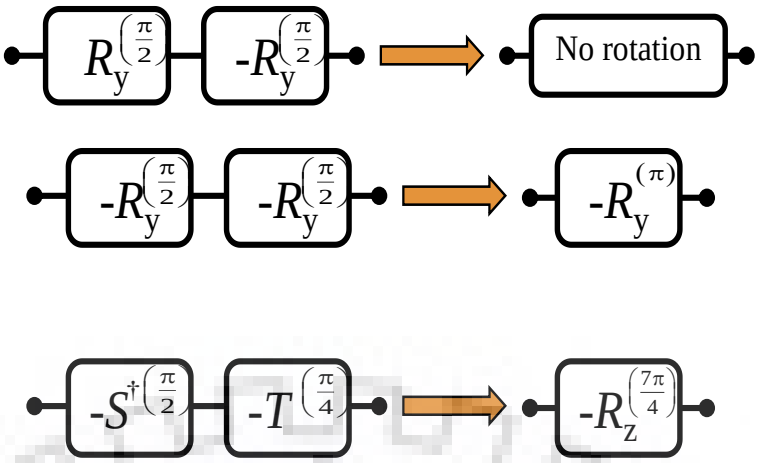

Figure 5.22 Optimization technique.

The decomposition of the reversible D-latch is achieved with the help of optimization technique (Figure 5.23).

With the help of optimization techniques, the number of elementary operations required for the realization of quantum circuits are considerably reduced. It helps in reducing the time required to realize a quantum circuit. The flowchart for the D-Latch realization with the help of transmission coefficient matrix based model is presented in Figure 5.24.

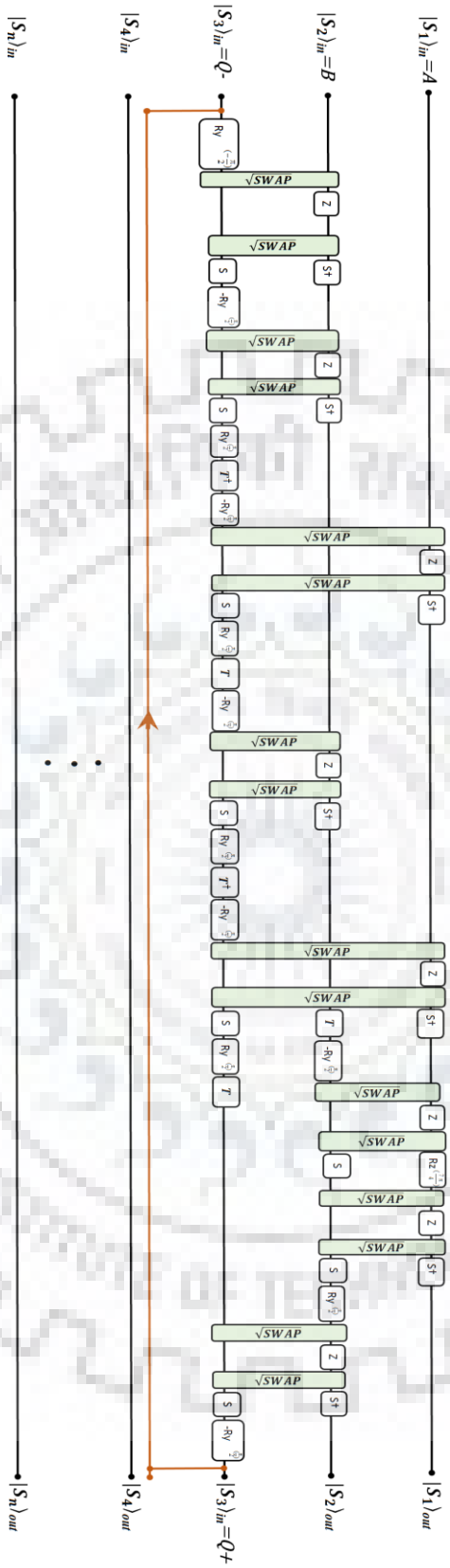

Figure 5.23 Optimal decomposition of reversible D-latch.

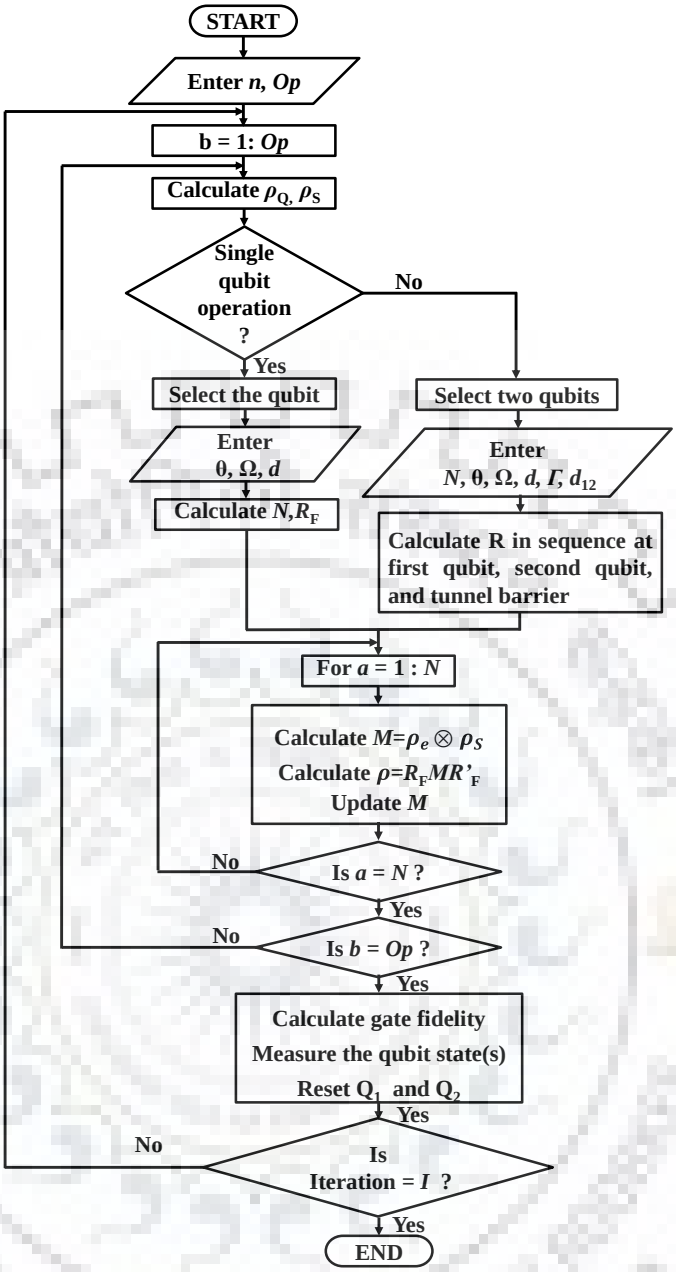

Figure 5.24 Flowchart for the spin-torque based reversible D-Latch.

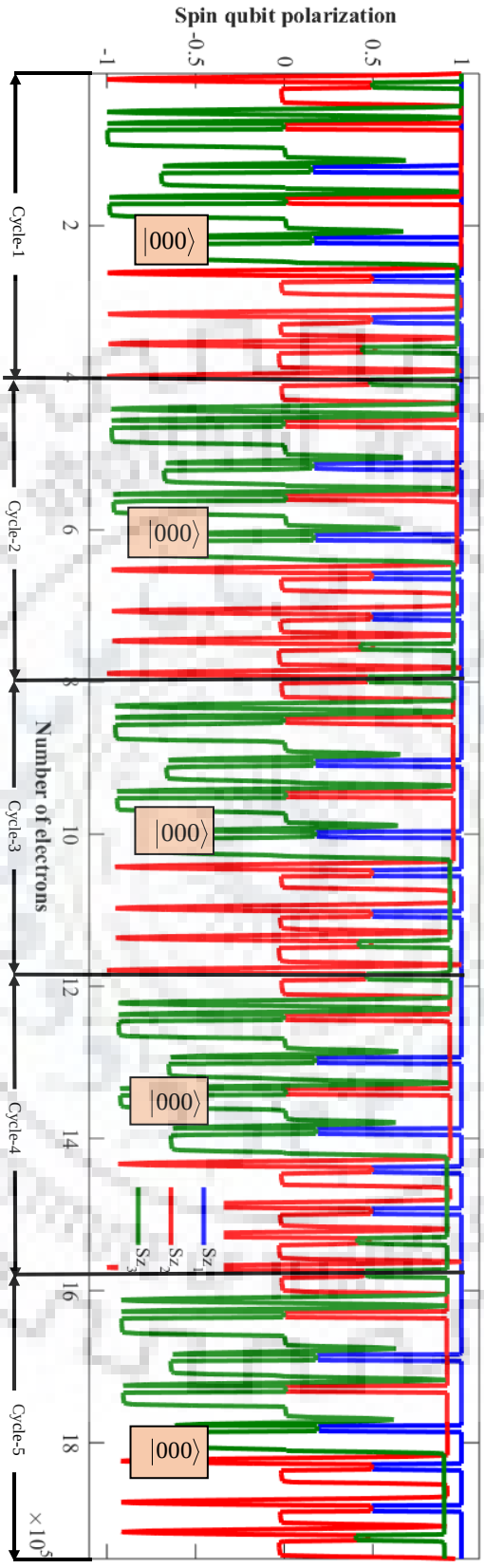

Figure 5.25 D-Latch state evolution for D=0, E=0, QPRV=0 (RESET).

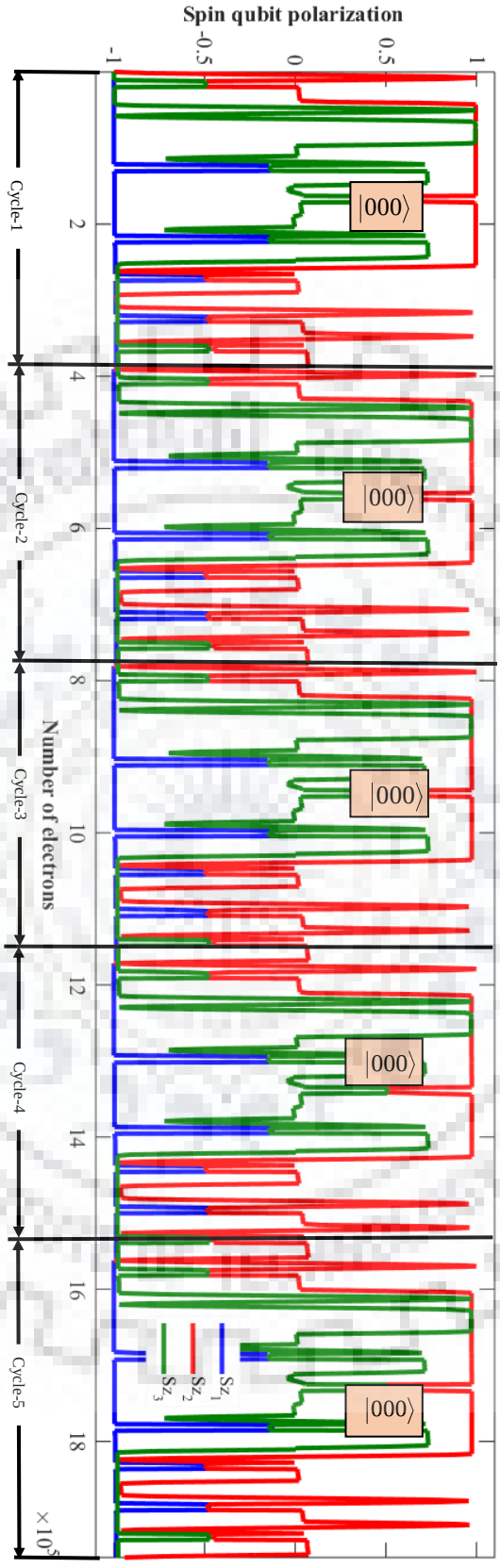

Figure 5.26 D-Latch state evolution for D=1, E=1, QPRV=1 (SET).

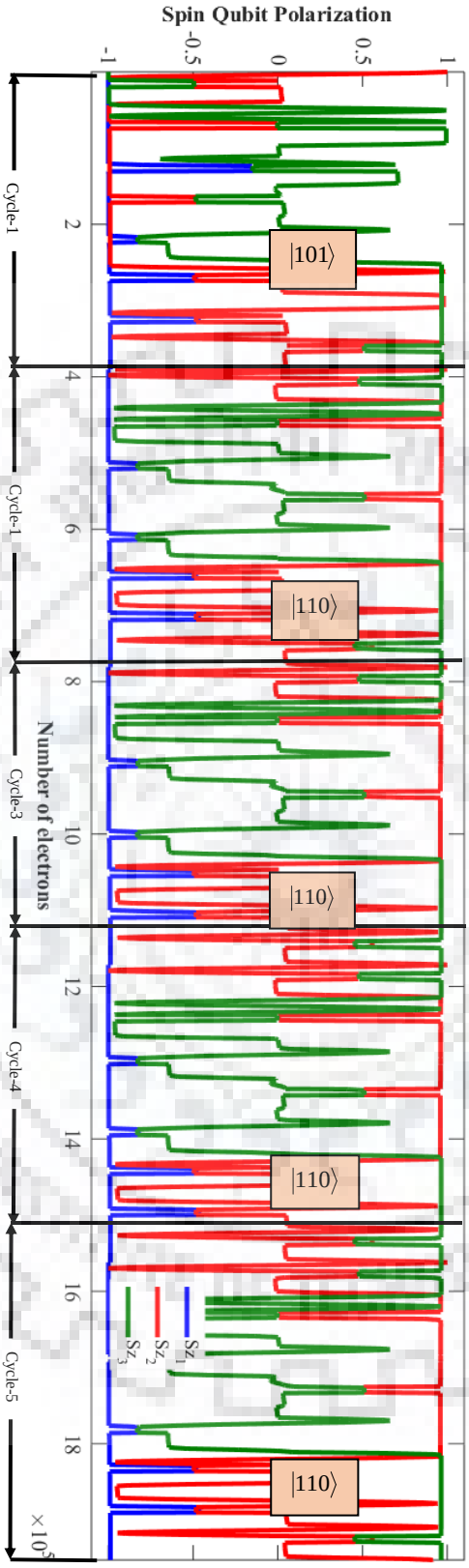

Figure 5.27 D-Latch state evolution for D=1, E=0, QPRV=1.

The present state output is given as input for the next state through the iterative process. The state evolution of the three-qubits utilized for the realization of the D-Latch is depicted in Figure 5.25, Figure 5.26, and Figure 5.27.

The fidelity comparison for the first order conventional and second order optimal decomposition for each of the 5 cycles is given in Table 5.6. It is observed that there is a slight reduction in the fidelity as number of cycles is increasing which results in small but incremental error at the end of each clock cycle. Therefore, we have approximated the obtained output at the end of each cycle for the error correction. The D-Latch with error correction is shown in Figure 6.11. It is observed that there is an improvement in the fidelity of the D-Latch. The fidelity comparison after the approximation is presented in Table 5.7. Therefore, there is a need of additional quantum circuits in feedback path for the error correction.

Table 5.6: Fidelity comparison without output state error correction

Inputs (DEQ_{PRV})	**Cycle 1**		**Cycle 2**		**Cycle 3**		**Cycle 4**		**Cycle 5**	
	1^{st} order Conv.	2^{nd} order opt.	1^{st} order Conv.	2^{nd} order opt.	1^{st} order Conv.	2^{nd} order opt.	1^{st} order Conv.	2^{nd} order opt.	1^{st} order Conv.	2^{nd} order opt.
000	99.52	99.09	99.29	98.55	99.06	98.07	98.84	97.63	98.62	97.24
001	98.22	98.83	97.16	98.20	96.12	97.52	95.09	96.79	94.08	96.01
010	99.01	98.70	98.78	98.09	98.55	97.51	98.34	96.94	98.12	96.40
011	98.62	98.99	97.55	98.37	96.50	97.74	95.47	97.12	94.45	96.50
100	99.05	98.44	98.68	97.50	98.67	97.51	98.67	97.51	98.67	97.51
101	98.51	98.58	98.49	98.58	98.45	98.58	98.42	98.58	98.41	98.58
110	98.51	98.58	98.51	98.58	98.51	98.58	98.51	98.58	98.51	98.58
111	98.33	99.09	97.29	98.15	97.29	98.15	97.29	98.15	97.29	98.15

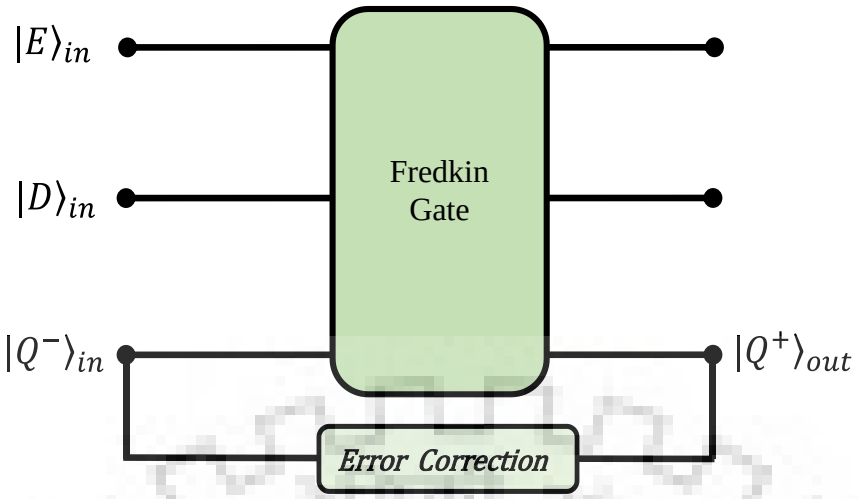

Figure 5.28 D-Latch with error correction.

Table 5.7: Fidelity comparison with output state error correction

Inputs (DEQ_{PRV})	Cycle 1		Cycle 2		Cycle 3		Cycle 4		Cycle 5	
	1st order Conv.	2nd order opt.	1st order Conv.	2nd order opt.	1st order Conv.	2nd order opt.	1st order Conv.	2nd order opt.	1st order Conv.	2nd order opt.
000	99.52	99.09	99.52	99.09	99.52	99.09	99.52	99.09	99.52	99.09
001	98.22	98.83	98.22	98.83	98.22	98.83	98.22	98.83	98.22	98.83
010	99.01	98.70	99.01	98.70	99.01	98.70	99.01	98.70	99.01	98.70
011	98.62	98.99	98.62	98.99	98.62	98.99	98.62	98.99	98.62	98.99
100	99.05	98.44	99.05	98.44	99.05	98.44	99.05	98.44	99.05	98.44
101	98.51	98.58	98.51	98.58	98.51	98.58	98.51	98.58	98.51	98.58
110	98.51	98.58	98.51	98.58	98.51	98.58	98.51	98.58	98.51	98.58
111	98.33	99.09	98.33	99.09	98.33	99.09	98.33	99.09	98.33	99.09

5.6. Summary

Semiconductor industry is facing two-fold challenge at sub-nanometer level. First, the high power dissipation in irreversible computing architectures due to information loss. Second, inability to handle large data due to sequential information processing. These issues create obstacles in producing the presumed low power complex computing outcomes. The heat dissipation can be reduced by utilizing the CMOS based reversible computing architectures. However, these architectures fail to

enhance the performance owing to inability to process large data. QC can circumvent these problems due to its fundamental ineffaceable characteristics of quantum mechanics based reversible computing and parallelism. Spin-torque based physical realization is the most suitable platform for reversible computing due to the electron spin analogous to the qubit. However, optimal quantum circuits are required to physically realize the complex Boolean logic due to spin-qubit decoherence and reduce the number of transistor switching activities for the spin generation and injection required for the spin-qubit rotation. Therefore, in this chapter, optimal quantum circuit decompositions are presented with the help of developed elementary quantum library $\{R_y^{(\theta)}, R_z^{(\theta)}, \sqrt{SWAP}\}$ for the spin-torque based QC architecture. The reversible Boolean logic performance is analyzed and compared for the conventional, reduced, and optimal decompositions on first and second order transmission coefficients based spin-torque QC architecture. The results encourage to set a path towards QC based reconfigurable complex computing systems in near future. The results presented in the chapter show that the Boolean logic computing fidelities satisfy the minimum requirement for fault-tolerant operations. Moreover, the average number of switching activities for optimal decompositions is reduced by 36.81% and 8.68% in comparison to conventional and reduced decompositions, respectively. We envision the considerable reduction in architecture power dissipation due to optimal decomposition of the computing blocks. Moreover, these optimal decompositions help to reduce the overall execution time of the reversible Boolean computing blocks to improve the qubit coherence. Moreover, the multiple Boolean computing blocks can be realized simultaneously with different sets of qubits by modulating respective qubit injection and reflection barrier heights.

Quantum computing due to its ability of inherent parallel processing has emerged as one of the novel solutions to the complex computing problems. In connection with this, several proposals have been given for the quantum circuits based design of the reversible combinational and sequential circuits. However, the implementation of the reversible sequential logic is challenging in comparison to the reversible combinational logic. Spin-torque based reconfigurable architecture is emerged as one of the novel technologies to realize the quantum circuits. However, the architecture needs the optimized decomposition of the quantum circuits utilized

for the reversible sequential logic due to required number of single qubit rotations and two-qubit entanglements. In this chapter, the elementary decomposition of the quantum circuits representing the reversible D-Latch is optimized with the help of elementary quantum library $\{R_y^{(\theta)}, R_z^{(\theta)}, \sqrt{SWAP}\}$. The number of elementary operations required to realize the D-Latch over 5 clock cycles is reduced by 43.56 %. The average fidelity of the D-Latch considered for the implementation and analysis at the end of each clock cycle is well above 97%. The fidelity is further improved by approximating the present state output utilized for the next state input.

Chapter 6

Spin-Torque Based Quantum Fourier Transform

6.1 Introduction

Complex computing problems can be solved efficiently by quantum computing (QC) in comparison to classical computing [192]. Quantum computers are able to efficiently solve the problems such as unorganized data searching [193], number factoring [194], counting solution problem [195], hidden subgroup problem [196], security of cryptographic systems [197], etc. Moreover, quantum computers can perform the operations in polynomial time as compared to the classical computer. However, the most critical issue with the QC is its physical realization. At present, the physical realization of QC is possible with the help of a classical computer and up to some extent by quantum computer. However, the technologies for the physical realization of quantum computer are not developed enough to deal with complex computing applications; therefore, most of QC based problems are solved on classical computers. To get rid of these obstacles, researchers are actively involved in the implementation of large scale QC. QC developed rapidly when Shor [17] through his algorithm showed that QC based integer number factoring could be performed in polynomial time. The integral component of the Shor's algorithm is Quantum Fourier Transform (QFT). From the computing point of view, QFT is one of the most imperative computational problems and finds its application in phase estimation [119], discrete algorithms [194], interchange of position and momentum states [119], quantum key distribution protocol [198], multiparty quantum telecommunication [199], and quantum arithmetic [200].

QFT is physically realized with the help of bulk resonance, atomic, and solid-state implementations [201, 202]. QFT based on solid-state technologies shows enormous prospects to realize the quantum computing at nanoscale. Recently, a spin-torque based architecture has emerged as one of the novel technologies to realize the single-qubit rotation and two-qubit entanglement [119]. However, the number of elementary operations required to realize the QC with this architecture is an issue due to the quantum circuit decomposition required for the elementary level. Therefore, in

this chapter, the optimal decomposition of the QFT and its realization with the generalized spin-torque based QC architecture is presented.

The chapter consists of eight sections including the introduction. Section 6.2 presents the mathematical treatment for the *n*-qubit QFT. The decomposition of the phase controlled gates used in quantum circuits for *n*-qubit QFT is elaborated in section 6.3. In section 6.4, decomposed quantum circuits are reduced and then optimized. The performance of the three-qubit QFT in terms of output state density matrix, magnitude/phase difference and fidelity comparison for the different forms of three-qubit QFT, is explained in section 6.5. The Clifford+T gate set based implementation of the QFT is presented in section 6.6. Finally, conclusions are drawn in section 6.7.

6.2 Multi-Qubit Quantum Fourier Transform

The Discrete Fourier Transform (DFT) finds its applications in digital signal processing for the conversion of time domain signals into frequency domain. The DFT of an *n*-bit input is given as

$$DFT(k) = \sum_{n=0}^{N-1} x(n) \cdot e^{\frac{-j2\pi nk}{N}} \tag{6.1}$$

where, *N* is the number of samples. However, for the complex signals, in comparison to QFT, DFT requires comparatively large time for the time domain to frequency domain conversion [1]. Therefore, QFT can be utilized for the time domain to the frequency domain conversion. The QFT on *n*-qubit states is expressed as

$$QFT_N |k\rangle = \frac{1}{\sqrt{N}} \sum_{n=0}^{2^N-1} e^{\frac{j2\pi nk}{N}} |n\rangle \tag{6.2}$$

where, $|n\rangle$ and $|k\rangle$ are the input and output states of the qubits, respectively, and *N* is the number of qubits. (6.2) is further decomposed as

$$QFT_N |k\rangle = \frac{1}{2^{\frac{N}{2}}} \sum_{n=0}^{1} \cdots \sum_{n_N=0}^{1} e^{\frac{j2\pi k(\sum_{l=1}^{N} n_l 2^{-l})|n_1.....n_N\rangle}{2^N}} |n\rangle \tag{6.3}$$

$$QFT_N |k\rangle = \frac{1}{2^{\frac{N}{2}}} \sum_{n=0}^{1} \cdots \sum_{n_N=0}^{1} e^{\frac{j2\pi nkl2^{-l}}{2^N}} |n_l\rangle \tag{6.4}$$

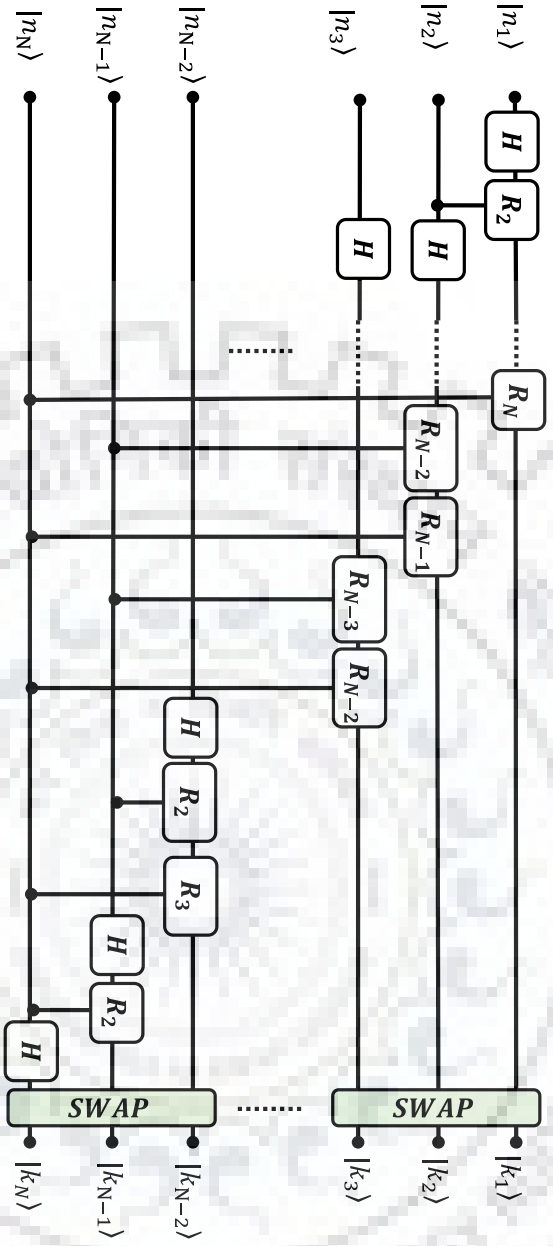

Figure 6.1 Multi-qubit QFT.

$$QFT_N|k\rangle = \frac{1}{2^{\frac{N}{2}}}\bigotimes_{l=1}^{N}\left(\sum_{n_l=0}^{1} e^{j2\pi nkl2^{-l}}|n_l\rangle\right) \tag{6.5}$$

$$QFT_N|k\rangle = \frac{1}{2^{\frac{N}{2}}}\bigotimes_{l=1}^{N}\left(|0\rangle + e^{j2\pi k}2^{-l}|1\rangle\right) \tag{6.6}$$

Based on (6.6), QFT is constructed for *n*-qubits (Figure 6.1). The quantum circuit for QFT consists of Hadamard and controlled phase shift gates [1]. *H* and *R* represent the Hadamard and controlled phase gate, respectively. A *SWAP* gate is utilized at the end

between successive odd and even numbered qubits, respectively (1and 3, 2 and 4). A four-qubit QFT for the unitary operation is represented as

$$QFT_4 = \begin{bmatrix} 1 & 1 & 1 & 1 \\ 1 & i & -1 & -i \\ 1 & -1 & 1 & -1 \\ 1 & -i & -1 & i \end{bmatrix} \tag{6.7}$$

6.3 Decomposition of Phase-Controlled Gate for multi-qubit QFT

A phase-controlled gate performs an unitary operation U[1] that is represented as

$$U = A \cdot X \cdot B \cdot X \cdot C \tag{6.8}$$

Therefore, the decomposition of phase-controlled gate [1] for (6.8) is shown in Figure 6.2.

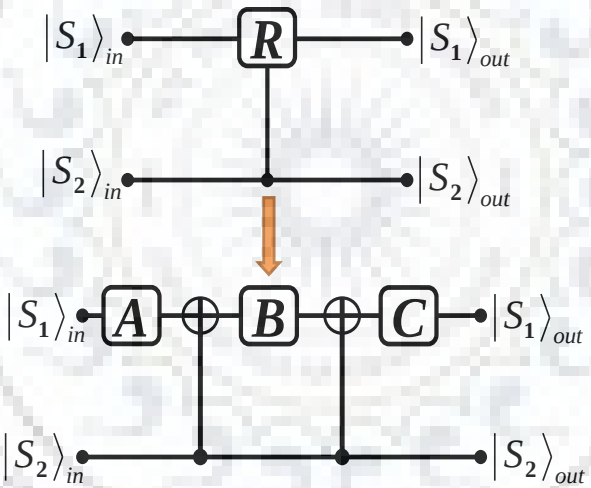

Figure 6.2 Controlled unitary gate.

The expressions for A, B, C, and X are given in (6.9), (6.10), (6.11), and (6.12).

$$A = \begin{bmatrix} e^{-i\left(\frac{\delta-\beta}{4}\right)} & 0 \\ 0 & e^{i\left(\frac{\delta-\beta}{4}\right)} \end{bmatrix} \tag{6.9}$$

$$B = \begin{bmatrix} \cos(\gamma/4)e^{i\left(\frac{\beta+\delta}{4}\right)} & -\sin(\gamma/4)e^{-i\left(\frac{\beta+\delta}{4}\right)} \\ \sin(\gamma/4)e^{i\left(\frac{\beta+\delta}{4}\right)} & \cos(\gamma/4)e^{-i\left(\frac{\beta+\delta}{4}\right)} \end{bmatrix} \tag{6.10}$$

$$C = \begin{bmatrix} \cos(\gamma/4)e^{-i\frac{\beta}{2}} & -\sin(\gamma/4)e^{-i\frac{\beta}{2}} \\ \sin(\gamma/4)e^{i\frac{\beta}{2}} & \cos(\gamma/4)e^{i\frac{\beta}{2}} \end{bmatrix} \tag{6.11}$$

$$X = \begin{bmatrix} 0 & 1 \\ 1 & 0 \end{bmatrix} \tag{6.12}$$

where, δ, β, and, γ are the phase angles such that the unitary operation U for the phase rotation is performed. Matrix X represents the CNOT gate operation. Therefore, (6.8) is modified to,

$$U = \begin{bmatrix} \sin^2\left(\frac{\gamma}{4}\right)e^{i\beta} + \cos^2\left(\frac{\gamma}{4}\right)e^{-i\left(\frac{\beta+\delta}{2}\right)\beta} & \sin\left(\frac{\gamma}{4}\right)\cos\left(\frac{\gamma}{4}\right)\left(e^{i\beta} - e^{-i\left(\frac{\beta+\delta}{2}\right)}\right) \\ \sin\left(\frac{\gamma}{4}\right)\cos\left(\frac{\gamma}{4}\right)\left(e^{i\left(\frac{\beta+\delta}{2}\right)} - e^{-i\beta}\right) & \sin^2\left(\frac{\gamma}{4}\right)e^{-i\beta} + \cos^2\left(\frac{\gamma}{4}\right)e^{i\left(\frac{\beta+\delta}{2}\right)\beta} \end{bmatrix} \tag{6.13}$$

The controlled rotations required in QFT are of the form

$$R_K = \begin{bmatrix} 1 & 0 \\ 0 & e^{\frac{i2\pi}{2^K}} \end{bmatrix} \tag{6.14}$$

The (6.13) is equivalent to (6.14) when $\delta = -3\beta$, and U is given below

$$U = \begin{bmatrix} e^{i\beta} & 0 \\ 0 & e^{-i\beta} \end{bmatrix} = \begin{bmatrix} e^{-i3\delta} & 0 \\ 0 & e^{i3\delta} \end{bmatrix} \tag{6.15}$$

6.4 Reduction/Optimization of QFT

The spin-torque based architecture needs further decomposition of the *H*, *R*, and CNOT into the single qubit rotations and two qubit entanglements. A conventional CNOT is decomposed into 11 elementary operations in sequence [108]. The R_x, R_z, and $\sqrt{\text{SWAP}}$ are single-qubit rotation about *x*-axis, single-qubit rotation about *z*-axis, and two-qubit entanglement, respectively. The matrix representation of the $\sqrt{\text{SWAP}}$ is given in (6.16).

$$\sqrt{SWAP} = \begin{bmatrix} 1 & 0 & 0 & 0 \\ 0 & \frac{1}{2}(1+i) & \frac{1}{2}(1-i) & 0 \\ 0 & \frac{1}{2}(1-i) & \frac{1}{2}(1+i) & 0 \\ 0 & 0 & 0 & 1 \end{bmatrix} \tag{6.16}$$

With the help of decomposed CNOTs, *H*s, and single qubit rotations, conventional decomposition of three-qubit QFT is achieved. For a hundred-qubit QFT, the number of operations required is 124050 (Table 6.1) which is very large, and will take longer time to perform the QFT. The elementary decomposition of the three-qubit QFT is shown in Figure 6.3.

QFT is optimized further by reducing the number of single qubit operations about the same axis at the interface of two quantum gates (Figure 6.4). The optimization of QFTs with more number of qubits can be performed with same methodology. There is a considerable reduction in the number of elementary operations due to optimization (Table 6.1). The number of elementary operations required to realize the QFT for their conventional, reduced, and optimized forms up to 10 qubits is given in this chapter.

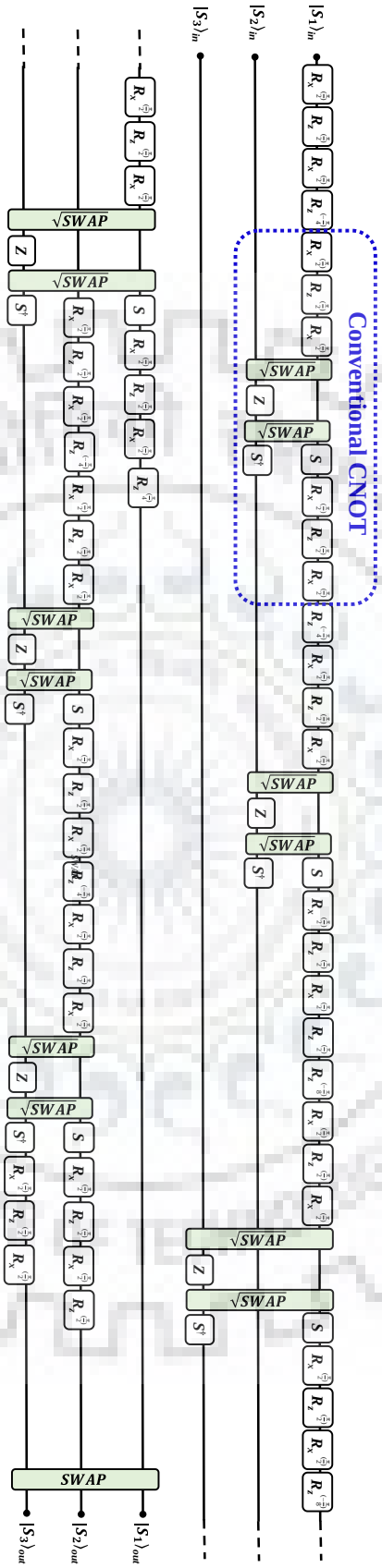

Figure 6.3 Conventional decomposition of three-qubit QFT.

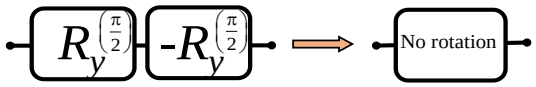

(a)

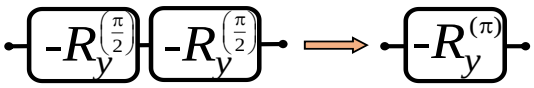

(b)

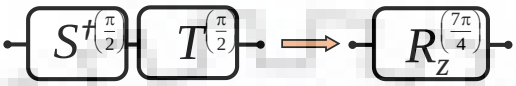

(c)

Figure 6.4 Reversible Boolean gates optimization (a) Removal of redundant single qubit rotations (b) Single rotation about y-axis by –π (c) Single qubit rotation about z-axis by 7π/4.

The reduction in the number of elementary operations helps in minimizing the number of switching activities needed for the spin generation and injection, preserve the spin-qubit coherence, and reduce overall switching power dissipation. For the spin-torque based QC architecture, the number of operations with the help of quantum gate library {R_y, R_z, $\sqrt{\text{SWAP}}$} are reduced. R_y is the qubit rotation about *y*-axis. The reduced/optimized decomposition of the three-qubit QFT is shown in Figure 6.5.

Table 6.1: Number of elementary operations

QFT size	Conventional decomposition	Reduced decomposition	Optimal decomposition
3	84	55	54
4	162	106	103
5	265	175	169
6	393	261	251
7	546	364	347
8	724	484	463
9	927	621	593
10	1155	775	739

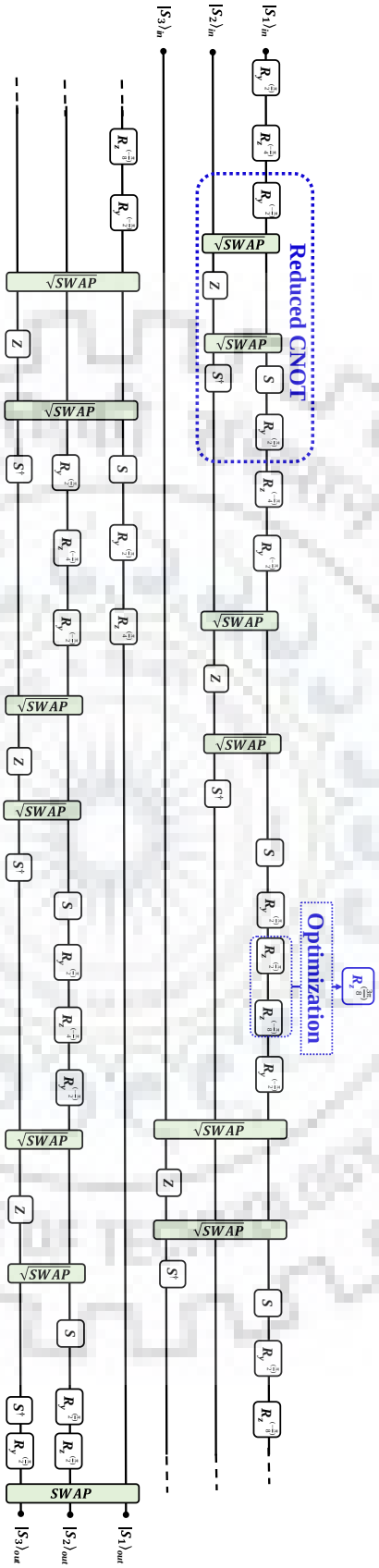

Figure 6.5 Reduced decomposition of three-qubit QFT.

The conventional, reduced, and optimized forms of the QFT are realized on the spin-torque based QFT. For the representation purpose, the state evolution of input state $|000\rangle$ is shown in Figure 6.6.

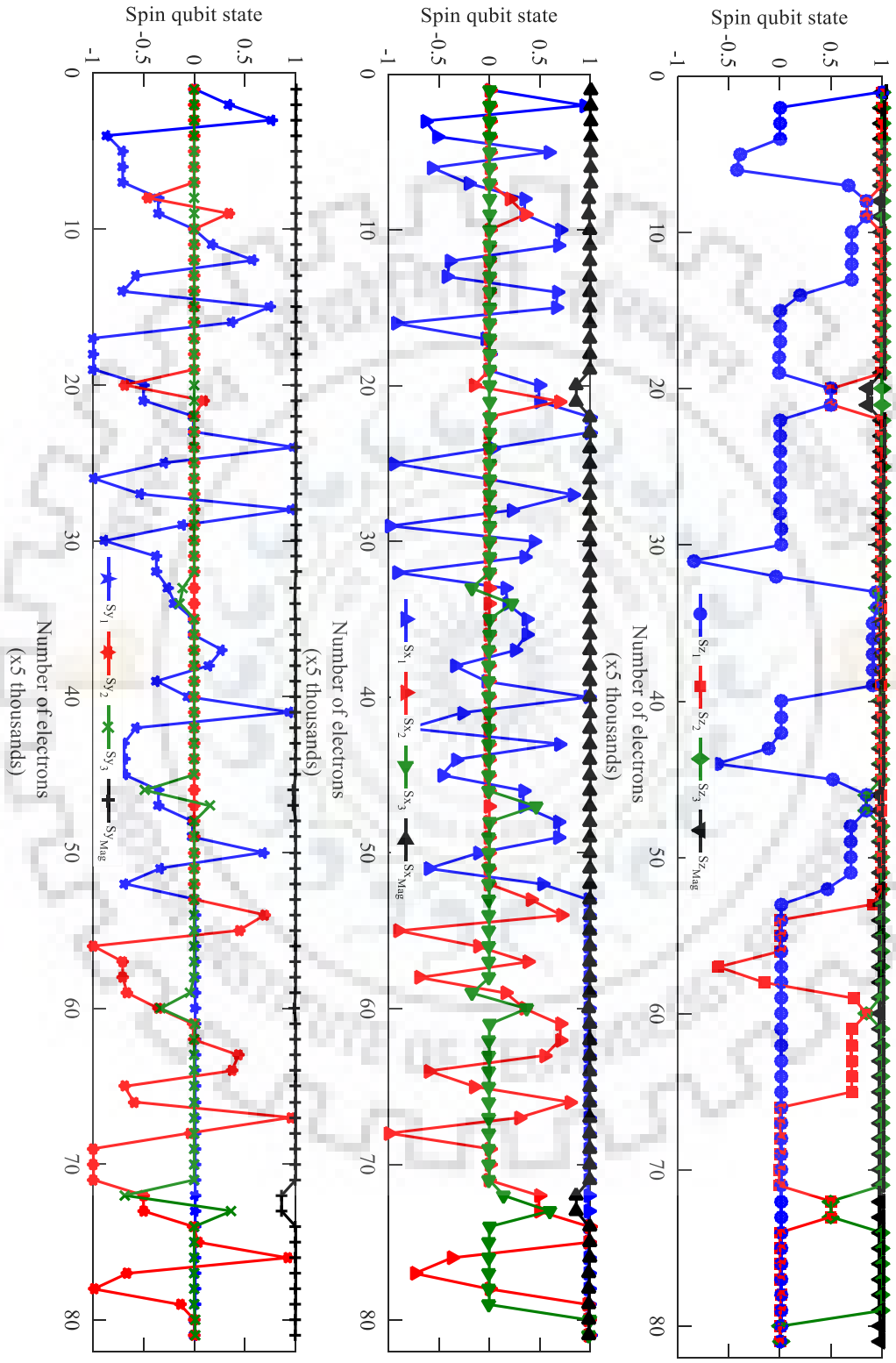

Figure 6.6 Qubit-state evolution for the input $|000\rangle$ for modified (second order) transmission coefficient based reduced/optimized decomposition of the QFT.

6.5 Performance Analysis of Three-Qubit QFT

The performance of the modified (second order) transmission coefficient based three-qubit QFT is analyzed based on the reduction in number of electrons required, deviation in the qubit states at the output, and QFT fidelity for all possible combinations of the input states, and its ability to trace the periodicity. The number of electrons required for the QFT realization depends on the number of operations involved to perform the QFT; angle of rotation for single qubit operations; and two-qubit entanglement. There is considerable reduction in the number of electrons required for the reduced/optimized forms of the QFT. The magnitude and phase difference between conventional, reduced, and optimized forms of the QFT for the input $|100\rangle$ are shown in Figure 6.7. Ideally, the respective phase difference and magnitude difference should be zero. However, the magnitude difference and phase difference between first order conventional and modified (second order) matrix based conventional QFTs is large in comparison to other respective magnitude and phase differences due to 34.52% more number of operations is required for the conventional decomposition; and the effect of the ratio of height of the injection side barrier to the exchange interaction on the single-qubit rotation and two-qubit entanglement.

The expression for the fidelity given in [203] for the model used in this chapter is

$$F = \frac{Tr(\rho_d \rho_o)}{\sqrt{Tr(\rho_d^2)}\sqrt{Tr(\rho_o^2)}} \sqrt{\frac{Tr(\rho_o^2)}{Tr(\rho_{in}^2)}} \tag{6.17}$$

where, ρ_d, ρ_o, and ρ_{in} are desired or, ideal output states spin density matrix, obtained states spin density matrix, and input states spin density matrix. The fidelity comparison for all forms of the three-qubit QFT is given in Table 6.2. The first order conventional, first order reduced, modified (second order) conventional, and modified (second order) reduced three-qubit QFTs have the average fidelities of 99.97%, 99.98%, 99.74%, and 99.90%, respectively.

The most important aspect of the QFT is periodicity extraction. An input state preparation (Figure 6.8a) is required to extract the periodicity of the three qubit QFT. Therefore, the input state is prepared (Figure 6.8b) and subsequently QFT is obtained for the input as shown in Figure 6.8(c). It is observed that the output density matrix is periodic with a period of four for the input of periodicity two.

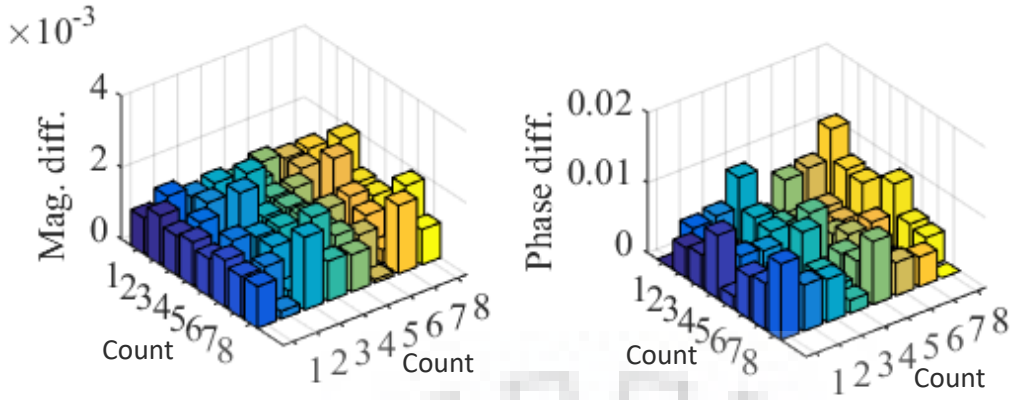
×10-3
Mag. diff.
4
2
0
Count
Count
Phase diff.
0.02
0.01
0
Count
Count

(a)

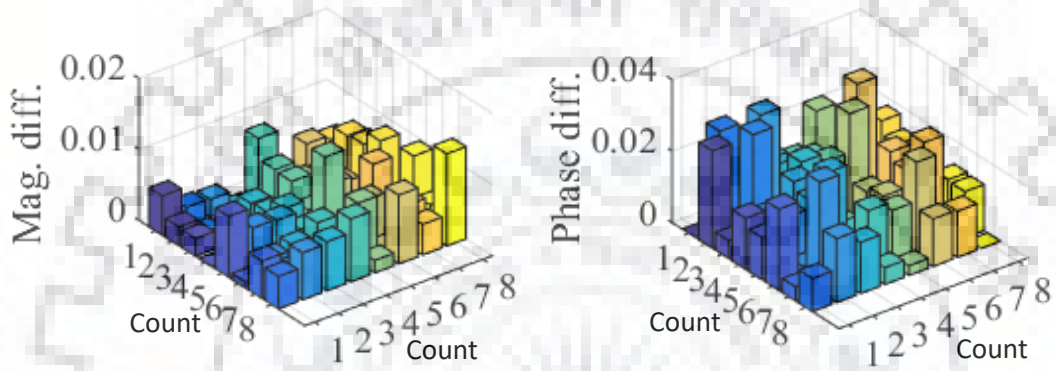
Mag. diff.
0.02
0.01
0
Count
Count
Phase diff.
0.04
0.02
0
Count
Count

(b)

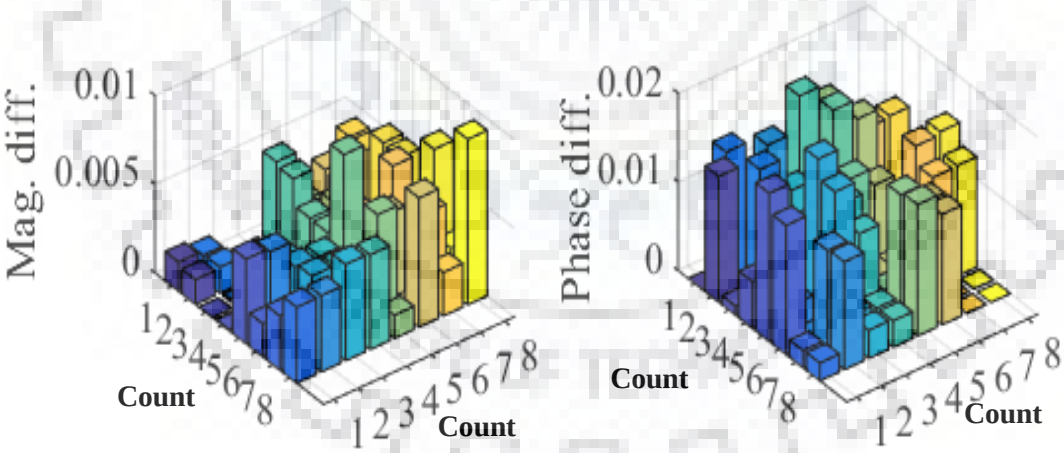
Mag. diff.
0.01
0.005
0
Count
Count
Phase diff.
0.02
0.01
0
Count
Count

(c)

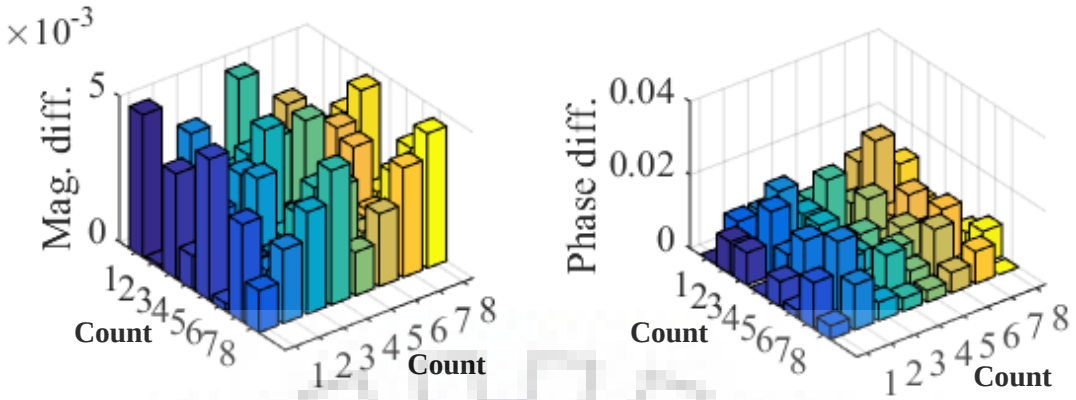

(d)

Figure 6.7 Magnitude and phase difference for the input $|000\rangle$ between (a) first order conventional and first order reduced QFT (b) first order conventional and modified (second order) matrix based conventional QFT (c) first order reduced and modified (second order) order reduced QFT (d) Modified (second order) order conventional and modified (second order) order reduced QFT.

Table 6.2: Fidelity for conventional and reduced three-qubit QFT

Input states	**First order conventional (%)**	**Modified (second) order conventional (%)**	**First order reduced (%)**	**Modified (second) order reduced (%)**
$\|000\rangle$	99.98	99.81	99.98	99.90
$\|001\rangle$	99.91	99.92	99.99	99.94
$\|010\rangle$	99.99	99.86	99.99	99.81
$\|011\rangle$	99.99	99.92	99.99	99.94
$\|100\rangle$	99.98	99.86	99.99	99.94
$\|101\rangle$	99.97	99.93	99.99	99.96
$\|110\rangle$	99.98	99.81	99.99	99.96
$\|111\rangle$	99.97	98.82	99.98	99.77

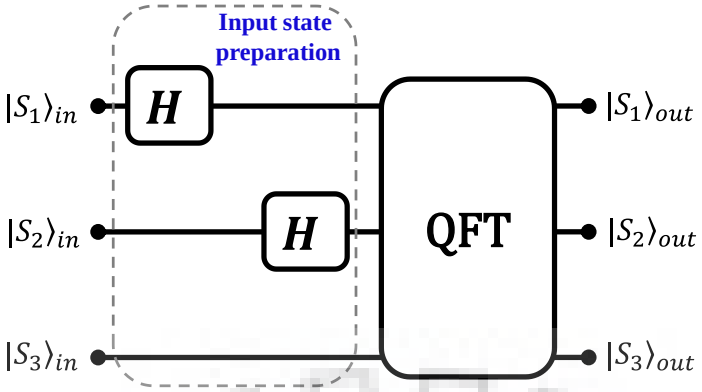

(a)

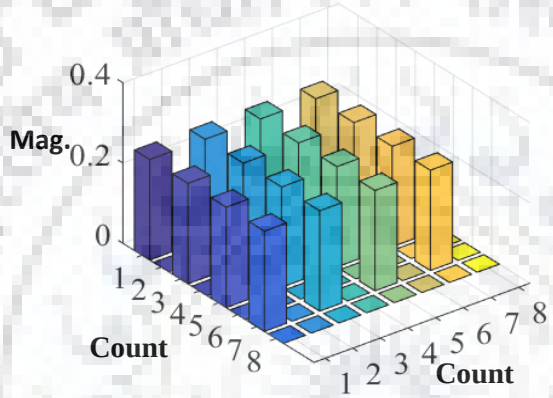

(b)

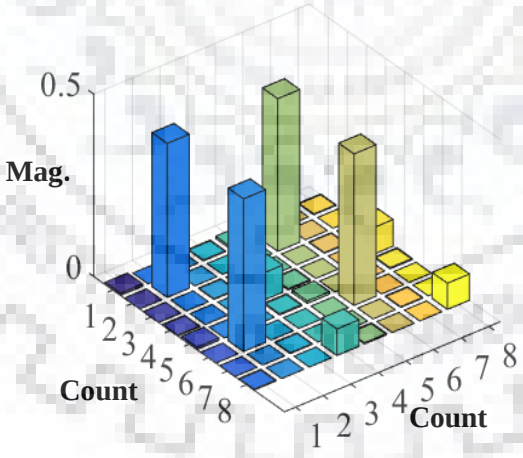

(c)

Figure 6.8 QFT Periodicity estimation for the input state (a) Quantum circuit (b) Periodicity 2 of the input state (c) Periodicity 4 of the output state.

6.6 Clifford+T Gate Set Based QFT Implementation

The quantum computation needs a finite gate set to solve the problem of efficient approximation. However, there is a limitation on the basic gates sets like

universal Clifford+T gate [204]. Therefore, there is a need of optimized Clifford+T gate set based quantum circuits with minimum depth [205]. In this chapter, an optimal-depth quantum circuit is utilized to implement the Clifford+T gate based three-qubit QFT (Figure 6.9). The number of elementary gates, *T*-depth, and total depth of the quantum circuit is 40, 9, and 32, respectively. The optimal decomposition of the Clifford+T gate based QFT is shown in Figure 6.10. The state evolution of the spin-qubit state is shown in Figure 6.11. It is observed from the Figs. 6.6 and 6.11 that the respective input and output states are the same. Therefore, it is possible to realize the Clifford+T gate set based QFT with the help of spin-toque-based single-qubit rotation and two-qubit entanglement model.

The number of elementary operations required for the three-qubit conventional QFT and reduced QFT is 84 and 55, respectively. However, the Clifford+T gate based QFT decomposition results in 188 elementary operations. After applying the reduction technique, it requires 134 elementary operations to realize the three-qubit QFT.

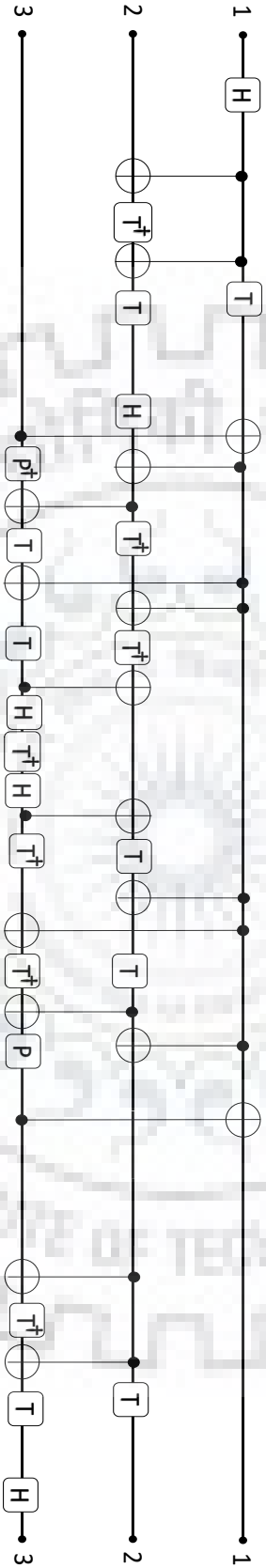

Figure 6.9 Clifford+T gate set based QFT.

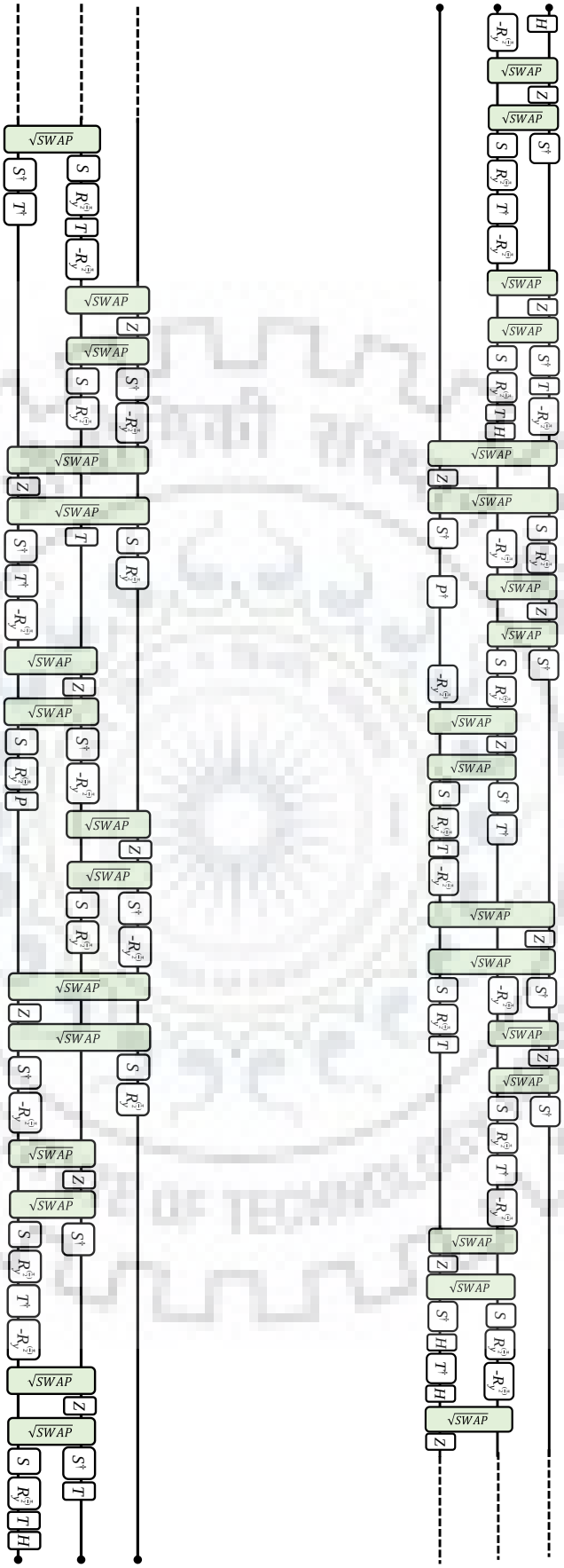

Figure 6.10 A reduced decomposition of the Clifford+ T based QFT.

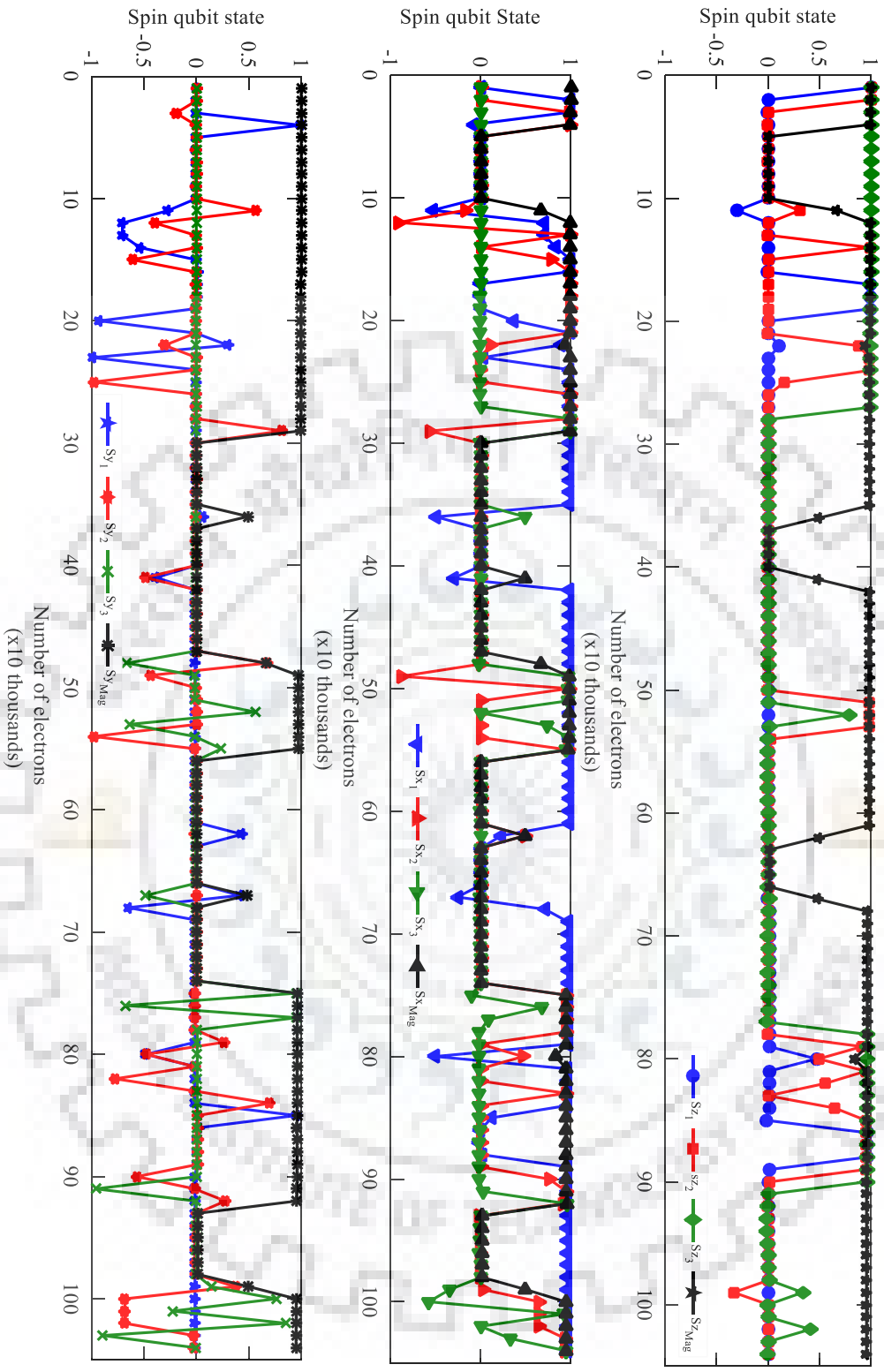

Figure 6.11 Qubit state evolution of the Clifford+T gate set based three-qubit QFT for $|000\rangle$ input.

6.7 Summary

Quantum computing (QC) provides an efficient platform to solve complex problems such as number factoring and searching. The Quantum Fourier Transform (QFT) is an integral part of quantum algorithms for integer number factoring, phase estimation, discrete algorithms, interchange of position and momentum states, quantum key distribution protocol, multiparty quantum telecommunication, and quantum arithmetic, etc. The theoretical and experimental implementations of QFT on various platforms have been proposed by researchers. Spin-torque-based qubit(s) manipulation is one of the encouraging solid-state device technologies. However, till date, QFT is not realized by spin-torque based QC architecture. In this chapter, the spin-torque based architecture has been modeled with the help of optimized decomposition of quantum circuits for the QFT. Moreover, an optimal-depth Clifford+T gates set based quantum circuit is utilized to implement the QFT. The performance analysis in terms of fidelity (>99%), magnitude, and phase difference of respective density matrices for different forms of three-qubit QFT, provides a novel way of its physical realization.

Chapter 7

Conclusions and Future Scope

The work presented in the thesis is concluded in this chapter. The modeling of single qubit rotation and two qubit entanglement; the reduction and optimization techniques to reduce the overall quantum operation time to preserve the spin coherence; and implementation and analysis of optimized three-qubit quantum Fourier transform (QFT) as an application, are presented in a systemic way in this thesis.

7.1 Conclusions

The thesis covers the work that is divided in five phases. In first phase, modified matrix based single-qubit rotation and two-qubit entanglement are performed on reconfigurable *n*-qubit architecture for the fault-tolerant QC. It is observed that interaction between flying electrons and static qubit is improved due to the inclusion of the reflection barrier height to exchange interaction ratio to modify the transmission coefficient matrix. Moreover, there is reduction in number of electrons required for single-qubit rotation and two-qubit entanglement. However, in case of single-qubit rotation, the component of spin qubit state along the axis of rotation deviates from reference. The deviation is negligble for smaller angles of rotation. However, it is observed that impact of deviation on fidelity is high for higher angle of rotations. In case of two qubit entanglement, there is increase in AEP due to effect of $\Gamma_{Rfl} / J = 0$.

In second phase of the thesis, the work is focused on performance of high fidelity conventional and reduced quantum gates evaluation with the help of quantum gate library $\{R_y, R_z, \sqrt{\text{SWAP}}\}$. It is observed that existing model based reduced gates have better fidelity and modified model based reduced gates require less number of electrons for the gate realization in comparison to other forms of realizations.

Performance of reversible Boolean computing blocks in *n*-qubit reconfigurable architecture is analyzed with the help of optimal decompositions in third phase of the thesis. The results presented in this work show that the Boolean logic computing fidelities satisfy the minimum requirement for fault-tolerant operations. Moreover, the

average number of switching activities for optimal decompositions is reduced by 36.81% and 8.68% in comparison to conventional and reduced decompositions, respectively. We envision the considerable reduction in architecture power dissipation due to optimal decomposition of the computing blocks. Moreover, these optimal decompositions help to reduce the overall execution time of the reversible Boolean computing blocks to improve the qubit coherence. Moreover, the multiple Boolean computing blocks can be realized simultaneously with different sets of qubits by modulating respective qubit injection and reflection barrier heights.

The reversible sequential circuits are considered in phase four of the thesis. The implementation and analysis of spin-torque based Reversible D-Latch is presented in this work. The optimized decomposition is realized through the iterative process for the next state output with the help of the modified transmission coefficient matrix. Due to the optimal decomposition of the Reversible D-Latch, the total number of elementary operations required for 5 cycles is 285 in comparison to the conventional decomposition that needs 505 numbers of operations. It is observed that the average fidelity of the D-Latch is close to the fault tolerant fidelity due the qubit state approximation at the end of each clock cycle.

In the final phase of the thesis, QFT's optimal decomposition is achieved for the spin-torque based QC architecture with the help of modified (second order) density matrix and optimized decomposition of the quantum circuit. Due to the optimization, there is a reduction in the number of transistor switching activities and the number of electrons required for the realization of the QFT. Moreover, the spin-torque based QFT is able to trace the periodicity of the prepared input states of periodicity of 4. The important outcome of the analysis is that the fidelity of the spin-torque-based three-qubit architecture is more than 99%, which encourages utilizing the spin-torque based architecture platform for the realization of complex computing applications of which QFT is an integral part.

7.2 Future Scope

The focus of the work is to have reduced and optimal quantum circuit decompositions to preserve the coherence of spin-qubits. However, the experimental verification of these circuit decompositions is not concealed in this thesis. Therefore, the experimental verification of fidelity and other parameters obtained in this thesis,

can be taken up as future work. Apart from this, the several potential problems that can be addressed in future as follows:

1. The challenges are qubit decoherence for realization of complex computing blocks and stability and precise control of qubit isolation and manipulation through barrier height control. Therefore, timing circuits are required to be developed for the effective control of the qubit barrier height so as to realize the sequence of elementary quantum operations for complex computing tasks.
2. The spin injection is an important aspect in designing the spintronics based devices. In the spin torque based QC, the single and two qubit operations are realized by considering the ideal conditions such as 100 % spin injection, and decoherence-free operations. However, in actual, the effect of low spin injection, and decoherence on the qubit manipulation are required to be considered to analyze the effect on qubit manipulation.
3. Unlike the classical Boolean operations, the quantum operations are prone to errors. The error correcting codes are bit flip, sign flip, and Shor codes. Therefore, the physical implementation of QC should have the ability to realize the error correcting codes. Previous models have performed low fidelity quantum operations in comparison to the spin torque based models. Therefore, the spin torque based high fidelity error correcting codes would be more suitable for the fault tolerant quantum computing.
4. There are several technologies proposed for the fabrication of the qubits. Therefore, fabrication of qubit could be seen as part of work to be done in future.

REFERENCES

[1] M. A. Nielsen and I. L. Chuang. *Quantum Computation and Quantum Information*. Cambridge: Cambridge University Press, 2000.

[2] D. P. DiVincenzo, "The physical implementation of quantum computation," *Fortschritte der Phys.*, vol. 48, no. 9–11, pp. 771–783, 2000.

[3] S. Bandyopadhyay and M. Cahay. *Introduction to Spintronics*. Boca Raton: CRC Press, 2008.

[4] M. Cahay, "An electron 's spin — part I," *IEEE Potentials*, pp. 31–35, 2009.

[5] W. Zhao and G. Prenat. *Spintronics-based Computing*. Switzerland: Springer, 2015.

[6] S. Bandyopadhyay, B. Das and A. E. Miller, "Supercomputing with spin polarized single electrons in a quantum coupled architecture", *Nanotech.*, vol. 5, no. 2, pp. 113-126, 1994.

[7] S. Bandyopadhyay, "Computing with spins: From classical to quantum computing", *Superlat. and Microstru.*, vol. 37, pp. 77-86, 2005.

[8] E. Y. Tsymbal, I. Žutic. *Handbook of Spin Transport and Magnetism*, New York: CRC press, 2012.

[9] Vladimir G. Plekhanov. *Isotope-Based Quantum Information*. Springer Briefs in Physics, 2012.

[10] A. Guzik, Alan, and P. Walther, "Photonic quantum simulators," *Nature Physics*, vol. 8, no. 4, pp. 285–291, 2012.

[11] C. Hennie, "One-tape, off-line Turing machine computations," *Elsevier*, vol.8, pp. 553-578, 1965.

[12] G. K. Brennen, C. M. Caves, P. S. Jessen, and I. H. Deutsch, "Quantum logic gates in optical lattices," *Phys. Rev. Lett.*, vol. 82, no. 5, p. 1060, 1999.

[13] A. C. C. Yao, "Classical physics and the Church-Turing thesis," *Jour. of the ACM*, vol. 50, no. 1, pp. 100–105, 2003.

[14] A. M. Turing, "On computable numbers, with an application to the Entscheidungs problem," *Proc. of the London Math. Soc.*, vol. s2-42, no. 1, pp. 230–265, 1937.

[15] E. Sakai, "On the principles of quantum mechanics," *Arxiv*, pp. 1-38, 2005.

[16] R. Landauer, "Irreversibility and heat generation in the computing process," *IBM Jour. of Res. and Dev.* , vol. 5, no. 3, pp. 183–191, 1961.

[17] P. W. Shor, "Polynomial-time algorithms for prime factorization and discrete logarithms on a quantum computer," *SIAM J. Comput.*, vol. 26, no. 5, pp. 1484–1509, 1997.

[18] L. K. Grover, "A framework for fast quantum mechanical algorithms," *Proc. of the 13th annual ACM symp. on Theory of comp.*, pp. 53–62, 1998.

[19] J. Fabian and I. Zutic, "The standard model of spin injection," *Arxiv.*, vol. 566, no. 2007, pp. 39, 2009.

[20] S. Bandyopadhyay, “Power dissipation in spintronic devices: A general perspective", *J. Nanosci. Nanotech.*, vol. 7, pp. 1-18, 2007.

[21] A. A. Tulapurkar and Y. Suzuki, "Boltzmann approach to dissipation produced by a spin-polarized current", *Phys. Rev. B*, vol. 83, pp. 1-4, 2011.

[22] D. D. Tang and Y. Lee. *Magnetic memory Fundamentals and Technology*. Cambridge: Cambridge University Press, 2010.

[23] L. I. Ying, “Dissertation on Mechanism and Assessment of Spin Transfer Torque (STT) based memory”, Massachusetts Institute of Technology, 2009.

[24] S. Rakheja, “Interconnects for Post-CMOS Devices : Physical Limits and Device and Circuit Implications”, Georgia Institute of Technology, 2012.

[25] D. P. DiVincenzo, “Quantum computation,” *Science*, vol. 270, no. 5234, pp. 255-261, 1995.

[26] R. P. Feynman, “Quantum mechanical computer,” *Springer*, vol. 16, no. 6, pp. 507- 531, 1986.

[27] P. Benioff, “Quantum mechanical Hamiltonian models of Turing machines,” *Jour. of Stat. Phy.*, vol. 29, no. 3, pp. 515-546, 1982.

[28] D. Loss and D. P. DiVincenzo, “Quantum computation with quantum dots,” *Phys. Rev. A*, vol. 57, no. 1, pp. 120-126, 1998.

[29] I. Žutić, J. Fabian, and S. D. Sarma, “Spintronics: Fundamentals and applications*,” Rev. Mod. Phys.*, vol. 76, no. 323, pp. 323-410, 2004.

[30] M. N. Leuenberger and D. Loss, “Spintronics and quantum computing: Switching mechanisms for qubits”, *Phys. E: Low-dimen. Sys. and Nano.*, vol. 10, no. 1, pp. 452-457, 2001.

[31] P. Benioff, “The computer as a physical system: A microscopic quantum mechanical Hamiltonian model of computers as represented by Turing machines,” *Jour. of Stat. Phy.*, vol. 22, no. 5, pp. 563-591, 1980.

[32] B. Schumacher, “Quantum coding,” *Phy. rev. A*, vol. 51, no. 4, pp. 2738-2747, 1995.

[33] V. Vedral, A. Barenco, and A. Ekert, “Quantum networks for elementary arithmetic operations,” *Phy. Rev. A*, vol. 54, no. 1, pp. 147-153, 1996.

[34] A. Barenco, C. H. Bennett, R. Cleve, D. P. DiVincenzo, N. Margolus, P. Shor, T. Sleator, J. Smolin, and H. Weinfurter, “Elementary gates for quantum computation,” *Phy. Rev. A*, vol. 52, no. 5, pp. 3457-3467, 1995.

[35] A. Barenco, “Quantum physics and computers,” *Cont. Phy.*, vol. 37, no. 5, pp. 375-389, 1996.

[36] P. W. Shor, “Polynomial-time algorithms for prime factorization and discrete logarithms on a quantum computer,” *SIAM Review*, vol. 41, no. 2, pp. 303-332, 1999.

[37] D. Deutsch, A. Barenco, and A. Ekert, “Universality in quantum computation,” *Proc. R. Soc. A*, vol. 449, no. 1937, pp. 669-677, 1995.

[38] S. Lloyd, “Almost any quantum logic gate is universal,” *Phy. Rev. Lett.*, vol. 75, no. 2, pp. 346-349, 1995.

[39] D. P. DiVincenzo, “Two-bit gates are universal for quantum computation,” *Phy. Rev. A*, vol. 51, no. 2, pp. 1015-1022, 1995.

[40] A. Barenco, "A universal two–bit gate for quantum computation," *Proc. R. Soc*., vol. 449, no. 1937, pp. 679-683, 1995.

[41] V. Buzek and M. Hillery, "Quantum copying: Beyond the no-cloning theorem," *Phy. Rev. A*, vol. 54, no. 3, pp. 1844-1852, 1996.

[42] S. Pirandola, J. Eisert, C. Weedbrook, A. Furusawa, and S. L. Braunstein, "Advances in quantum teleportation," *Nature Photo.*, vol. 9, no. 1, pp. 641-652, 2015.

[43] L. A. Rozema, D. H. Mahler, A. Hayat, P. S. Turner, and A. M. Steinberg, "Quantum data compression of a qubit ensemble," *Phys. Rev. Lett.*, vol. 113, no. 160504, pp. 1-5, 2014.

[44] A. Broadbent and C. Schaffner, "Quantum cryptography beyond quantum key distribution," *Designs, Codes and Cryptography*, vol. 78, no. 1, pp. 351-382, 2016.

[45] M. Rahami, D. Shamanta, and A. Tasnim, "Basic quantum algorithms and applications," *Int. Jour. of Comp. App.*, vol. 56, no. 4, pp. 26-31, 2012.

[46] C. A. P. Delgado and P. Kok, "Quantum computers: Definitions and implementations," *Phy. Rev. A*, vol. 83, no. 12303, pp. 1-15, 2011.

[47] Q. A. Turchette, C. J. Hood, W. Lange, H. Mabuchi, and H. J. Kimble, "Measurement of conditional phase shifts for quantum logic," *Phy. Rev. Lett.*, vol. 75, no. 25, pp. 4710-4713, 1995.

[48] R. Dumke, M. Volk, T. Muther, F. B. J. Buchkremer, G. Birkl, and W. Ertmer, "Micro-optical realization of arrays of selectively addressable dipole traps: A scalable configuration for quantum computation with atomic qubits," *Phy. Rev. Lett.*, vol. 89, no. 9, pp. 1-4, 2002.

[49] L. M. Duan, E. Demler, and M. D. Lukin, "Controlling spin exchange interactions of ultracold atoms in optical lattices," *Phy. Rev. Lett.*, vol. 91, no. 9, pp. 1-4, 2003.

[50] A. Blais, R. S. Huang, A. Wallraff, S. M. Girvin, and R. J. Schoelkopf, "Cavity quantum electrodynamics for superconducting electrical circuits: An architecture for quantum computation," *Phy. Rev. A*, vol. 69, no. 6, pp. 1-14, 2004.

[51] Z. X. Man, Y. Z. Xia, and R. L. Franco, "Cavity-based architecture to preserve quantum coherence and entanglement," *Sci. Rep.*, vol. 5, no. 13843, pp. 1-13, 2015.

[52] Y. L. Lim, S. D. Barrett, A. Beige, P. Kok, and L. C. Kwek, "Repeat-until-success quantum computing using stationary and flying qubits," *Phy. Rev. A*, vol. 73, no. 1, pp. 1-14, 2006.

[53] Y. L. Lim, A. Beige, and L. C. Kwek, "Repeat-until-success linear optics distributed quantum computing," *Phy. Rev. Lett.*, vol. 95, no. 3, pp. 1-4, 2005.

[54] S. Ritter, C. Nolleke, C. Hahn, A. Reiserer, A. Neuzner, M. Upho, M. Mucke, E. Figueroa, Jorg Bochmann, and G. Rempe, "An elementary quantum network of single atoms in optical cavities," *Nature*, vol. 484, no. 1, pp. 195-200, 2012.

[55] A. Serafini, S. Mancini, and S. Bose, "Distributed quantum computation via optical fibres," *Phy. Rev. Lett.*, vol. 96, no. 1, pp. 1-4, 2006.

[56] Z. Y. Xue and Z. D. Wang, "Simple unconventional geometric scenario of one-way quantum computation with superconducting qubits inside a cavity," *Phy. Rev. A*, vol. 75, no. 6, pp. 1-4, 2007.

[57] A. J. Daley, M. M. Boyd, J. Ye, and P. Zoller, "Quantum computing with alkaline earth atoms," *Phy. Rev. Lett.*, vol. 101, no. 17, pp. 1-4, 2008.

[58] M. Saffman and T. G. Walker, "Quantum information with Rydberg atoms," *Rev. of Mod. Phy.*, vol. 82, no. 3, pp. 2313-2363, 2010.

[59] C. M. Tesch and R. Vivie-Riedle, "Quantum computation with vibrationally excited molecules," *Phy. Rev. Lett.*, vol. 89, no. 9, pp. 1999-2008, 2002.

[60] T. Brecht, W. Pfaff, C. Wang, Y. Chu, L. Frunzio, and M. H. Devoret, "Multilayer microwave integrated quantum circuits for scalable quantum computing," *npj Quan. Info.*, vol. 2, no. 16002, pp. 1-4, 2016.

[61] B. Lekitsch, S. Weidt, A. G. Fowler, K. Mølmer, S. J. Devitt, C. Wunderlich, and W. K. Hensinger, "Blueprint for a microwave trapped ion quantum computer," *Sci. Adv.*, vol. 3, no. 2, 2017.

[62] S. Muralidharan, L. Li, J. Kim, N. Lutkenhaus, M. D. Lukin and, L. Jiang, "Optimal architectures for long distance quantum communication," *Sci. Rep.*, vol. 6, no. 20463, pp. 1-4, 2016.

[63] M Saffman, "Quantum computing with atomic qubits and Rydberg interactions: Progress and challenges," *Jour. of Phy. B: Atom., Mole. and Opt. Phy.*, vol. 49, no. 20, pp. 1-24, 2016.

[64] Richard J. Warburton, "Self-assembled semiconductor quantum dots," *Cont. Phy.*, vol. 43, no. 5, pp. 351-364, 2002.

[65] S. Bandyopadhyay, "Self-assembled quantum dots and nanostructures," *Nanophase and Nanostructured Materials*, Chapter 3, pp. 119-145, 2003.

[66] R. Hanson, L. P. Kouwenhoven, J. R. Petta, S. Tarucha, and L. M. K. Vandersypen, "Spins in few-electron quantum dots," *Rev. of Mod. Phy.*, vol. 79, no. 4, pp. 1217-1265, 2007.

[67] P. Kouwenhoven, T. H. Oosterkamp, M. W. S. Danoesastro, M. Eto, D. G. Austing, T. Honda, and S. Tarucha "Excitation spectra of circular, few-electron quantum dots," *Science*, vol. 278, no. 5344, pp. 1788-1792, 1997.

[68] V. I. Klimov, "Nanocrystal quantum dots: From fundamental photophysics to multicolor lasing," *Los Ala. Sci.*, vol. 28, no. 1, pp. 214-220, 2003.

[69] V. N. Golovach, M. Borhani, and D. Loss, "Electric dipole induced spin resonance in quantum dots," *Phy. Rev. B*, vol. 74, no. 16, pp. 1-10, 2006.

[70] M. A. Wilde and D. Grundler, "Alternative method for the quantitative determination of Rashba and Dresselhaus spin–orbit interaction using the magnetization," *New Jour. of Phy.*, vol. 15, no. 115013, pp. 1-18, 2013.

[71] O. G. Heinonen, P. K. Muduli, E. Iacocca, and J. Åkerman, "Decoherence, mode hopping, and mode coupling in spin torque oscillators," *IEEE Transactions on Magnetics*, vol. 49, no. 7, pp. 4398-4404, 2013.

[72] D. Klauser, D. V. Bulaev, W. A. Coish, and D. Loss, "Electron and hole spin dynamics and decoherence in quantum dots," in *Semi. Quant. Bits*, F. Henneberger, Ed. Singapore, Pan Stanford Publishing, 2008, pp. 229-245.

[73] A. Laraoui, F. Dolde, C. Burk, F. Reinhard, J. Wrachtrup, and C. A. Meriles, "High-resolution correlation spectroscopy of ^{13}C spins near a nitrogen-vacancy centre in diamond," *Nature Comm.*, vol. 4, no. 1651, pp. 1-7, 2013.

[74] J. Fischer, B. Trauzettel, and D. Loss, "Hyperfine interaction and electron-spin decoherence in graphene and carbon nanotube quantum dots," *Phy. Rev. B*, vol. 80, no. 15, pp. 1-9, 2009.

[75] M. Trif, P. Simon, and D. Loss, 'Relaxation of hole spins in quantum dots via two-phonon processes," *Phy. Rev. Lett.*, vol. 103, no. 10, pp. 1-4, 2009.

[76] T. A. Baart, T. Fujita, C. Reichl, W. Wegscheider, and L. M. K. Vandersypen, "Coherent spin-exchange via a quantum mediator," *Nature Nanotech.*, vol. 12, pp. 26-30, 2017.

[77] B. Bertrand, S. Hermelin, S. Takada, M. Yamamoto, S. Tarucha, A. Ludwig, A. D. Wieck, C. Bäuerle, and T. Meunier, "Fast spin information transfer between distant quantum dots using individual electrons," *Nature Nanotech.*, vol. 11, pp. 672-676, 2016.

[78] R. Hanson and G. Burkard, "Universal set of quantum gates for double-dot spin qubits with fixed inter-dot coupling," *Phy. Rev. Lett.*, vol. 98, no. 5, pp. 1- 4, 2007.

[79] C.H. Bennett, "Logical reversibility of computation," *IBM J. Res. Dev.*, vol. 17, no. 6, pp. 525-532, 1973.

[80] A. R. Trivedi and S. Bandyopadhyay, "Single spin Toffoli–Fredkin logic gate," *Jour. of App. Phy.*, vol. 103, no. 10, pp. 1- 5, 2008.

[81] Y. Weiss, M. Goldstein, and R. Berkovits, "Significant g-factor values of a two-electron ground state in quantum dots with spin-orbit coupling," *Phys. Rev. B*, vol. 78, no. 195306, pp. 1-7, 2008.

[82] P. Recher and B. Trauzettel, "Quantum dots and spin qubits in graphene," *IOP Science*, vol. 21, no. 30, pp. 1-13, 2010.

[83] J. Yoneda, K. Takeda, T. Otsuka, T. Nakajima, M.R. Delbecq, G. Allison, T. Honda, T. Kodera, S. Oda, Y. Hoshi, N. Usami, K. M. Itoh, and S. Tarucha, "A quantum dot spin qubit with coherence limited by charge noise and fidelity higher than 99.9%," *Nature Nanotechnology*, vol. 13, pp. 102-106, 2018.

[84] R. B. Chen, C. P. Chang, and M. F. Lin, "Electric-field-tunable electronic properties of graphene quantum dots," *Phy. E: Low-dimen. Sys. and Nano.*, vol. 42, no. 10, pp. 2812-2815, 2012.

[85] C. Kloeffel, M. Trif, P. Stano, and D. Loss, "Circuit QED with hole-spin qubits in Ge/Si nanowire quantum dots," *Phy. Rev. B*, vol. 88, no. 24, pp. 1-5, 2013.

[86] J. Tejada, E. M. Chudnovsky, E. del Barco, J. M. Hernandez, and T. P. Spiller, "Magnetic qubits as hardware for quantum computers," *Nanotech.*, vol. 12, pp. 181–186, 2001.

[87] G. Schmidt, "Concepts for spin injection into semiconductors— A review," *J. Phys. D. Appl. Phys.*, vol. 38, no. 7, pp. R107–R122, 2005.

[88] Y. Suzuki, A. A. Tulapurkar, and C. Chappert, "Spin injection phenomena and applications," *Nanomag. and Spintron.*, chapter 3, pp. 93-153, 2009.

[89] D. Banerjee, R. Adari, S. Sankaranarayan, A. Kumar, S. Ganguly, R. W. Aldhaheri, M. A. Hussain, A. S. Balamesh, and D. Saha, "Electrical spin injection using GaCrN in a GaN based spin light emitting diode,"*Appl. Phys. Lett.*, vol. 103, pp. 1-4, 2013.

[90] S. Gundapaneni, S. Ganguly, W. Van Roy, S. Kaushal and K. Sugishima, "Effect of sputtering on ferromagnet-oxide-silicon spin injection contacts,"*J. Vac. Sc. & Tech. B*, vol. 29, pp. 1-5, 2011.

[91] R. Adari, M. Murthy, T. Patil, R. Maheshwari, G. Vaidya, S. Ganguly, and D. Saha, "Geometric enhancement of spin injection and detection in semiconductors

for high-temperature operation," *in 55th Annual Conference on Magnetism and Magnetic Materials*, Atlanta, November 14-18, 2010, p.1.

[92] L. Liu, C. F. Pai, Y. Li, H. W. Tseng, D. C. Ralph, and R. A. Buhrman, "Spin-torque switching with the giant spin Hall effect of tantalum," *Science*, vol. 336, no. 6081, pp. 555–558, 2012.

[93] R Sbiaa and S. N. Piramanayagam, "Recent developments in spin transfer torque MRAM," *Physica status solidi RRL*, vol. 11, pp. 1-8, 2017.

[94] R. Sbiaa, R. Law, S.Y.H. Lua, E.L. Tan, T. Tahmasebi, and C.C. Wang, "Spin transfer torque switching for multi-bit per cell magnetic memory with perpendicular anisotropy," *App. Phy. Lett.*, vol. 99, pp. 1-3, 2011.

[95] L Wang, K Shi, S Peng, K Cao, H Yang, J Gao, W Zhao, and C Zha, " Large spin Hall effect of perpendicularly magnetized β-W/CoFeB/MgO layers with high thermal stability," *Japan. Journ. of App. Phy.*, vol. 58, pp. 1-4, 2019.

[96] D. Tiwari, N. Behera, A. Kumar, P. Dürrenfeld, S. Chaudhary, D. K. Pandya, J. Åkerman, and P. K. Muduli, "Antidamping spin-orbit torques in epitaxial-Py(100)/beta-Ta," *App. Phy. Lett.*, vol. 111, no. 23, pp. 1-4, 2017.

[97] A. Kumar, R. Bansal, S. Chaudhary, and P. K. Muduli, "Large spin current generation by the spin Hall effect in mixed crystalline phase Ta thin films," *Phy. Rev.*, vol. 98, no. 10, pp. 1-6, 2018.

[98] M. Ranjbar, S. N. Piramanayagam, S. K. Wong, R. Sbiaa, and T. C. Chong, "Anomalous Hall effect measurements on capped bit-patterned media," *App. Phy. Lett.*, vol. 99, no. 14, pp. 1-3, 2011.

[99] S. Wong, B. H. Chia, K. Srinivasan, R. Law, E. Tan, H. K. Tan, R. Sbiaa, and S. N. Piramanayagam,"Anomalous Hall effect measurement of novel magnetic multilayers," Jour. of App. Phy., vol. 106, no. 9, pp. 1-4, 2009.

[100] D. Bhowmik, "Spin orbit torque driven magnetic switching for low power computing and memory," University of California, Berkeley, 2015.

[101] D. Bhowmik, O. Lee, L. You, S. Salahuddin, "Magnetization switching and domain wall motion due to spin orbit torque," *in Nanomagnetic and Spintronic Devices for Energy Efficient Memory and Computing*, Chichester, Wiley and Sons Publishing, 2016, pp. 165-186.

[102] M. Kazemi, E. Ipek, and E. G. Friedman, "Switching of perpendicularly magnetized nanomagnets with spin-orbit torques in the absence of external magnetic fields," USA, 20180350498, 2018.

[103] M. Kazemi, G. E. Rowlands, S. Shi, R. A. Buhrman, and E. G. Friedman, "All-spin-orbit switching of perpendicular magnetization," *IEEE Trans. on Elect. Dev.*, vol. 63, no. 11, pp. 4499-4505, 2016.

[104] M. Kazemi, G. E. Rowlands, E. Ipek, R. A. Buhrman, and E. G. Friedman, "Compact Model for spin–orbit magnetic tunnel junctions," *IEEE Trans. on Elect. Dev.*, vol. 63, no. 2, pp. 848-855, 2016.

[105] K. Yagami, A. A. Tulapurkar, A. Fukushima and Y. Suzuki, "Inspection of intrinsic critical currents for spin-transfer magnetization switching," *IEEE Trans. on Mag.*, vol. 41, pp. 2615, 2005.

[106] T. Devolder, A. A. Tulapurkar, K. Yagami, P. Crozat, C. Chappert, A. Fukushima, Y. Suzuki, "Ultra-fast magnetization reversal in magnetic nano-pillars by spin-polarized current," *Jour. of Mag. and Mag. Mat.*, vol. 286, pp. 77-86, 2005.

[107] B. Kaestner, C. Leicht, V. Kashcheyevs, K. Pierz, U. Siegner, and H. W. Schumacher, "Single-parameter quantized charge pumping in high magnetic fields," *Appl. Phys. Lett.*, vol. 94, no. 1, pp. 92–95, 2009.

[108] B. Sutton and S. Datta, "Manipulating quantum information with spin torque," *Sci. Rep.*, vol. 5, no. November, p. 17912, 2015.

[109] A. S. Dzurak, L. C. L. Hollenberg, D. N. Jamieson, F. E. Stanley, C. Yang, T. M. Buhler, V. Chan, D. J. Reilly, C. Wellard, A. R. Hamilton, C. I. Pakes, A. G. Ferguson, E. Gauja, S. Prawar, G. J. Milburn, and R. G. Clark, " Charge-based silicon quantum computer architectures using controlled single-ion implantation," *Arxiv*, pp. 1-9, 2003.

[110] R. J. Schoelkopf, P. Wahlgren, A. A. Kozhevnikov, P. Delsing, and D. E. Prober, " The radio frequency single-electron transistor (RF-SET)," A FUS Science, vol. 280, no. 1238, 1998.

[111] M. Mitic, S. E. Andersen, C. Yang, T. Hopf, V. Chan, E. Gauja, F. E. Hudson, T. M. Buehler, R. Brenner, A. J. Ferguson, C. I. Pakes, S.M. Hearne, G. Tamanyan, D. J. Reilly, A. R. Hamilton, D. N. Jamieson, A. S. Dzurak, and R. G. Clark, " Single atom Si nanoelectronics using controlled single-ion implantation," *Elsevier*, vol. 78, pp. 279-286, 2005.

[112] J. V. Donkelaar, C. yang, A. D. C. Alves, J. C. McCallum, C. Hougaard, B. C. Johnson, F. E. Hudson, A. S. Dzurak, A. Morello, D. Spemann, and D. N. Jamieson, "Single atom devices by ion implantation," *J. Phys.: Condens. Matt.*, vol. 27, p. 154204 (1-9), 2015.

[113] S. R. Schofield, N. J. Curson, M. Y. Simmons, F. J. Rueb, T. Halllam, L. Oberbeck, and R. G. Clark, "Atomically precise placement of single dopants in silicon," *Phy. Rev. lett.*, vol. 91, no. 13, pp. 136104(1-2), 2003.

[114] T. Shinada, M. Hori, K. Taira, T. Endoh, and I. Ohdomari, "Recent advance in single-ion implantation method for single dopant devices," *9th Int. Works. on Junct. Tech.*, 2009, pp. 96-99.

[115] D. N. Jamieson, C. Yang, T. Hopf, S. M. Hearne, C. I. Pakes, S. Prawer, M. Mitic, E. Gauja, S. E. Andersen, F. E. Hudson, A. S. Dzurak, and R. G. Clark, " Controlled shallow single-ion implantation in silicon using an active substrate for sub-20-keV ions," *App. Phy. Rev. Lett.*, vol. 86, pp. 202101(1-3), 2005.

[116] C. Yang, D. N. Jamieson, S. M. Hearne, T. Hopf, C. I. Pakes, S. Prawer, S. E. Andersen, A. S. Dzurak, E. Gauja, F. E. Hudson, and R. G. Clark, " Integration of single ion implantation method in focused ion beam system for nanofabrication," *ICONN*, Brisbane, July 3-7, 2006, pp. 567-569.

[117] P. Hoyer, "Efficient quantum transforms," *Arxiv*, pp. 1-30, 1997.

[118] R. Cleve and J. Watrous, "Fast parallel circuits for the quantum Fourier transform," *Proc. 41st Annu. Symp. Found. Comput. Science*, pp. 526–536, 2000.

[119] Y. S. Weinstein, M. A. Pravia, E. M. Fortunato, S. Lloyd, and D. G. Cory, "Implementation of the quantum Fourier transform," *Phys. Rev. Lett.*, vol. 86, no. 9, pp. 1889–1891, 2001.

[120] A. Muthukrishnan and C. R. Stroud, "Quantum fast Fourier transform using multilevel atoms," vol. 49, no. 13, p. 8, 2001.

[121] R. Barak and Y. Ben-aryeh, "Fourier Transform of linear optics operators," *Journ. Opt. Soc. Am. B*, vol. 24, no. 2, pp. 231–240, 2007.

[122] M. Scully and M. Zubairy, "Cavity QED implementation of the discrete quantum Fourier transform," *Phys. Rev. A*, vol. 65, no. 5, p. 52324, 2002.

[123] H. F. Wang, A. D. Zhu, S. Zhang, and K. H. Yeon, "Simple implementation of discrete quantum Fourier transform via cavity quantum electrodynamics," *New J. Phys.*, vol. 13, 2011.

[124] S. Dogra and K. Dorai, "Implementation of the quantum Fourier transform on a hybrid qubit – qutrit NMR quantum emulator," *Int. Jour. of Quant. Info.*, vol. 13, no. 7, pp. 12–14, 2016.

[125] S. Weimann, A. Perez-leija, M. Lebugle, and A. Szameit, "Implementation of the classical and quantum Fourier transform in photonic lattices," *in Conf. on Lasers and Electro-Optics (CLEO)*, San Jose, CA, USA, May 10–15, 2015, no. 3, pp. 6–7.

[126] D. R. Tobergte and S. Curtis, "Emerging nanoelectronic devices," *J. Chem. Inf. Mod.*, vol. 53, no. 9, pp. 1689–1699, 2013.

[127] A. Fert, "The present and the future of spintronics," *Thin Solid Films*, vol. 517, no. 1, pp. 2–5, 2008.

[128] M. Cahay, "An electron's spin — part II," *IEEE Potentials*, vol. 28, no. 4, July, pp. 36–39, 2009.

[129] B. E. Kane, "A silicon-based nuclear spin quantum computer," *Nature*, vol. 393, pp. 133–137, 1998.

[130] C. Kloeffel and D. Loss, "Prospects for spin-based quantum computing in quantum dots," *Annu. Rev. Cond. Matter Phy.*, vol. 4, no. 1, pp. 51–81, 2013.

[131] B. Trauzettel, D. V. Bulaev, D. Loss, and G. Burkard, "Spin qubits in graphene quantum dots," *Nature*, vol. 3, pp. 192- 196, 2007.

[132] L. Jindal, A. D. Rane, H. S. Dhar, A. S. De, U. Sen, "Patterns of genuine multipartite entanglement in frustrated quantum spin systems," vol. 89, no. 1, pp. 1-9, 2014.

[133] D. Gunlycke, J. H. Jefferson, T. Rejec, A. Ramšak, D. G. Pettifor, and G. A. D. Briggs, "Entanglement between static and flying qubits in a semiconducting carbon nanotube," *J. Phys. Condens. Matter*, vol. 18, no. 21, pp. S851–S866, 2006.

[134] G. Cordourier-Maruri, Y. Omar, R. de Coss, and S. Bose, "Graphene enabled low-control quantum gates between static and mobile spins," *Phys. Rev. B*, vol. 89, pp. 1–6, 2014.

[135] M. Habgood, J. H. Jefferson, A. Ramšak, D. G. Pettifor, and G. A. D. Briggs, "Entanglement of static and flying qubits in degenerate mesoscopic systems," *Phys. Rev. B - Cond. Matter Mater. Phy.*, vol. 77, no. 7, pp. 1–10, 2008.

[136] G. Cordourier-Maruri, F. Ciccarello, Y. Omar, M. Zarcone, R. de Coss, and S. Bose, "Implementing quantum gates through scattering between a static and a flying qubit," *Phys. Rev. A - At. Mol. Opt. Phys.*, vol. 82, no. 5, pp. 1–7, 2010.

[137] M. Yamamoto, S. Takada, C. Bäuerle, K. Watanabe, A. D. Wieck, and S. Tarucha, "Electrical control of a solid-state flying qubit," *Nat. Nanotech.*, vol. 7, no. 4, pp. 247–251, 2012.

[138] X. Fong, Y. Kim, K. Yogendra, D. Fan, A. Sengupta, A. Raghunathan, and K. Roy, "Spin-transfer torque devices for logic and memory prospects and perspectives," *IEEE Trans. on Com.-Aid. Des. of Int. Cir. and Sys.*, vol. 35, no. 1, pp. 1–22, 2016.

[139] R. Adari, T. Patil, S. Murthy, S. Ganguly, and D. Saha, "Enhanced magnetoresistance in lateral spin-valves," *Appl. Phys. Lett.,* vol. 97, pp. 1-3, 2010.

[140] D. P. DiVincenzo, "Quantum gates and circuits," *Proc. R. Soc.,* vol. 454, no. 1969, p. 18, 1997.

[141] C. C. Lin, A. Chakrabarti, and N. K. Jha, "Optimized quantum gate library for various physical machine descriptions," *IEEE Trans. on Ver. Lar. Sca. Int. Sys.*, vol. 21, no. 11, pp. 2055–2068, 2013.

[142] J. E. Hirsch, "Spin Hall effect," *Phy. Rev. Lett.,* vol. 83, no. 9, pp.1834–1837, 1999.

[143] D. Bhowmik, L. You, and S. Salahuddin, "Spin Hall effect clocking of nanomagnetic logic without a magnetic field," *Nat. Nanotechnol.,* vol. 9, no. 1, pp. 59-63, 2013.

[144] Y. Ji, A. Hoffmann, J. S. Jiang, J. E. Pearson, and S. D. Bader, "Non-local spin injection in lateral spin valves," *Journ. Phy. D. App. Phy.*, vol. 40, no. 5, pp. 1280–1284, 2007.

[145] J. P. Gordon and K. D. Bowers, "Microwave spin echoes from donor electrons in silicon," *Phy. Rev. Lett.,* vol. 1, no. 10, pp. 368–370, 1958.

[146] A. M. Tyryshkin, S. A. Lyon, A. V. Astashkin, and A. M. Raitsimring, "Electron spin-relaxation times of phosphorus donors in silicon," *Phy. Rev. B*, pp. 12–15, 2003.

[147] T. Schenkel, J. A. Liddle, A. Persaud, A. M. Tyryshkin, S. A. Lyon, R. D. Sousa, K. B. Whaley, J. Bokor, J. Shangkuan, and I. Chakarov, "Electrical activation and electron spin coherence of ultralow dose antimony implants in silicon," *App. Phy. Lett.*, vol. 88, no. 11, pp. 1–3, 2006.

[148] A. M. Tyryshkin, S. A. Lyon, W. Jantsch, and F. Schaffler, "Spin manipulation of free two-dimensional electrons in Si/SiGe quantum wells," *Phy. Rev. Lett.*, vol. 94, no. 12, pp. 1–4, 2005.

[149] B. Huang, D. J. Monsma, and I. Appelbaum, "Coherent spin transport through a 350 micron thick silicon wafer," *Phy. Rev. Lett.*, vol. 99, p. 177209, 2007.

[150] R. Jansen, "Silicon spintronics," *Nat. Mater.*, vol. 11, no. 5, pp. 400–408, 2012.

[151] J. Ghosh, D. Osintsev, V. Sverdlov, and S. Ganguly, "Multilevel parallelization approach to estimate spin lifetime in silicon: Performance analysis*," in IEEE EUROSOI-ULIS*, Granada, 2018, pp. 1-4.

[152] Y. Gao, Y. J. Kubo, C. C. Lin, Z. Chen, and J. Appenzeller, "Optimized spin relaxation length in few layer graphene at room temperature," *Tech. Dig. -Int. Elec. Dev. Meet. IEDM*, no. I, pp. 80–83, 2012.

[153] R. Farshchi and M. Ramsteiner, "Spin injection from Heusler alloys into semiconductors: A materials perspective," *Journ. of Appl. Phy.*, vol. 113, no. 19, 2013.

[154] A. Hirohata, H. Sukegawa, H. Yanagihara, I. Zutic, T. Seki, S. Mizukami, and R. Swaminathan, "Roadmap for emerging materials for spintronic device applications," *IEEE Trans. on Magn.*, vol. 51, no. 10, 2015.

[155] R. Barends, J. Kelly, A. Megrant, A. Veitia, D. Sank, E. Jeffrey, T. C. White, J. Mutus, A. G. Fowler, B. Campbell, Y. Chen, Z. Chen, B. Chiaro, A. Dunsworth, C. Neill, P. O'Malley, P. Roushan, A. Vainsencher, J. Wenner, A. N. Korotkov, A. N. Cleland, and J. M. Martinis, "Superconducting quantum circuits at the

surface code threshold for fault tolerance," *Nature*, vol. 508, no. 7497, pp. 500–503, 2014.

[156] P. M. N. Rani, A. Kole, K. Datta, and I. Sengupta, "Improved decomposition of multiple-control ternary Toffoli gates using Muthukrishnan-Stroud quantum gates*," in Int. Conf. on Rev. Comp. RC2017*, Kolkata, 2017, pp. 202-213.

[157] S. Datta, *Electronic Transport in Mesoscopic Systems*. Cambridge, U.K.: Cambridge Univ. Press, 1995.

[158] J. Gubbi, R. Buyya, S. Marusic, and M. Palaniswami, "Internet of Things (IoT): A vision, architectural elements, and future directions," *Fut. Gen. Comp. Sys.*, vol. 29, no. 7, pp. 1645–1660, 2013.

[159] C. H. Bennett, "Notes on Landauer's principle, reversible computation, and Maxwell's demon," *Stud. Hist. Philos. Sci. Part B - Stud. Hist. Philos. Mod. Phys.*, vol. 34, no. 3, pp. 501–510, 2003.

[160] S. Tiwari, "Implications of scales in processing of information," *Proc. of IEEE*, vol. 103, no. 8, pp. 1250–1273, 2015.

[161] M. P. Frank, "Introduction to reversible computing: motivation, progress, and challenges," in *Proc. 2nd Conf. on Comp.*, Ischia, Italy, May 04 – 06, 2005, pp. 385–390.

[162] V. P. Roychowdhury, D. B. Janes and S. Bandyopadhyay, "Nanoelectronic architecture for Boolean logic," *in Proc. of the IEEE*, vol. 85, no. 4, pp. 574-588, 1997.

[163] Y. Zhao, P. Ouyang, W. Kang, S. Yin, Y. Zhang, S. Wei, W. Zhao, "An STT-MRAM based in memory architecture for low power integral computing*," IEEE Trans. on Computers*, vol. 68, no. 4, pp. 617-623, 2018.

[164] Q. An, S. L. Beux, I. O'Connor, J. O. Klein, and W. Zhao, "Arithmetic logic unit based on all-spin logic devices," *in 15th IEEE International New Circuits and Systems Conference (NEWCAS)*, Strasbourg, France, June 25 – 28, 2017, pp. 317-320.

[165] W. Hung, X. Song, G. Yang, J. Yang, and M. Perkowski, "Optimal synthesis of multiple output Boolean functions using a set of quantum gates by symbolic reachability analysis," *IEEE Trans. on CAD*, vol. 25, no. 9, pp. 1652–1663, 2006.

[166] K. Datta, I. Sengupta, and H. Rahaman, "A post-synthesis optimization technique for reversible circuits exploiting negative control lines," *IEEE Trans. on Comp.*, vol. 64, no. 4, pp. 1208-1214, 2015.

[167] D. K. Kole, H. Rahaman, D. K. Das, and B. B. Bhattacharya, "Derivation of test set for detecting multiple missing-gate faults in reversible circuits," *in International Symposium on Electronic System Design*, Kochi, Kerala, India, December 19 – 21, 2011, pp. 200-205.

[168] H. Rahaman, D. K. Kole, D. K. Das, and B. B. Bhattacharya, "Fault diagnosis for missing-gate fault (SMGF) model in reversible quantum circuits," *in 21st International Conference on VLSI Design (VLSID)*, Hyderabad, India, January 4-8, 2008, pp. 163-168.

[169] B. Parhami, "Fault tolerant reversible circuits", *in 40th Asimolar Conf. Signals, Systems, and Computers*, Pacific Grove, CA, USA, October 29-November 1, 2006, pp. 1726-1729.

[170] M. Nachtigal and N. Ranganathan, "Design and analysis of a novel reversible encoder/decoder", *in 11th IEEE Int. Con. on Nanotech.*, Portland, OR, USA, August 15-18, 2011, pp. 1543-1546.

[171] M. Nachtigal, H. Thapliyal, and N. Ranganathan, "Design of a reversible floating-point adder architecture, " *in 11th IEEE Conf. Nanotech.*, Portland, OR, USA, August 15-18, 2011, pp.451-456.

[172] C. Bandyopadhyay, H. Rahaman, and R. Drechsler, "Improved cube list based cube pairing approach for synthesis of ESOP based reversible logic," *Springer Trans. on Comp. Science XXIV*, LNCS 8911, pp. 129–146, 2014.

[173] A. J. Genot, J. Bath, and A. J. Turber, "Reversible logic circuits made of DNA," *J. of the Ameri. Chem. Soc.*, vol. 133, pp. 20080–20083, 2011.

[174] P. K. Lala, J. P. Parkerson, and P. Chakraborty, "Adder designs using reversible logic gates," *WSEAS Trans. on Cir. and Sys.*, vol. 9, no. 6, pp. 369–378, 2010.

[175] J. W. Bruce, M. A. Thornton, L. Shivakumaraiah, P. S. Kokate, and X. Li., "Efficient adder circuits based on a conservative reversible logic gate," *in IEEE Symposium on VLSI*, Pittsburgh, PA, USA, USA, April 25-26, 2002, pages 83–88.

[176] H. Thapliyal and M. Srinivas, "Novel Reversible 'TSG' gate and its application for designing components of primitive reversible/quantum ALU, " *in 5th International Conference on Information, Communications and Signal Processing*, Bangkok, Thailand, December 6-9, 2005, pp. 1425-1429.

[177] Z. Zhang, V. Dunjko, and M. Olshanii, "Atom transistor from the point of view of nonequilibrium dynamics," *New J. Phys.*, vol. 17, no. 12, p. 125008, 2015.

[178] W. C. Athas and L. J. Svensson, "Reversible logic issues in adiabatic CMOS," *in Proc. Work. Phys. Comput. Phy. Comp '94*, Dallas, TX, USA, November 17-20, 1994, pp. 111–118.

[179] P. Andrei and I. Mayergoyz, "Quantum mechanical effects on random oxide thickness and random doping induced fluctuations in ultra-small semiconductor devices," *J. Appl. Phys.*, vol. 94, no. 11, pp. 7163–7172, 2003.

[180] V. V Shende, A. K. Prasad, I. L. Markov, and J. P. Hayes, "Synthesis of reversible logic," *IEEE Trans. on Comp.-Aid. Des. of Int. Cir. and Sys.*, vol. 22, no. 6, pp. 710–722, 2003.

[181] B. Behin-Aein, D. Datta, S. Salahuddin, and S. Datta, "Proposal for an all-spin logic device with built-in memory," *Nature Nanotech.*, no. **5**, pp. 266 – 270, 2010.

[182] J. A. Jones, "Implementation of a quantum algorithm on a nuclear magnetic resonance quantum computer," J. *Chem. Phy.*, vol. 109, no. 5, pp. 1648–1653, 1998.

[183] C. A. Mack, "Fifty years of Moore's Law," *IEEE Trans. on Semi. Manufac.*, vol. 24, no. 2, pp. 202–207, 2011.

[184] A. Allan, H. William, and B. Andrew, "2001 Technology roadmap for semiconductors," *ITRS*, pp 42-53, 2002.

[185] A. D. Vos and Y. V. Rentergem, "Reversible Computing : From mathematical group theory to electronical circuit experiment," *in Proc. of the 2nd con. on Comp. front. (CF'05)*, Ischia, Italy, May 04 - 06, 2005, pp. 35–44.

[186] M. Saeedi, R. Wille, and R. Drechsler, "Synthesis of quantum circuits for linear nearest neighbor architectures," *Quant. Info. Proc.*, pp. 355–377, 2011.

[187] J. E. Rice, "A new look at reversible memory elements," *in IEEE Int.Symp. on Cir.and Sys.(ISCAS)*, Island of Kos, Greece, 2016, pp. 5–8.

[188] T. Song and S. Wang, "The design of reversible gate and reversible sequential circuit based on DNA computing," *in 3rd Inter. Conf. on Intel. Syst. and Know. Engin.*, Xiamen, China, 2008, pp. 114–118.

[189] H. Thapliyal and N. Ranganathan, "Design of reversible sequential circuits optimizing quantum cost, delay, and garbage outputs," *ACM Jour. on Emer. Tech. in Comp. Syst.*, vol. 6, no. 4, pp. 1201-1209, 2010.

[190] K. Veezhinathan, "Constructing online testable circuits using reversible logic," *IEEE Trans. on Instru. and Meas.*, vol. 59, no. 1, pp. 101–109, 2010.

[191] H. Thapliyal , S. Kotiyal, and N. Ranganathan, "Design of testable reversible sequential circuits," *IEEE Trans. on VLSI*, vol. 21, no. 7, pp. 1201–1209, 2013.

[192] C. H. Bennett, E. Bernstein, and G. Brassard, "Strengths and weaknesses of quantum computing," *SIAM J. Comp.*, vol. 26, no. 5, pp. 1510–1523, 1997.

[193] E. Rieffel and W. Polak, "An introduction to quantum computing for non-physicists," *ACM Comp. Sur.*, vol. 32, no. 3, pp. 300-335.

[194] W. Peter, A. B. Labs, M. Ave, and M. Hill, "Algorithms for quantum computation : discrete logarithms and factoring," in *Proc. 35th Ann. Symp. on Found. of Comp. Sci.*, Santa Fe, NM, USA, November 20-22, 1994, pp. 124–134.

[195] C. M. Dawson, H. L. Haselgrove, A. P. Hines, D. Mortimer, M. A. Nielsen, and T. J. Osborne, "Quantum computing and polynomial equations over the finite field Z2," *Jour. of Quant. Info. and Comp.*, vol. 5, no. 2, pp. 102–112, 2005.

[196] W. Wang, X. Jiang, L. Mu, and H. Fan, "A quantum algorithm for greatest common divisor problem," *Arxiv*, pp. 3–7, 2017.

[197] C. Cheng, R. Lu, A. Petzoldt, and T. Takagi, "Securing the internet of things in a quantum world," *IEEE Comm. Mag.*, pp. 116–120, 2017.

[198] X. Tan, S. Cheng, J. Li, and Z. Feng, "Quantum key distribution protocol using quantum Fourier transform," *IEEE Comp. Soc.*, no. 1, pp. 0–5, 2015.

[199] D. O. N. Diep, "Multiparty quantum telecommunication using quantum Fourier transforms," *Arxiv*, pp. 1–11, 2017.

[200] L. Ruiz-perez and J. C. Garcia-escartin, "Quantum arithmetic with the quantum Fourier transform," *Quant. Inf. Pro.*, vol. 16, no. 6, pp. 1–14, 2017.

[201] C. Feature, "The future of nanocomputing," *IEEE Comp. Soc.*, pp. 44-53, 2016.

[202] Q. Guo, X. Guo, R. Patel, E. Ipek, and E. G. Friedman, "AC-DIMM: Associative computing with STT-MRAM," in *Proceedings of the 40th Annual International Symposium on Computer Architecture (ISCA)*, Tel-Aviv, Israel, June 23 – 27, 2013, pp. 189-200.

[203] K. Dorai and D. Suter, "Efficient implementations of the quantum Fourier transform: An experimental perspective," *Int. Jour. of Quant. Info.*, vol. 3, no. 2, pp. 413–424, 2005.

[204] V. Kliuchnikov, D. Maslov, and M. Mosca, "Fast and efficient exact synthesis of single qubit unitaries generated by Clifford and T gates," *Jour. of Quant. Info. and Comp.*, vol. 13, no. 7, pp. 607-630, 2013.

[205] M. Amy, D. Maslov, M. Mosca, and M. Roetteler, "A meet-in-the-middle algorithm for fast synthesis of depth-optimal quantum circuits," *IEEE Trans. on CAD of Int. Cir. and Sys.*, vol. 32, no.6, pp. 818-830, 2013.

LIST OF PUBLICATIONS

Journals/Magazines

[1] **Anant Kulkarni** and Brajesh Kumar Kaushik, "Spin-torque based quantum Fourier transform," ***IEEE Transactions on Magnetics*** **(Article in Press)**.

[2] **Anant Kulkarni**, Sanjay Prajapati, Shivam Verma, and Brajesh Kumar Kaushik, "Optimal Boolean logic quantum circuits decomposition for spin-torque based *n*-qubit architecture," ***IEEE Transactions on Magnetics***, vol. 54, no. 10, pp. 1-9, 2018.

[3] **Anant Kulkarni**, Sanjay Prajapati, and Brajesh Kumar Kaushik, "Transmission coefficient matrix modeling of spin-torque based *n*-qubit architecture," ***IEEE Transactions on VLSI***, vol. 26, no. 8, pp. 1461-1470, 2018.

[4] Shivam Verma, **Anant Kulkarni**, and Brajesh Kumar Kaushik, "Spintronics based devices to circuits: Perspectives and challenges," ***IEEE Nanotechnology Magazine***, vol. 10, no. 4, pp. 13-28, 2016.

[5] **Anant Kulkarni**, Namita Bindal, and Brajesh Kumar Kaushik, "Quantum computing circuits based on spin-torque qubit architecture," ***IEEE Nanotechnology*** **Magazine (Article in Press).**

Conference

[1] **Anant Kulkarni**, Brajesh Kumar Kaushik, and Zeljko Zilic, "Implementation and analysis of spin torque based reversible D-Latch," ***IEEE Canadian Conference on Electrical and Computer Engineering (CCECE)***, Quebec City, QC, Canada, 2018.

Book

[1] Brajesh Kumar Kaushik, Shivam Verma, **Anant Kulkarni**, and Sanjay Prajapati. *Next Generation Spin Torque Memories*. Singapore: Springer Nature, 2017.